

The University of Manitoba

Evaluation of Novel Sample Preparation
and Purification Methods for
Mass Spectrometry of Peptides

by

Colin Lee

B.Sc. University of Manitoba 1995

A thesis submitted to the Faculty of Graduate Studies in partial fulfillment of the
requirements for the degree of

Doctor of Philosophy

Department of Chemistry

2009

Winnipeg, Manitoba

Copyright © 2009 Colin Lee

THE UNIVERSITY OF MANITOBA
FACULTY OF GRADUATE STUDIES

COPYRIGHT PERMISSION

**Evaluation of Novel Sample Preparation and Purification Methods for Mass Spectrometry
of Peptides**

BY

Colin Lee

**A Thesis/Practicum submitted to the Faculty of Graduate Studies of The University of
Manitoba in partial fulfillment of the requirement of the degree**

Of

Doctor of Philosophy

Colin Lee © 2009

**Permission has been granted to the University of Manitoba Libraries to lend a copy of this
thesis/practicum, to Library and Archives Canada (LAC) to lend a copy of this
thesis/practicum, and to LAC's agent (UMI/ProQuest) to microfilm, sell copies and to
publish an abstract of this thesis/practicum.**

**This reproduction or copy of this thesis has been made available by authority of the
copyright owner solely for the purpose of private study and research, and may only be
reproduced and copied as permitted by copyright laws or with express written
authorization from the copyright owner.**

Abstract

The onus of providing a highly pure biological sample for mass spectrometric analysis is daunting. For the predominant types of analytes such as proteins, peptides, and nucleic acids, their polymeric nature inherently implies only small differences in their physical properties to draw upon in developing analytical strategies.

Our research focuses on the development of novel analytical tools for the purification of biological samples to be analyzed by mass spectrometry. First, we evaluate surface adsorption of proteins to polyurethane substrates to capture target molecules. Samples of β -casein are adsorbed onto a polyether type polyurethane surface. Wash steps, and the evaluation of on-membrane digestion parameters are performed to yield peptides suitable for mass spectrometric analysis. In comparison, online CE-MS is evaluated to determine its efficacy in yielding complete peptide maps of phosphorylated peptides.

In addition, we examine methods of producing a thinner polyurethane surface to reduce space charge effects in a linear TOF system. The formation of thin, poreless polyurethane films was evaluated, as well as the effects of solvent composition on surface artifacts.

The performance of a prototype MALDI-QqTOF was evaluated for the analysis of multiply-phosphorylated peptides. Analysis of the tryptic fragment T1-2 of β -casein was performed, showing in-source fragmentation of the phosphate moieties. Further MS/MS analysis of the fragment shows the formation of dehydroalanine residues from phosphoserine. In addition, the formation of multiple ion series arising from differing fragmentation pathways of phosphoserine is also

seen. Further MS/MS studies of prompt decay products shows similar results, concluding that phosphoserine fragmentation yields multiple ion series even if all phosphoserine have been reduced to dehydroalanine by in-source decay prior to MS/MS analysis.

The evaluation of an on-target electrophoresis system was evaluated for the separation of peptide standards. Samples were electrophoretically separated in a Teflon channel, immobilized by freezing, and lyophilized to remove water prior to deposition of matrix and analysis by MALDI-TOF. Results show separation occurring, though sensitivity is low. Though the Teflon channel allows for electrophoretic separation, it reduces sensitivity in direct MALDI analysis of components, as well as problems in matrix deposition.

Acknowledgements

I would like to thank Dr. H el ene Perreault for the opportunity to study and work in her lab. These years spent studying bioanalytical chemistry has greatly expanded my horizons as a scientist. Her constant support in my professional career has led me to develop not only as a scientist, but also to mature and grow as a person.

Special thanks go to Dr. Mark E. McComb for introducing me to the field of biological mass spectrometry. His guidance during my initiation into graduate school taught me much about surviving graduate school and to approach research with enthusiasm. I will always fondly remember late nights conducting research and many coffee breaks for “fresh air”.

Graduate studies is no small task, and no man stands alone. Heartfelt thanks go to Mr. R.J. McNabb, without whom, some projects would have never been attempted, or gone unfinished. But beyond his incredible technical expertise, he has been a great friend. Coffee breaks and late night discussions over things technical as well as philosophical took on new meaning. Being in a technical field implied a level of cleverness and savvy in Jim, but I learned much from him about intangible things such as work ethic and integrity. Kudos to you, my friend. Keep your powder dry....

Dedication

This thesis is dedicated to my parents, whom without their support I could not have achieved this work.

To David, who has always led by example as both a scientist and a big brother.

And to my darling Leanne, who makes my world shine and brings feelings to my life that science will never understand.

“Character, like a photograph, develops in darkness.”
- **Yousuf Karsh**

“Never doubt that a small group of thoughtful, committed
citizens can change the world; indeed, it's the only thing that
ever has.”
- **Margaret Mead**

“Character is higher than intellect. A great soul will be strong to
live as well as think.”
- **Ralph Waldo Emerson**

Table of Contents

1 Introduction

1.1 Mass Spectrometry.....	1
1.1.1 MALDI.....	2
1.1.2 Electrospray Ionization.....	5
1.1.3 Quadrupole Mass Spectrometers.....	7
1.1.4 Time of Flight Mass Spectrometers.....	10
1.1.5 Post Source Decay.....	15
1.1.6 Collision Induced Dissociation.....	16
1.1.7 Hybrid Mass Spectrometers.....	18
1.1.8 Collisional Damping Interface.....	21
1.1.9 Concluding Statement.....	23
1.2 References.....	25

2 Profiling of Polyurethane Film Structure by Scanning Electron Microscopy

2.1 Introduction.....	27
2.1.1 Scanning Electron Microscopy.....	33
2.2 Experimental	
2.2.1 Materials and Method.....	38
2.3 Results and Discussion	
2.3.1 THF vs. distilled THF as solvent for PU.....	41
2.3.2 Alcohols and Chloromethanes.....	45
2.3.3 Other Solvents.....	53
2.3.4 Dissimilar Solvents to THF.....	53
2.3.5 Spin Coating.....	60
2.4 Conclusion.....	74
2.5 References.....	77

3 Determination of Protein Phosphorylation Sites by MALDI-QqTOF MS

3.1 Introduction.....	79
3.2 Experimental	
3.2.1 Materials and Methods.....	81
3.3 Results and Discussion	
3.3.1 MS of β -casein and dephosphorylated β -casein.....	83
3.3.2 MS/MS of $[M+H]^+$ dephosphorylated T1-2.....	87
3.3.3 MS of $[M+H]^+$ of phosphorylated T1-2.....	88
3.3.4 MS/MS of $[M+H]^+$ of phosphorylated T1-2 by QqTOF.....	92

3.3.5 MS/MS of prompt decay products.....	99
3.3.6 MS/MS of doubly charged ions.....	103
3.4 Conclusions.....	105
3.5 References.....	107

4 A Comparison of Sheathless Capillary Electrophoresis with LC-ESI-MS and MALDI-MS for Evaluation of Phosphoprotein Mapping

4.1 Introduction	
4.1.1 Capillary Electrophoresis.....	109
4.1.2 Interfacing CE to Mass Spectrometry.....	116
4.1.2.1 Sheathless Interface.....	117
4.1.2.2 Liquid Junction Interface.....	120
4.1.2.3 Sheath-flow Interface.....	122
4.1.2.4 Comparison of Interface Designs.....	124
4.1.2.5 Mass Spectrometers Suitable for CE.....	126
4.2 Experimental	
4.2.1 Materials and Method.....	129
4.3 Results and Discussion	
4.3.1 MALDI-TOF MS.....	130
4.3.2 HPLC-MS.....	134
4.3.3 CE-TOF-MS.....	137
4.4 Conclusion.....	143
4.5 References.....	144

5 Evaluation of On-Target Electrophoresis as a Sample Preparation Method for MALDI-MS

5.1 Introduction.....	147
5.2 Materials and Methods	
5.2.1 Electrophoresis Targets.....	150
5.2.2 Cooling System.....	150
5.2.3 Method.....	150
5.3 Results and Discussion	
5.3.1 Proof of concept.....	156
5.3.2 Design Considerations and Prototyping of On-target Electrophoresis System.....	159
5.3.3 Peptide Standard Results.....	163
5.4 Conclusion.....	181
5.5 References.....	185

List of Figures

Page

Figure 1.1: Illustration of MALDI ionization process.....	4
Figure 1.2: Illustration of electrospray ionization process	7
Figure 1.3: RF Field Applied to quadropoles.....	8
Figure 1.4: Motion of ions through a quadrupole.....	9
Figure 1.5: Linear TOF diagram, showing differing velocities for ions of different masses.....	12
Figure 1.6: Ion mirror compensating for ions of equal mass but different velocities.....	14
Figure 1.7: Collision induced dissociation process.....	17
Figure 1.8: Schematic of an orthogonal acceleration QqTOF instrument	19
Figure 1.9: Schematic drawing of a MALDI-QqTOF, with a collisional damping interface.....	22
Figure 2.1: Chemical structure of polyether type PU.....	30
Figure 2.2: Interaction volume of a SEM electron beam on a sample surface.....	34
Figure 2.3: Interaction volume of SEM electron beam.....	36
Figure 2.4: Schematic drawing of SEM microscope.....	37
Figure 2.5: SEM of PU film cast with bottled THF.....	43
Figure 2.6: SEM of PU film cast with distilled THF.....	43
Figure 2.7: SEM of PU films cast from 10% water.....	44
Figure 2.8: SEM of PU film cast with 10% methanol.....	46
Figure 2.9: SEM of PU film cast with 10% ethanol.....	46
Figure 2.10: SEM of PU film cast with 10% ethanol.....	46
Figure 2.11: SEM of PU film cast with 10% 1-butanol	48
Figure 2.12: SEM of PU film cast from 10% dichloromethane.....	50
Figure 2.13: SEM of PU film cast from 10% trichloromethane	50
Figure 2.14: SEM of PU film cast from 10% tetrachloromethane	51
Figure 2.15: SEM of PU film cast from 10% acetone	55
Figure 2.16: SEM of PU film cast from 10% acetonitrile.....	55
Figure 2.17: SEM of PU film cast from 10% toluene.....	56
Figure 2.18: SEM of PU film cast from 10% DMSO.....	59
Figure 2.19: SEM of PU film spin coated at 100% speed.....	62
Figure 2.20: SEM of PU film spin coated at 80% speed.....	62
Figure 2.20c: SEM of PU film formed by spin coating at 80% speed.....	64
Figure 2.21a: SEM of PU film formed by spin coating at 60% speed	64
Figure 2.21b: SEM of PU film formed by spin coating at 60% speed.....	65
Figure 2.22: Images of PU film formed by spin coating at 40% speed.....	68
Figure 2.23: SEM of PU films from spin coating a 10% water spiked solution spun at 100% speed.....	69
Figure 2.24: SEM of PU film formed from a 10% water solution spin coated at 80% speed.....	71
Figure 2.25: SEM of PU film formed from 10% water spike spun at 60% speed...	73
Figure 2.26: SEM of PU film formed from 10% water spike spun at 40% speed...	73

Figure 3.1: Peptide sequence of T1-2 tryptic fragment of bovine β -casein with schematic fragmentation pattern.....	86
Figure 3.2a: MALDI QqTOF MS/MS spectrum of $[M+H]^+$ ions of dephosphorylated T1-2 digestion products of β -casein.....	89
Figure 3.2b: MALDI QqTOF MS/MS spectrum of $[M+H]^+$ ions of dephosphorylated T1-2 digestion products of β -casein.....	90
Figure 3.3: Portion of MALDI MS spectrum of β -casein digest products showing prompt decay loss of H_3PO_4	91
Figure 3.4: MALDI QqTOF MS/MS spectrum of $[M+H]^+$ ions of dephosphorylated T1-2 digestion product of β -casein.....	95
Figure 3.5: Formation of dehydroalanine residues via β -elimination of H_3PO_4	96
Figure 3.6: Portions of MALDI QqTOF MS/MS spectrum of T1-2 showing isotope distributions of fragments.....	98
Figure 3.7: MALDI QqTOF MS/MS spectrum of prompt decay product of $[M+H-4 H_3PO_4]^+$ ions.....	100
Figure 3.8: Proposed formation of b_n+18 ions in MS/MS of $[M+H-4H_3PO_4]^+$	102
Figure 3.9: MALDI QqTOF MS/MS spectrum of $[M+H]^{2+}$ of T1-2.....	104
Figure 4.1: Schematic representation of the inner and outer Helmholtz layers of a CE capillary wall.....	111
Figure 4.2: Comparison of variable flow velocities at walls and center of capillaries for (a) EOF and (b) Parabolic flow.....	112
Figure 4.3: Schematic representation of separation of positive, neutral, and negatively charged species by CE.....	114
Figure 4.4: Schematic representation of a CE apparatus.....	115
Figure 4.5: Schematic diagram of a sheathless interface.....	119
Figure 4.6: Schematic diagram of a liquid junction interface.....	121
Figure 4.7: Schematic diagram of a sheathflow interface.....	123
Figure 4.8: Peptide map of β -casein generated by MALDI-MS of on-membrane digestion products.....	132
Figure 4.9: Comparison of MALDI spectra of on-membrane digestion products...	133
Figure 4.10: Total ion chromatogram of HPLC-MS of β -casein tryptic digest.....	135
Figure 11: Selected Ion Chromatograms of HPLC-MS of β -casein digestion products.....	136
Figure 4.12: Total ion electropherogram of sheathless electrospray CE of β -casein digest.....	138
Figure 13: Selected ion electropherograms of β -casein digestion products.....	139
Figure 4.14: Comparison of sensitivity and resolution of HPLC-ESI-MS and CE-TOF-MS.....	140
Figure 4.15: Peptide map of β -casein generated by CE-TOF-MS.....	141
Figure 5.1: Schematic representation of Teflon Channel.....	152
Figure: 5.2a: Schematic of Target holder for Bruker Biflex IV.....	153
Figure 5.2b: Photo of Target holder with Teflon channel.....	153
Figure 5.3: Cooling apparatus for freezing Teflon channel.....	154

Figure 5.4: Workflow for open channel electrophoresis on a Teflon channel.....	155
Figure 5.5a: Chemical structure of Congo Red.....	157
Figure 5.5b: Chemical structure of Malachite Green	157
Figure 5.6: Migration of ionic dyes.....	158
Figure 5.7: MALDI-MS of peptide standard mixture.....	165
Figure 5.8: MALDI-MS of surface extract from Zone 1.....	166
Figure 5.9: MALDI-MS of surface extract from Zone 2.....	167
Figure 5.10: MALDI-MS of surface extract from Zone 3.....	168
Figure 5.11: MALDI-MS of surface extract from Zone 4.....	169
Figure 5.12: MALDI-MS of surface extract from Zone 5.....	170
Figure 5.13: MALDI-MS of surface extract from Zone 6.....	171
Figure 5.14: Trace spectra of MALDI-MS of zone surface extracts.....	172
Figure 5.15: MALDI-MS showing increased oxidation of bombesin.....	179
Figure 5.16: MALDI-MS spectrum directly acquired from Teflon surface	180
Figure 5.17: Schematic workflow of joined Teflon targets showing	184

List of Tables	Page
Table 2.1: Solvents and physical data.....	39
Table 3.1: Measured m/z values of [M+H] ⁺ ion of on-membrane tryptic digestion products of bovine β-casein.....	85
Table 5.1: Peptide Standards and properties.....	164
Table 5.2: Absolute peak counts of peptides from extraction zones	176
Table 5.3: Peak counts for oxidized bombesin peaks in Standard Sample and Zone 4.....	178

List of Abbreviations

oa	orthogonal acceleration
BHT	Butylated HydroxyToluene
CAD	Collision Activated Dissociation
CE	Capillary Electrophoresis
CID	Collision Induced Dissociation
CDI	Collisional Damping Interface
CZE	Capillary Zone Electrophoresis
DHB	2,5 Dihydroxy Benzoic acid
DMSO	DiMethyl Sulfoxide
EOF	ElectroOsmotic Flow
ESI	Electrospray Ionization
FAB	Fast Atom Bombardment
FT-ICR	Fourier Transform Ion Cyclotron Resonance
HPLC	High Performance Liquid Chromatography
IR	Infra-Red
MALDI	Matrix-Assisted Laser Desorption/Ionization
MS	Mass Spectrometry
MS/MS	Tandem Mass Spectrometry
PSD	Post-Source Decay
QqTOF	Quadrupole-quadrupole Time of Flight mass spectrometer
RF	Radio Frequency
SDS	Sodium Dodecyl Sulfate

SELDI	Surface Enhanced Laser Desorption/Ionization
SEM	Scanning Electron Microscope
THF	TetraHydro Furan
TOF	Time of Flight mass spectrometer
UV	Ultra-Violet

1 INTRODUCTION

1.1 Mass Spectrometry

Since the sequencing of the human genome in the early part of the twenty-first century, many initiatives have formed to analyze the proteins encoded by the genes of an organism. The existence of intron genes makes the prediction of final amino acid sequences difficult, while the addition of post-translational modifications often governs the functionality of the protein. The significant differences between an encoded base pair sequence and the functional protein transcribed spurred the need to directly analyze the proteins present, forming the field of proteomics.

Mass spectrometry has found great use in the analysis of biological samples in fields such as proteomics largely due to the sensitivity of the method, the broad range of molecules to which it can be applied, and the standard behavior of such protein molecules which fragment to give sequence information. Two critical areas of interest in mass spectrometry are the ionization methods, and the methods of determining the charge-to-mass ratio (m/z) of the resulting ion.

In mass spectrometry, identification of an unknown molecule is often possible through measurement of its m/z (mass to charge) ratio. With sufficient accuracy on m/z , identification of an unknown is possible due to the limited number of possible candidates given the common structure of biological molecules such as proteins and glycans. The two most common methods for the ionization of biomolecules used are matrix-assisted laser desorption/ionization (MALDI) and electrospray ionization (ESI).

1.1.1 Matrix-Assisted Laser Desorption/Ionization

Sample materials which are subjected to heat or radiation can undergo numerous changes such as change of phase, decomposition of the material, and ionization. If the energy is applied over a sufficiently long period of time however, equilibration of the excess internal energy of analyte biomolecules to surrounding molecules results in little or no change to the analyte's molecular structure.

However, when a large amount of energy is delivered into a small enough area over a very short period of time, the excess energy cannot be dissipated rapidly enough, resulting in localized vaporization of the material (desorption), and possible excitation of the electrons, giving rise to decomposition and/or ionization.

Pulsed lasers are very suited to material desorption/ionization since they are able to focus the light into a small area, and they are sufficiently powerful while delivering the energy in a short period of time (ie. pulse). The capacity of the laser to desorb any material will depend on the wavelength of the laser, the power output from the laser, and the physical properties of the materials being analyzed.

When the material exhibits sufficiently strong absorption for light at the wavelength of the laser, the energy is efficiently transferred, facilitating vaporization and desorption of the material. However, if the material does not absorb at the appropriate wavelength, increased laser power will be required to desorb the material.

The addition of a light absorbing matrix to a sample was introduced in the late 1980s by Hillenkamp and Karas [1]. In MALDI, a sample of interest is co-crystallized with an acidic matrix material with energy absorbing characteristics similar to the

wavelength of emission of the laser. When the laser is fired upon the sample spot, the energy is efficiently absorbed by the crystalline matrix, with some of the energy also being passed on to the sample embedded with the matrix, resulting in the vaporization of both the matrix material and sample (Figure 1.1) [2,3]. Once in the gas phase, proton transfer from the matrix material to the analyte results in a positively charged ion, $[M+H]^+$. Possibly more than one proton is transferred, resulting in multiply charged ions, $[M+nH]^{n+}$. Similarly, it is possible for the analyte to lose a proton, resulting in $[M-H]^-$ species, as well as $[M-nH]^{n-}$.

The use of a matrix makes laser desorption/ionization a soft technique, in that the analyte is not fragmented readily by the laser pulse. A matrix is chosen for its high molar absorptivity at the laser's wavelength, miscibility with the analyte in the solid phase, good vacuum stability, and ability to transfer protons to the analyte in the gas phase. For these reasons, matrices tend to be acidic, low molecular weight aromatic solids. Commonly used matrices are 2,5 dihydroxybenzoic acid (DHB), sinapinic acid, and alpha-cyano 4-hydroxy cinnamic acid.

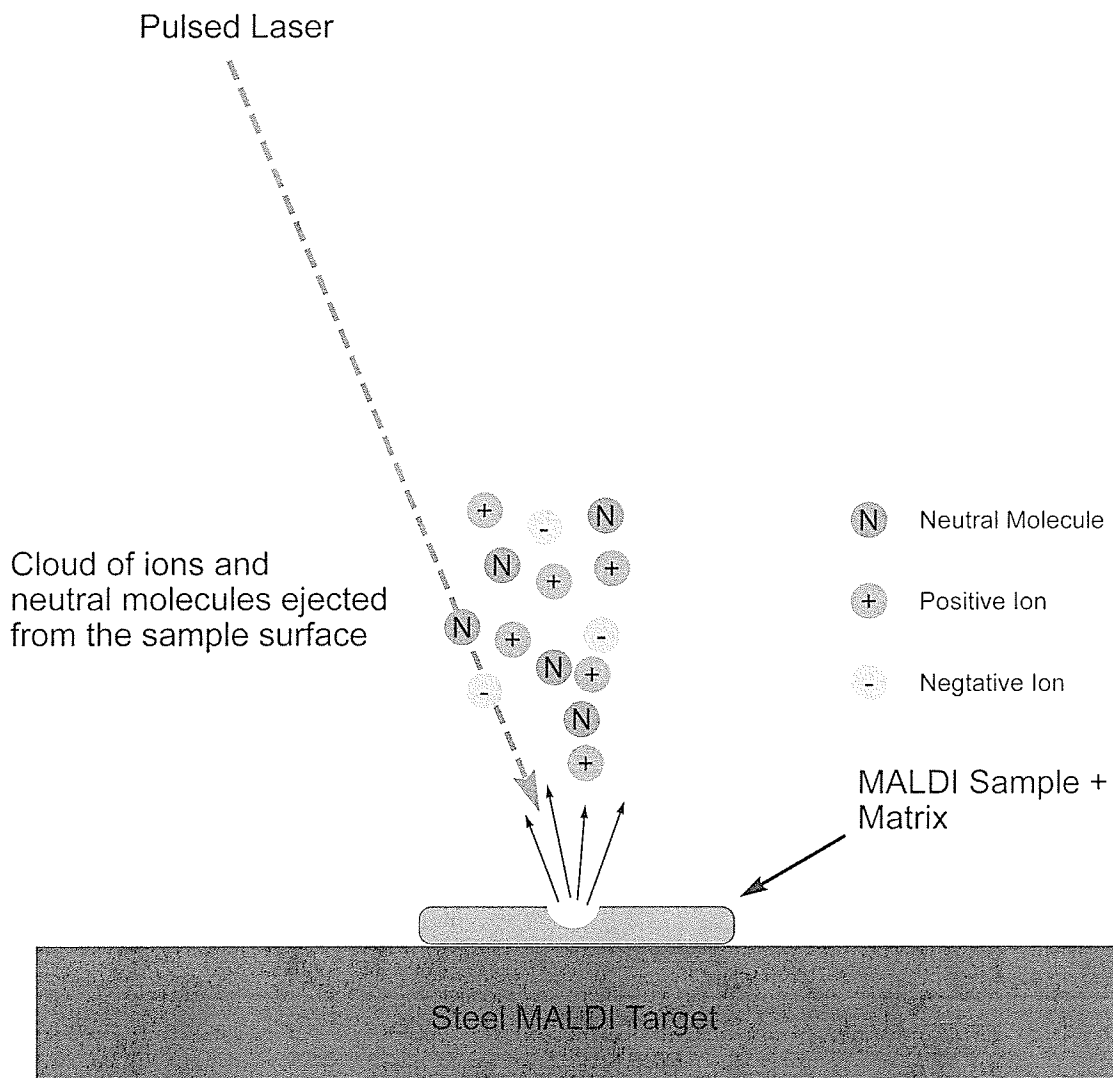


Figure 1.1: Illustration of MALDI ionization process

1.1.2 Electrospray Ionization

While the electrospray ionization (ESI) process was first observed by Dole [4] during the late 1960's, the ESI process used for modern mass spectrometric analysis was pioneered by Yamashita and Fenn in 1984 [5]. A liquid sample is moved by a carrier liquid and pumped through a narrow conductive capillary. When a potential is applied to the capillary, analyte molecules are drawn to the tip of the capillary based on their charge (Figure 1.2). As the charge accumulates at the tip, the increasing force destabilizes the surface tension. When the force exceeds the surface tension, 'budding' occurs at the tip. Small droplets pull free from the capillary and fly towards a skimmer cone held at the reverse potential. During flight, the droplets which contain the accumulated analyte from the capillary tip continue to evaporate. When the droplet size reduces sufficiently to concentrate the ionic charge further, the droplets undergo coulombic fission and further disintegrate into smaller droplets and continue the process until single analyte ions remain in the gas phase. The analyte ions are drawn into the skimmer cone and into the mass spectrometer. The resulting analyte ions may possess multiple charges, creating an envelope of m/z ratios [6].

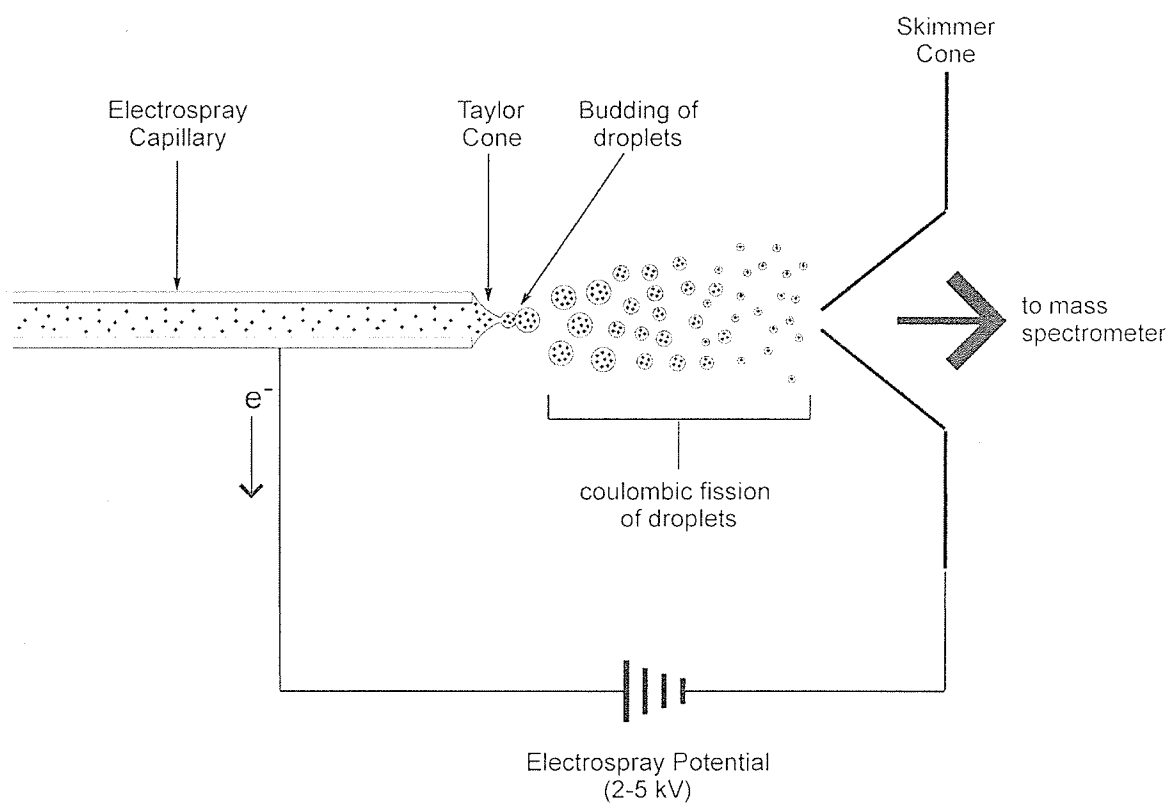


Figure 1.2: Illustration of electro spray ionization process

1.1.3 Quadrupole Mass Spectrometers [7]

Originally developed in 1953 by Paul and Steinwedel [8], the quadrupole mass spectrometer is one of the most commonly used mass analyzers today. Quadrupole mass analyzers consist of four parallel rods, equally spaced. Ions enter the quadrupoles along the central axis from one end. A fixed DC (U) voltage with a radio frequency (RF) field and amplitude potential ($V\cos \omega t$) is applied to the rods (Figure 1.3).

As ions enter the electric field established by the quadrupoles, they move in an oscillating motion as the RF field oscillates with time between both pairs of opposite rods. For a given m/z , there exist suitable values of U , V , and ω where the ion oscillates with a stable motion and passes through the quadrupole. All ions of other values of m/z will oscillate with increasing amplitude until they impact one of the quadrupoles and are grounded or neutralized. Operating in this method, quadrupoles act as m/z filters, and must scan through a m/z range to obtain spectra (Figure 1.4). Therefore quadrupole mass analyzers are more suitably coupled with continuous ionization sources such as ESI. Quadrupoles can also operate in RF (radio frequency only) mode, where they allow all ions through. By use of this mode, quadrupoles constrain ion motion and act as guides.

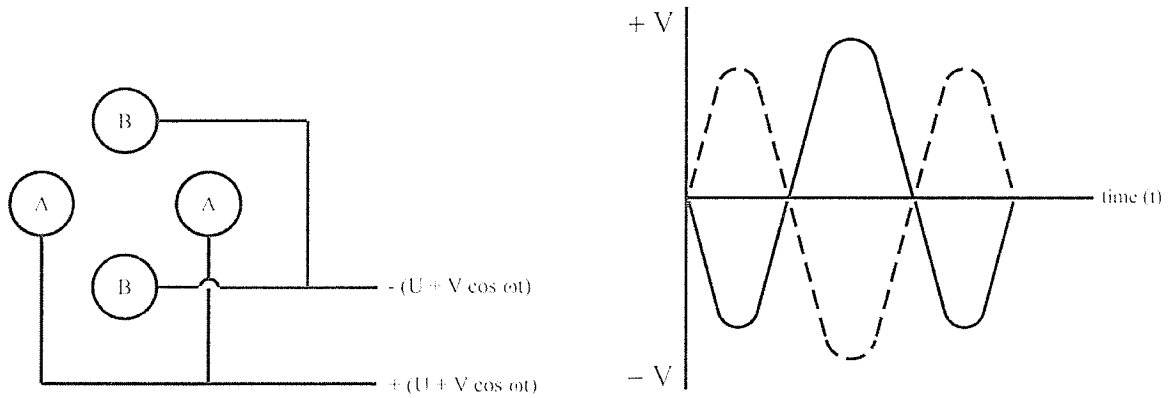


Figure 1.3: RF Field Applied to quadrupoles. Cross section of quadrupoles show opposing quadrupoles with same field potential while adjacent quadrupoles have opposing fields. Positive and negative fields inversely rise and fall with each other.

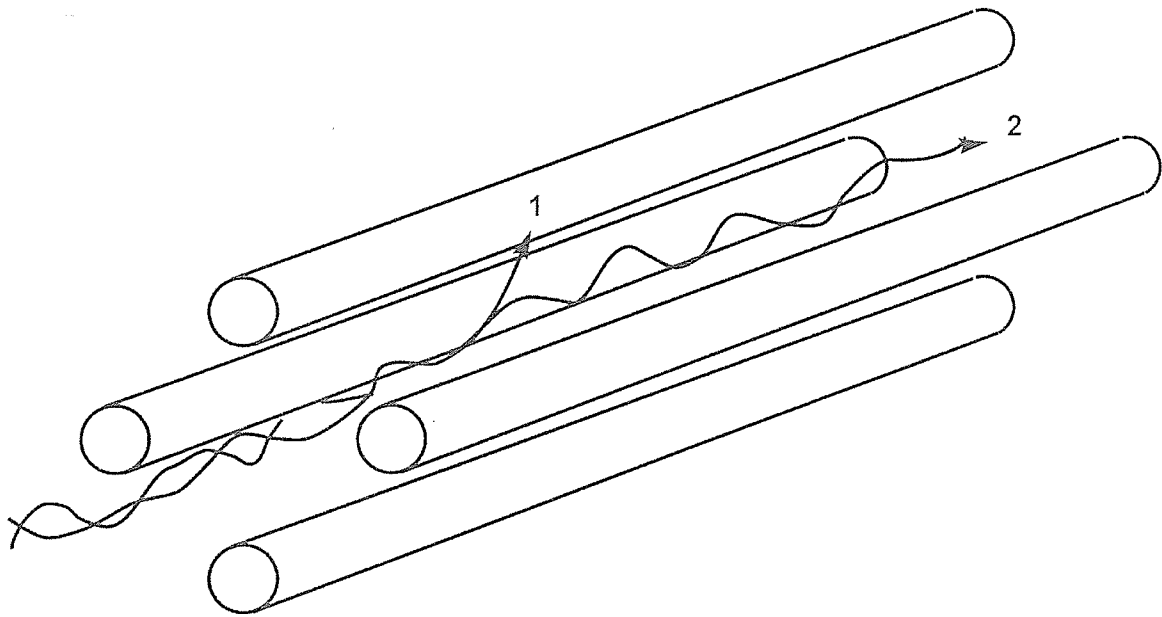


Figure 1.4: Motion of ions through a quadrupole showing (1) ions filtered and impacting one of the rods, and (2) ions passing through the quadrupole filter

1.1.4 Time-of-Flight Mass Spectrometers

Time-of-flight (TOF) mass spectrometers were first used to measure the m/z of a sample in the 1950s [9, 10]. Because of the pulsed nature of the TOF analyzer, it is ideally suited to be paired to the MALDI process. In the source, ions produced by MALDI are accelerated by a pulsed electric potential applied to the target plate and accelerating grids, giving approximately equal kinetic energy to all ions in the field:

$$\text{Kinetic Energy} = qV = \frac{1}{2} mv^2$$

q = charge of ion

V = voltage of the electric field

m = mass of the ion

v = velocity of the ion

Equation 1: Kinetic energy of a charged particle (q) accelerated by an electric field (V) of mass (m) and resultant velocity (v)

Under these conditions, ions with different masses will have different velocities. As the electric field accelerates the ions through a field free drift region, the faster ions (ie: lighter ions) move ahead of the slower ions and reach the detector first (Figure 1.5). Upon calibration of the system, it is possible to determine the m/z ratio of ions based on their time of flight. Pulsed firing of the laser is coordinated with the pulsed acceleration of the TOF source.

Several advantages are associated with the use TOF mass analyzers. The pulsed nature of the TOF system with parallel detection results in high sensitivity. Secondly, TOF analyzers have no upper limit to the mass range they can detect, which makes them highly desirable for use in biological applications (e.g. protein

analysis) which often have masses in the tens of thousands. Thirdly, TOF mass analyzers are robust, and relatively simple to construct, requiring no magnetic fields. The only requirement that is required is high vacuum (typically 10^{-7} Torr). Many other types of mass spectrometers operate in this vacuum range.

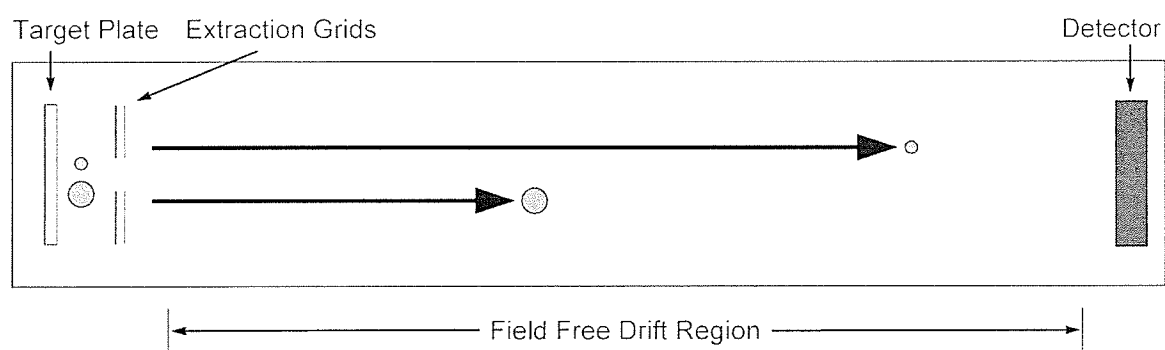


Figure 1.5: Linear TOF diagram, showing differing velocities for ions of different masses

Though the electric field used to accelerate ions from the source gives approximately equal kinetic energy to all ions at the source, ions formed by laser desorption still have a distribution of velocities despite having equal masses. The resulting differences in velocities gives rise to broadening of peaks and hence lower resolution.

To correct for this phenomenon, a reflecting mirror analyzer is used [11-13]. Composed of a series of concentric rings held at increasing voltages, the mirror turns around the trajectory of the ions from the source towards a detector. However, because the ion mirrors are set up in a voltage gradient, ions with greater momentum penetrate further into the field before being turned around. If set up correctly, ions with the same m/z but different velocities are time and space focused to arrive at the detector at the same time to first or second order, since the faster ions must travel a longer path to reach the detector (Figure 1.6). Though they correct for a large range of energy distributions, the ion mirrors do result in a lower ion transmission.

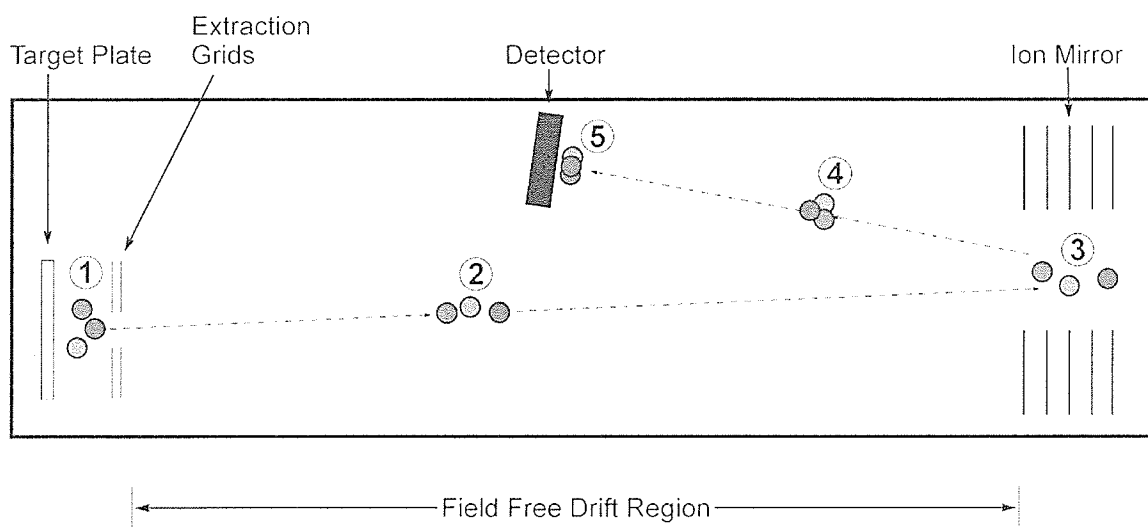


Figure 1.6: Ion mirror compensating for ions of equal mass but different velocities. Ions formed at the source (1) travel through the field free region, separating due to their different velocities (2). Faster ions penetrate further into the gradient field of the reflectron (3) before trajectories are reversed (4) and arrive simultaneously at a detector (5).

1.1.5 Post Source Decay

One important disadvantage of TOF analyzers is the limited ability to fragment molecules to further elucidate structure and identity. Prior to the advent of TOF-TOF mass spectrometers, TOF analyzers primarily employed post-source decay (PSD) [14-17] to fragment molecules and measure the m/z of the fragments. In PSD, a stronger than normal laser pulse is used to vaporize the sample and matrix. If sufficient energy is imparted into the system, the resulting energy causes the fragmentation of the molecule during its flight through the field free region. After entering the ion mirror region, the fragments are reflected to a detector where the individual fragment m/z ratios are determined by their TOF from the mirror.

The main drawbacks to the PSD method are twofold. First, the lack of a mirror to compensate for the kinetic energy distribution in the fragments results in low resolution spectra. The second drawback is the possible lack of fragmentation observed due to the nature of the sample. By this method, the fragmentation pattern induced by the laser energy is limited by the nature of the molecule itself. Hence the observed fragmentation pattern is largely beyond the control of the operator.

1.1.6 Collision Induced Dissociation

Tandem mass spectrometry (MS/MS) was pioneered by Beynon, Cooks, and coworkers [18] during instrument development, while collision activated dissociation (CAD) was pioneered by McLafferty [19] and Jennings [20] as a method to fragment molecules. More commonly now, the technique is referred to as collision induced dissociation (CID). In CID, molecules are collided with an inert collision gas causing the molecules to fragment.

As the velocity of ionized molecules (and hence the energy of collision) is adjustable by varying the accelerating potential, the user can adjust the degree of fragmentation to generate a variety of product ions related to the original molecule.

This ability to optimize the fragmentation conditions to suit the user's needs makes CID much more useful than PSD as a means of fragmenting molecules. However, because of the high vacuum constraints involved in TOF, most instruments cannot accommodate a collision gas being introduced between the source and detector.

With respect to MS/MS, there exist two distinct classes of mass spectrometers: instruments which can store ions, and instruments which must be connected in tandem to function. The former type can store and selectively eject ions. Within the storage chamber, a collision gas can be introduced to cause fragmentation.

Tandem instrument configurations cannot simultaneously analyze masses and provide the collision conditions for CID. Therefore, instruments are connected so that each section provides one of the required functions of mass selection, CID, and/or mass analysis (Figure 1.7) [21].

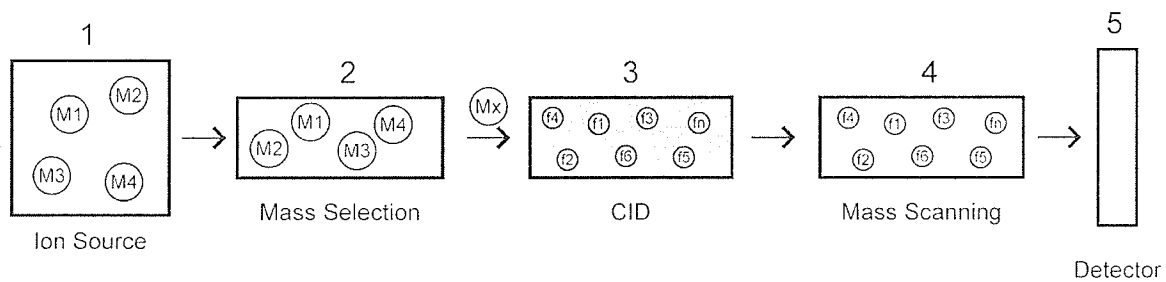


Figure 1.7: Collision induced dissociation process. Ions formed from an ion source (1) are mass selected to pass ion of a single m/z value (2) to the CID cell where the parent ions are fragmented by collision with an inert gas (3). The resulting fragments are then mass analyzed and detected (4 and 5).

1.1.7 Hybrid mass spectrometers

Hybrid mass spectrometer designs incorporate multiple mass analyzers. A common arrangement is the coupling of double quadrupole mass analyzer system with a single time of flight mass analyzer. The resulting instrument configuration, commonly referred to as a QqTOF arrangement, offers numerous advantages (Figure 1.8) [22-26].

In normal MS mode, the quadrupoles act as ion guides, passing all masses through to the TOF analyzer. However, the presence of two quadrupole sections allows MS/MS to be performed by collision induced dissociation, which TOF by itself does not easily allow for. The first quadrupole (Q) acts as a mass filter, allowing selection of the desired m/z value. The second quadrupole (q) acts as a collision cell, where an accelerating voltage causes the collision of the selected ions with an inert collision gas, rendering it into smaller ion fragments. Subsequent variation of the accelerating voltage affects the collision energy, and therefore affects the degree of fragmentation. Fragments of ions ejected from the collision cell enter the TOF chamber and are detected as described previously in Section 1.1.3.

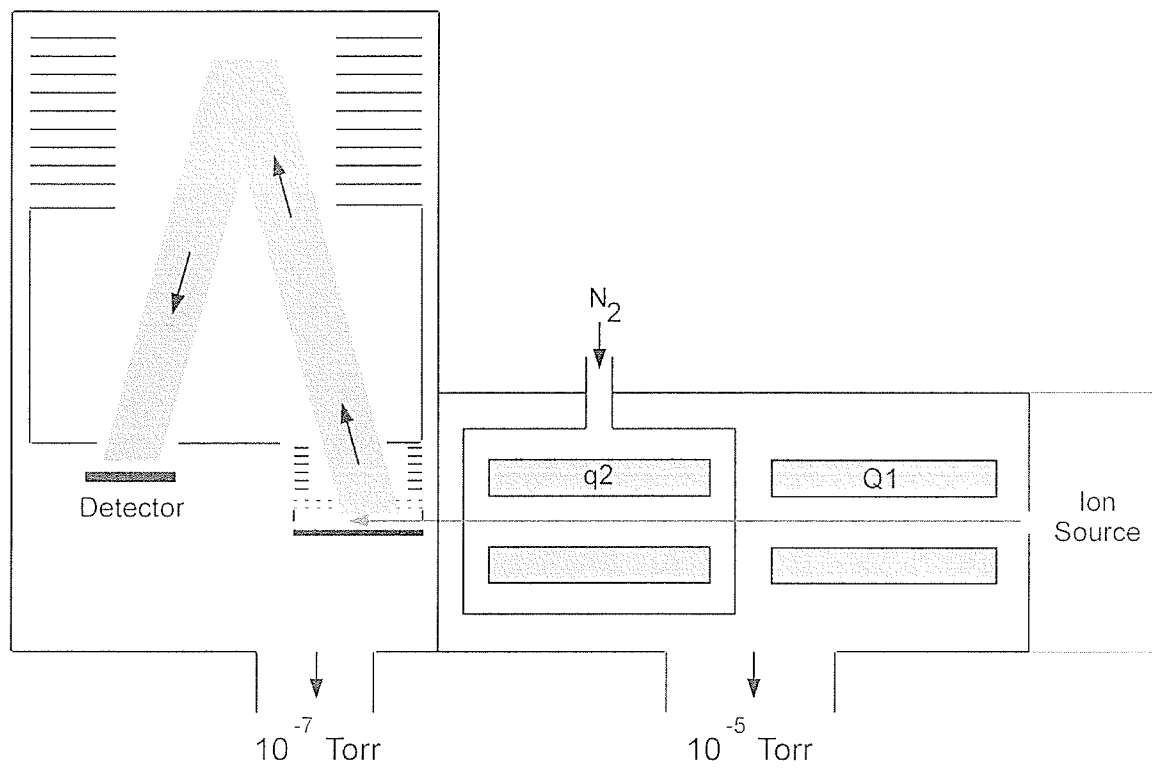


Figure 1.8: Schematic of an orthogonal acceleration QqTOF instrument.

Different mass analyzers have different ideal uses. But due to the mixed mass analyzer design, various ion sources can be used with QqTOF instruments. ESI sources are commonly used, but suffer from lower duty cycles, due to the continuous nature of the ion source coupled to the pulsed TOF analyzer .

One of the greatest benefits of the QqTOF arrangement is the orthogonal orientation of the source with respect to the TOF axis. In traditional axial linear TOF or reflecting TOF, variability in the ion velocity or spacing at the source causes loss of resolution which can be corrected for, to some degree by methods such as time lag focusing or by the use of an ion mirror as already discussed. However, in a QqTOF arrangement, the ions formed travel in a direction orthogonal to the TOF direction (decoupled from the source). Hence the final resolution of ions detected is largely insensitive to the conditions under which the ions are formed, but depends instead on the height of the ion beam entering the TOF analyzer.

Because of this, MALDI sources can be operated differently than those used in traditional instruments. Typically, laser fluence is held to threshold levels in MALDI-TOF instruments, as any energy beyond the minimum threshold will result in an exponential increase in the amount of material vapourized. The increased energy and number of collisions of ions within the larger ion plume formed result in a loss of resolution. In a QqTOF arrangement, however, the collisions and ions energies do not affect the final resolution. Any variations in ion velocity which occurs are negated due to the orthogonal motion of the ions to the direction of the TOF analyzer. Hence, MALDI sources can be run with higher than normal laser fluences, thereby increasing

sensitivity. Running the laser at high repetition rates also produces a quasi-continuous ion beam, approaching a constant ion source.

1.1.8 Collisional Damping Interface

One drawback to the use of a MALDI source on a QqTOF arrangement is the high initial velocity of ions formed in the ion plume. Typically on the order of several hundreds of meters per second, the velocity is too fast for efficient transmission through a quadrupole. To improve ion transmission, the ions must first be slowed. This is made possible by the use of a collisional damping interface (CDI) [27-29].

With a CDI, MALDI ions are formed at high pressures (10^{-2} Torr) in an inert atmosphere (Figure 1.9). While constrained by a quadrupole in RF mode, high velocity ions formed by MALDI collide with inert gas molecules, thereby reducing their velocity before being passed to the mass filtering quadrupole. Both MALDI and ESI sources have proven to be valuable tools for proteomics analysis [30-32].

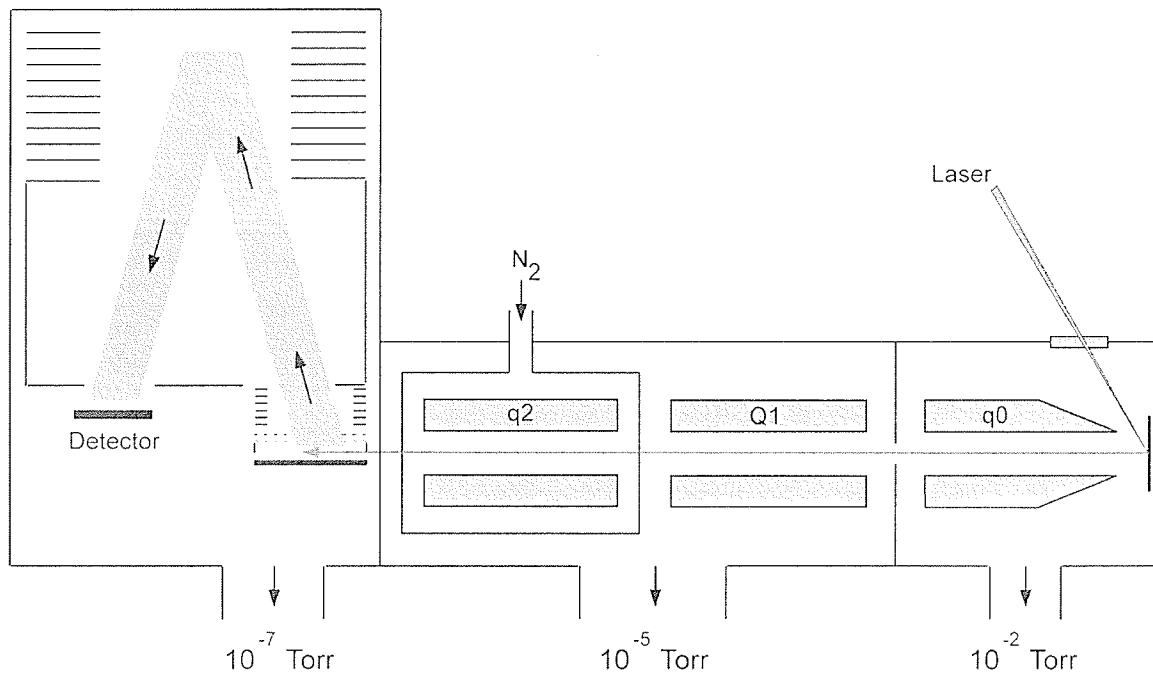


Figure 1.9: Schematic drawing of a MALDI-QqTOF, with a collisional damping interface (q_0)

1.2.0 Concluding Statement

Due to its high sensitivity and ability to conclusively identify analytes through structural information, mass spectrometry has proven to be useful in a large variety of applications. The high sensitivity of the method requires an increasingly pure sample however, as sample impurities can interfere with analysis. In these cases, sample workup, pre-concentration and purification is a requirement, but further handling of samples containing trace amounts of materials often reduces the sample integrity. The objective of this thesis is to evaluate novel methods of sample fractionation, as well as to assess existing methods combined with novel prototype instrumentation.

In my work, the results of a sheathless capillary electrophoresis system combined with a high resolution reflecting TOF analyzer are compared with a commercial HPLC-triple quadrupole instrument to evaluate their ability to detect the fragments of a tryptic digest of a phosphoprotein. A phosphoprotein was used as a standard test material since the peptides are often difficult to detect by mass spectrometry as phosphate moieties often exhibit reduced ionization efficiencies. In addition, the results of the digestion are compared with an on-membrane digestion method suitable for MALDI. As the digestion is performed on-target, sample handling is minimized giving better sensitivity.

In the second part of this thesis, I examine the fragmentation of a phosphopeptide in a MALDI-QqTOF instrument. Due to the unique collisional damping interface of this instrument, the MS spectra shows artifact peaks not present in the MS spectra of the same phosphopeptide from an axial TOF instrument.

The third chapter of the thesis qualitatively examines polyurethane films. From previous research, it has been shown the application of PU membranes has been useful as a sample support directly on a MALDI target. The advantage of the method is the affinity for proteins for the PU surface, allowing washing of salts from samples deposited on the surface. However, the PU membrane exhibits space charge effects due to the nonconductive nature of the material. The theory was that a sufficiently thin PU film would allow for sufficient charge dissipation while also being much simpler to apply to a steel MALDI target. Initial attempts to create a PU film also resulted in a porous surface which may trap analyte molecules, rendering them inaccessible for analysis. My research goal was to determine the cause of the pores, and create a thin non-porous PU film.

One of the largest limitations of MALDI is the fact the samples are crystallized into a solid matrix. In doing so, the sample cannot be further purified. Therefore, all sample purification is performed off-line before being deposited on the MALDI target surface, often from analytical purification methods such as HPLC or CE. My research examines the possibility of creating an electrophoresis based sample handling system integrated into a MALDI target, capable of rapid sample purification followed by direct MALDI-MS analysis.

1.2 References

- [1] Karas, M., Hillenkamp, F., *Anal. Chem.* **60**, 2299 (1988)
- [2] Hillenkamp, F., Karas, M., Beavis, R.C., Chait, B.T., *Anal. Chem.*, **63** (24), 1193A-1202A (1991)
- [3] Juhasz, P., Costell, C., Biemann, K., *J. American Soc. Mass Spectrom.*, **4**, 399-409 (1993)
- [4] Dole, M., Mack, L.L., Hines, R.L., *J. Chem. Phys.* **49**, 2240 (1968)
- [5] Yamashita, M., Fenn, J.B., *J. Phys. Chem.* **88**, 4451 (1984)
- [6] Gieniec, J., Mack, L., Nakamae, K., Gupta, C., Kumar, V., Dole, M., *Biomed. Mass Spectrom.* **11**, 259 (1984)
- [7] Ferguson, R.E., McKulloh, K.E., Rosenstock, H.m., *J. Chem. Phys.*, **42**, 100 (1965)
- [8] Paul, W., Steinwedel, H.S.Z., *Naturforsch.*, **8a**, 448 (1953)
- [9] Cameron, A.E., Eggers, Jr., D.F., *Rev. Sci. Instrum.*, **19**, 605 (1948)
- [10] Wiley, W.C., McLaren, J.B., *Rev. Sci. Instrum.* **26**, 1150 (1955)
- [11] Karataev, V.I., Mamyrin, B.A., Shmikk, D.V., *Soviet Physics-Technical Physics* **16**(7), 1177-9 (1972)
- [12] Mamyrin, B.A., Karataev, V.I., Shmikk, D.V., Zagulin, V.A., *Soviet Physics JETP*, **37**(1) 45-8 (1973)
- [13] Mamyrin, B.A., Shmikk, D.V., *Sov. Phys. JETP* **49**, 762, (1979)
- [14] Kaufmann, R., Spengler, B., Lützenkirchen, F., *Rapid Commun. Mass Spectrom.* **7**, 902 (1993)
- [15] Kaufmann, R., Kirsch, D., Spengler, B., *Int. J. Mass Spectrom. Ion Processes* **131**, 355 (1994)
- [16] Spengler, B., Kirsch, D., Kaufmann, R., *J. Phys. Chem.*, **96**, 9678 (1992)
- [17] Spengler, B., Kirsch, D., Kaufmann, R., Jaeger, E., *Rapid Commun. Mass Spectrom.* **6**, 105 (1992)

- [18] Cooks, R.G., Beynon, J.H., Caprioli, R.M., Lester, G.R., *Metastable Ions*, Elsevier, Amsterdam (1973)
- [19] McLafferty, F.W., Bente III, R.F., Kornfeld, R., Tsai, S.C., Howe, I., *J. Am. Chem Soc.* **95**, 2120 (1973)
- [20] Jennings, K.R., *Int. J. Mass Spectrom. Ion Phys.* **1**, 227 (1968)
- [21] Yost, R.A., Boyd, R.K., *Methods Enzymol.* **193**: 154, 1990
- [22] Morris, H.R., Paxton, T., Dell, A., Langhorne, J., Berg, M., Bordoli, R.S., Hoyes, J., Bateman, R.H., *Rapid Commun. Mass Spectrom.* **10**, 889 (1996)
- [23] Chernushevich, I.V., Ens, W., Standing, K.G., *Electrospray Ionization Mass Spectrometry Fundamentals, Instrumentation, & Applications*, Cole R. (editor) John Wiley & Sons: New York, 1997; Chapter 6, 203
- [24] Chernushevich, I.V., Ens, W., Standing, K.G., *Anal. Chem.* **71**, 452A (1999)
- [25] Guilhaus, M., Selby, D., Mlynski, V., *Mass Spectrom. Rev.* **19**, 65, (2000)
- [26] Krutchinsky, A.N., Chernushevich, I.V., Spicer, V.L., Ens, W., Standing, K.G., *J. Am. Soc. Mass Spectrom.* **9**, 569 (1998)
- [27] Krutchinsky, A.N., Loboda, A.V., Spicer, V.L., Dworschak, R., Ens, W., Standing, K.G., *Rapid Commun. Mass Spectrom.* **12**, 508 (1998)
- [28] Loboda, A.V., Krutchinsky, A.N., Bromirski, M., Ens, W., Standing, K.G., *Rapid Commun. Mass Spectrom.* **14**, 1047 (2000)
- [29] Chernushevich, I.V., Loboda, A.V., Thomson, B.A., *J. Mass Spectrom.* **36**, 849 (2001)
- [30] Shevchenko, A., Loboda, A., Shevchenko, A., Ens, W., Standing, K.G., *Anal. Chem.* **72**, 2132 (2000)
- [31] Kristensen, D.B., Imamura, K., Miyamoto, Y., Yoshizato, K., *Electrophoresis* **21**, 430 (2000)
- [32] Verhaert, P., Uttenweiler-Joseph, S., de Vries, M., Loboda, A., Ens, W., Standing, K.G., *Proteomics* **1**, 118 (2001)

2 Profiling of Polyurethane Film Structure by Scanning Electron Microscopy

2.1 Introduction

Mass spectrometry has seen great advances in the last decade. With increasing sensitivity, resolution, and mass accuracy, mass spectrometry has become an invaluable tool in the biological sciences. Biomolecules which once could not be accurately analyzed due to instrumental m/z constraints and ionization problems are routinely analyzed today.

Because of the theoretically unlimited mass range analyzable by TOF mass analyzers, they have become much more prominent in their application to large biomolecule analysis than in the past. Due to the pulsed nature of the TOF experiment, TOF mass analyzers are ideally suited to the pulsed nature of the MALDI process.

Constrained by the high vacuum requirements of TOF and the solid nature of the matrix sample, sample preparation methods for MALDI-TOF are limited in number. Sample purification and pre-concentration must be performed offline prior to the crystallization into the matrix. Comparatively, ESI-MS methods have the benefit of on-line sample preparation methods such as HPLC-MS which effectively removes interfering impurities such as salts and buffers, while fractionating sample components for detailed online ESI analysis.

While MALDI has been shown to have high tolerance towards impurities, due to the crystallization of the matrix drying process, the heterogeneity of the resulting sample-embedded matrix crystal cannot provide a completely pure sample without

using a sample pre-purification method. Results from a MALDI-TOF analyzer need to be assessed on a per-shot basis to determine if a particular spot on the sample crystal is sufficiently free of impurities. In addition, sample heterogeneity is a challenge, as analysis of a single laser spot will not necessarily be representative of the sample itself.

Research groups have developed on-target sample purification methods to remove buffers and salts from biological samples [1-8]. Previous research has shown that polyurethane (PU) has a preferential uptake of neutral species over a charged species [9-13]. Published results from our group have shown that polyurethane (PU) membranes are a suitable sample support for MALDI in the analysis of proteins [14]. The straight chain hydrocarbon segments in the polyether type PU [15] possess hydrophobic characteristics while the hard segments exhibit hydrogen bonding and affinity for proteins deposited on the PU surface [11,16] (Figure 2.1a). Adsorption of the protein to the surface of the membrane allows for subsequent washing steps to remove salts and buffers which have little to no affinity for the PU surface.

However, the use of the membrane is difficult and time consuming. The membrane must adhere to the surface of the MALDI target as smoothly as possible. Surface irregularities result in incorrect mass determinations, as ions formed from desorption at a higher point of a target arrive at the the detector sooner than ions of the same mass from a desorbed lower point (Figure 2.1b). Also, any substantial defects will limit the accessibility of the laser to the substrate. Handling of the 25 μm thick membrane is difficult, as wrinkles are inevitable. The adhesive used to fix the PU membrane onto the target also contributes as a possible source of contamination,

as solvents used in the adhesive may become trapped in the polymer and off gas under high vacuum.

(a)

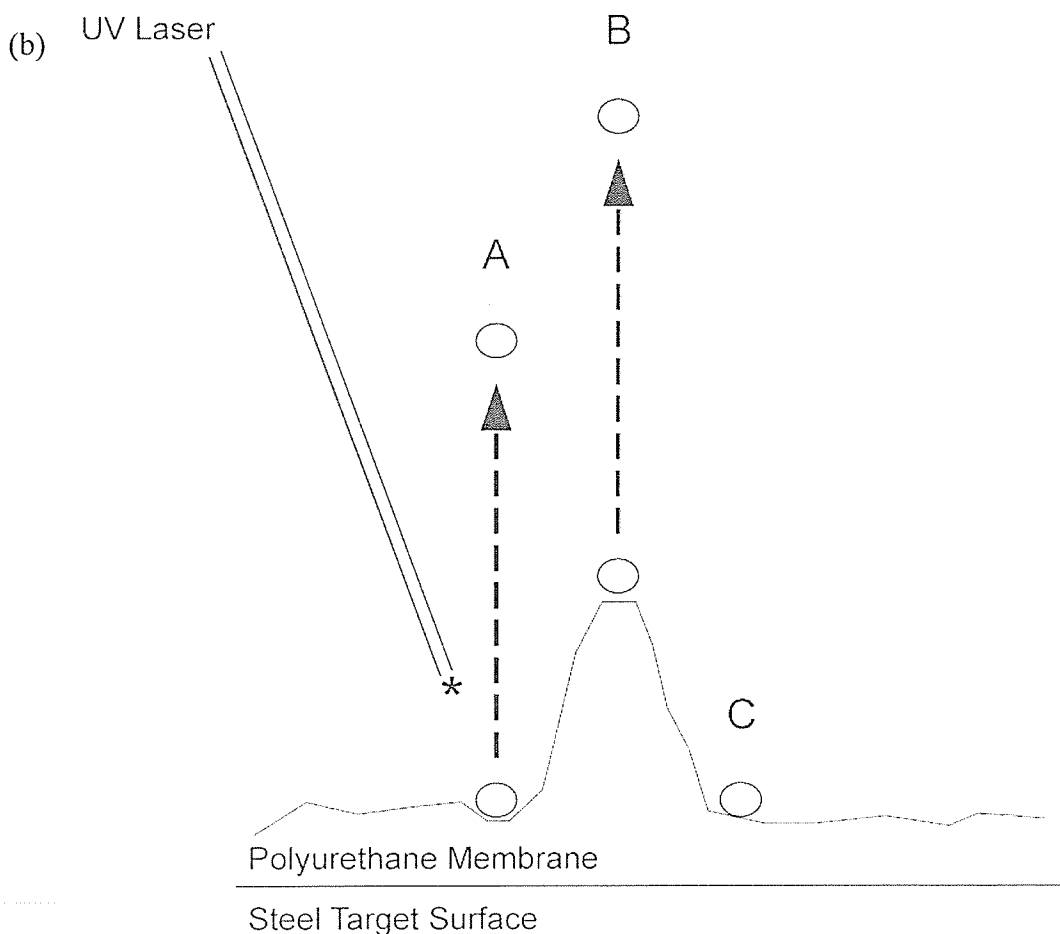
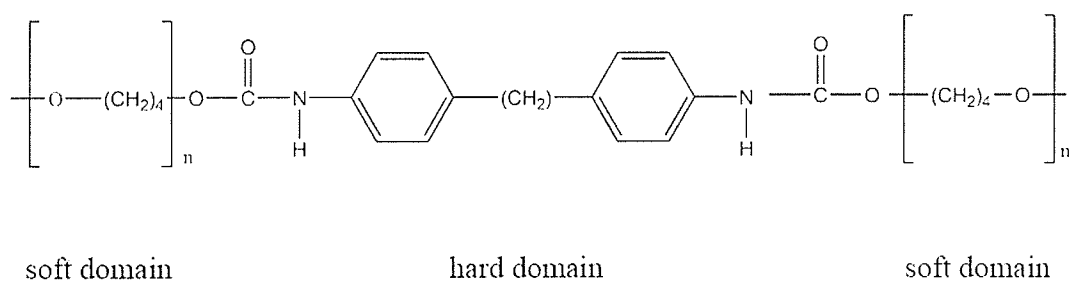


Figure 2.1: (a) Chemical structure of polyether type PU, and (b) Schematic drawing of an irregular polyurethane surface used as a MALDI target. (A) MALDI from a relatively flat position, (B) resulting MALDI from a raised position (C) Sample inaccessible to MALDI laser

The most serious issue arising from using PU membrane as a sample support is the non-conductive nature of the polymer. Normally, ions formed by the MALDI process consist of a cloud of positive and negative ions, as well as neutral molecules in the gas phase. When operating in positive mode, the negative ions are drawn towards the positive potential, and are electrically neutralized on contact. When the extraction pulse is applied, the remaining positive ions are accelerated towards the detector.

When using a PU sample support, the negative ions are prevented from electrically neutralizing immediately on the steel surface due to the non-conductive nature of the PU membrane. Despite being only 25 μm thick, the membrane is sufficiently insulating to partly prevent electrical neutralization. As a result, a cloud of negative ions builds on the surface of the target, creating an electrostatic-charging effect [17]. As the negatively charge accumulates with each laser pulse and extraction pulse, the negative ions exerts an increasing pull towards the positive ions thereby retarding their velocity towards the detector. Consequently, the apparent m/z values of the ions gradually shift towards higher masses during data acquisition, resulting in loss of resolution and mass accuracy.

The use of a PU film (instead of a membrane) was proposed to resolve these technical issues. If the PU film could be applied to the surface of the steel target in a liquid form, the technical hurdles of wrinkles in the PU membrane and use of the adhesive could be eliminated. Secondly, a sufficiently thin PU film could reduce the electrostatic charging effect. With a sufficiently thin layer of PU, the insulating

effects could be reduced to eliminate or decrease the build up of ions on the target surface.

Previously, our research group had successfully created a PU film which demonstrated the same affinity properties as the PU membrane. However, the film topography contained some features which were not conducive to the analysis of biological samples. The film thickness was still substantial, giving rise to the same electrostatic-charging effect seen with the PU membrane. Secondly, the film topography showed numerous pores throughout the surface of the membrane, ranging from 2 to 20 μm in diameter [18]. Concerns existed regarding analyte samples infiltrating themselves into the pores and becoming inaccessible to the washing procedure, or inaccessible to the matrix added, and thus being inaccessible to the laser [19].

Our primary goal is to produce a PU film without pores, suitable as a physical support for MALDI. The removal of pores would eliminate any sample loss inside the pores during the sample purification stages. Ideally, this film would be sufficiently thin to exhibit no charging effects resulting from insulating effects of the PU film. The secondary goal is to identify the parameters which cause the formation pores in the PU film, and determine if any other physical features may be developed by dissolution of the PU membrane and drying of the deposited solution.

2.1.1 Scanning Electron Microscopy

Scanning electron microscopes have been used in research for many decades. They provide information about samples such as surface topography and limited elemental composition. From their initial development starting in the 1930's, they have become widely used in scientific research, giving scientists images far beyond the limitations of the light microscope.

Scanning electron microscopes function by focusing an electron beam from an electron gun via a series of lenses and condensers onto a sample surface. Incidence of an electron beam onto a sample surface gives rise to a number of effects such as x-ray fluorescence, heat, light, backscattered electrons, and secondary electrons.

Secondary electrons ejected from the sample surface are used to map the surface topography of a sample. As the incident beam strikes the surface of the sample and penetrates inwards, the electrons scatter within an area called the interaction volume (Figure 2.2). Secondary electrons ejected from the sample surface are drawn towards a positively charged Faraday cup built around the detector. The captured electrons are used to build the resulting image. Any secondary electrons produced deeper within the interaction volume do not have sufficient energy to escape and are therefore not detected. Backscattered electrons from deeper within the interaction volume do escape the sample surface, but are mostly too high in energy to be captured by the Faraday cup.

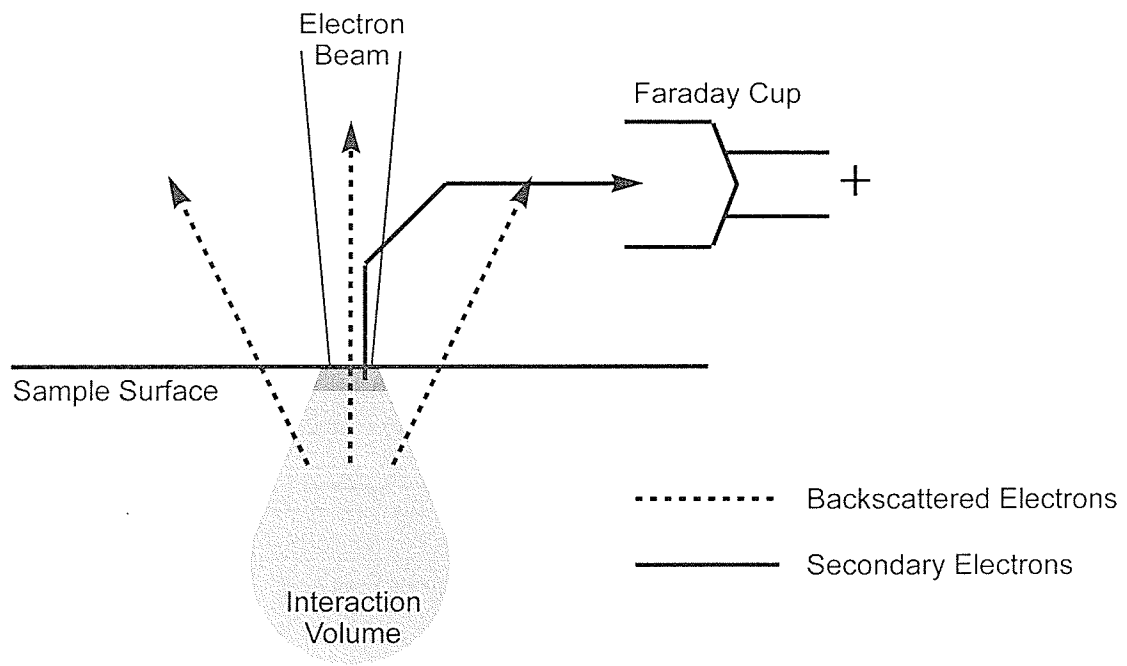


Figure 2.2: Interaction volume of a SEM electron beam on a sample surface

For any particular spot scanned by the SEM, the spot brightness is dependent on the current of electrons from the electron gun, and/or the topography of the sample. If the electron beam interacts at a point where the surface topography is raised, more edge effects are seen and the sample spot is seen as being brighter, since more secondary electrons are captured by the faraday cup. This phenomenon is commonly called the 'edge effect', as edges are seen as being brighter, providing image contrast (Figure 2.3). Conversely, secondary electrons from valley areas of the sample surface are not efficiently captured by the Faraday cup, and are thus seen as being dark due to fewer secondary electrons being emitted.

As the scan coil rapidly rasters the surface of the target, the secondary electrons for each point are captured, measured, and used to produce a black and white image point by point (Figure 2.4).

All samples analyzed by SEM must be able to dissipate accumulated charges from the resulting electron bombardment. As PU membranes are not conductive, they must be sputter coated with a metal layer to make them conductive. The coating is sufficiently thin as to not alter the topography of the sample, but substantial enough to conduct an electric charge. The coating must also be inert, so as not to cause any chemical degradation of the sample. Typically, a gold-palladium alloy is sputter coated onto the target under high vacuum, giving a coating several angstroms thick, which is beyond the resolution of the instrument. Gold-palladium alloys also produce high yields of secondary electrons, giving a better dynamic range for the image produced.

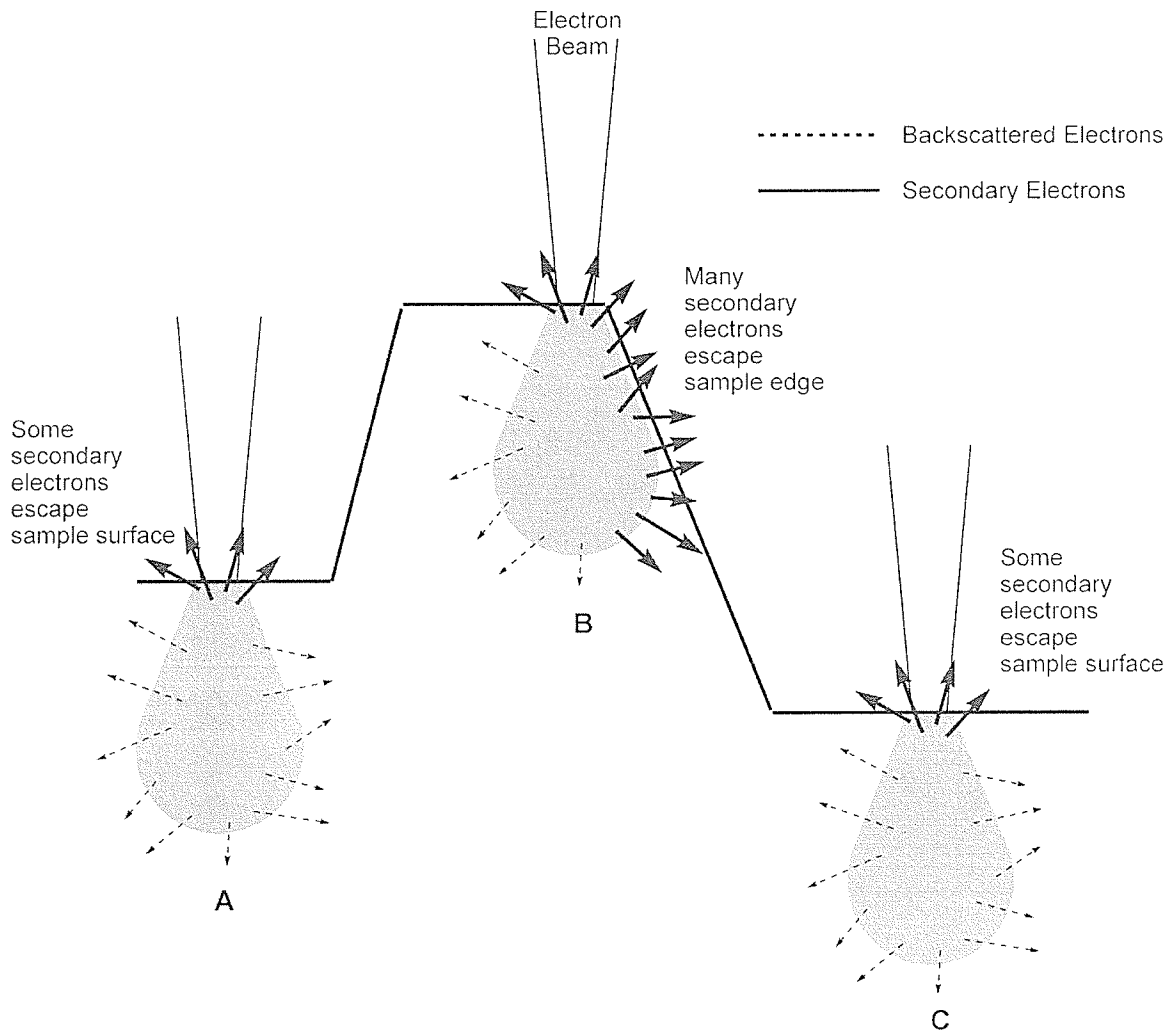


Figure 2.3: Interaction volume of SEM electron beam at various features topographical points of the sample surface. (A) Interaction volume and secondary electrons from a normal sample surface, (B) Interaction volume from sample edge showing many secondary electrons detected, (C) Interaction volume from a valley in the sample surface, with few detectable secondary electrons available for capture.

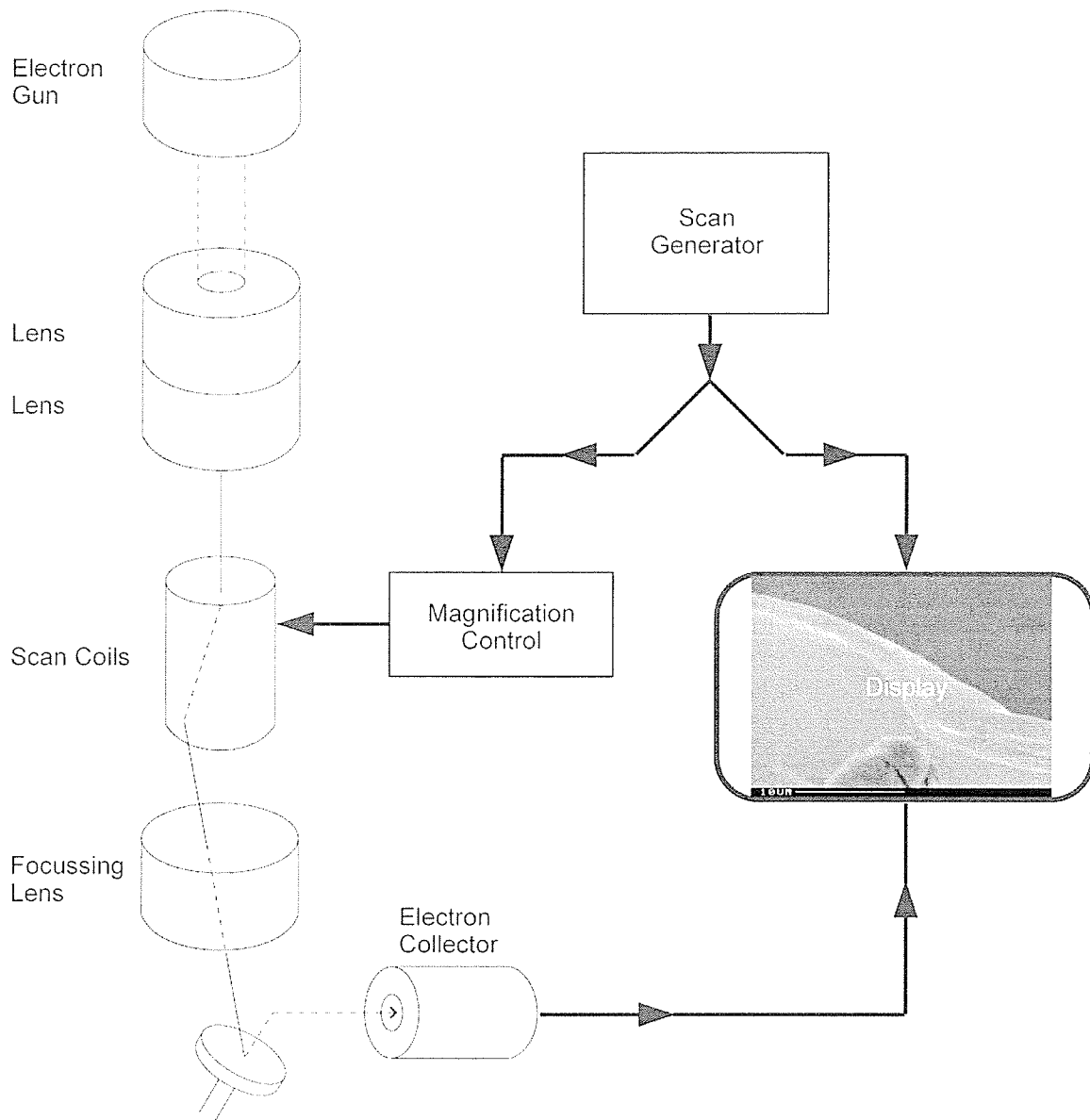


Figure 2.4: Schematic drawing of SEM microscope

2.2 Experimental

2.2.1 Materials and Method

Approximately 100 cm² of 25 µm thick polyether type polyurethane (JPS Elastomerics, XPR625-FS) were dissolved in 8 ml of tetrahydrofuran (Sigma Aldrich) from both a commercial bottle and a benzophenone distillation. Benzophenone distillation of THF was performed to remove trace amounts of water as well as butylated hydroxyl toluene (BHT, 0.025%) that manufacturers add, to prevent peroxide formation in ethers.

The PU solution was centrifuged at 5000 RPM for 15 minutes. The supernatant was separated from precipitates and sealed in a tube until ready to use. Sample PU films were formed by applying a 20 µL droplet onto a stainless steel disk (1 cm diameter, 10 µm thickness) to simulate a MALDI target and allowing to air dry. The resulting film spot measured approximately 5-6 mm in diameter.

To further observe changes in PU morphology with different solvent mixtures, solutions comprising of PU solution (90% v/v, prepared with distilled THF) and a significant amount of a second solvent (10% v/v) to exacerbate any changes to the topography of the PU film. Solvents were chosen to represent a range of boiling points, density, viscosity, and polarity, as listed in Table 2.1.

Testing of electrostatic charging of PU films were acquired on an in-house built linear TOF system, Manitoba TOF-II (Dept. of Physics, University of Manitoba) [20].

Table 2.1: Solvents and physical data

Solvent	Boiling Point (°C) @ 1 atm	Polarity (dielectric constant)	Density (g/ml)
Tetrahydrofuran	65-67	7.5	0.866
Water	100	80	1.000
Methanol	65	33	0.791
Ethanol	78	24	0.789
1-Propanol	81-83	20	0.803
1-Butanol	117.7	18	0.810
Dichloromethane	40	9.1	1.326
Trichloromethane	61	4.8	1.498
Tetrachloromethane	75	2.2	1.584
Ethyl Acetate	76.5-77.5	6.0	0.894
Acetonitrile	81-82	37	0.786
Acetone	56	21	0.786
Hexanes	68-70		
Toluene	111	2.4	0.867
Dimethyl Sulfoxide	189	47	1.092

PU solvent spiked films were prepared by applying a 20 uL droplet to a stainless steel disk and allowing to air dry.

Spin coating of targets was performed using a tabletop centrifuge (Waco Separator, Wilkins Anderson, Chicago Ill) fitted with a Delrin stage aligned to the central axis of rotation. While spinning, a 100 uL aliquot of PU solution was applied to the center of the steel disk, and allowed to air dry while spinning. The effect of varying speeds of rotation on the polymer topography was examined. Actual rotation speeds are not available, as the centrifuge was only designed with an on/off switch.

Speed of rotation was controlled using a variable autotransformer. Films were cut with a razor after drying, to give a clear view of the cross section and resulting film thickness.

2.3 Results and Discussion

2.3.1 THF vs. distilled THF as solvent for PU.

The choice of THF as the casting solvent was necessary as PU would not dissolve in other common solvents. Previous results showed that small surface pores were created in the polymer surface. Increasing the concentration of PU in THF to 12 cm²/ml showed large improvements, resulting in the formation of undesirable small bubbles trapped in the film. These defects ranged in size from 3 to 20 μm, and were found in a localized area in the film (Figure 2.5a and 2.5b).

In comparison, an equivalent concentration of PU prepared in THF distilled from benzophenone showed no bubbles or pores in the surface. The resulting film appeared very uniform and featureless to the SEM (Figure 2.6). The use of purified THF appears to be an important element in producing a non-porous PU film. The reported water content by the manufacturer of 0.05 % v/v and/or the BHT peroxide stabilizer (0.025% v/v) was enough to cause visible artifacts in the polymer topography. It should also be noted that the proportion of water may not be accurate as the bottle would absorb atmospheric water once opened. As atmospheric water must have been present during the drying stage of the film, the system is shown to be tolerant of only trace levels of impurities.

A water spiked sample of THF was prepared to simulate an exaggerated high water content in this solvent. The resulting polymer film showed very irregular surface characteristics, that were apparent without the aid of a SEM (Figure 2.7a-d). The details of the surface showed large peaks, holes, pores, and bubbles. A large, coarse peak structure (~ 500 μm long) was found between the center and edge with

indentations all over it. The center of the film showed a region characterized by small bubbles only a single micron in diameter, some surface pores of similar size, as well as some large but shallow surface pores measuring 5-50 μm in length. A small separate region of the film was populated with small, circular pores measuring 5-25 μm in diameter. The distinct regions were likely formed as a result of the strong hydrogen bonding of water, allowing it to pool into distinct regions as the THF evaporated.

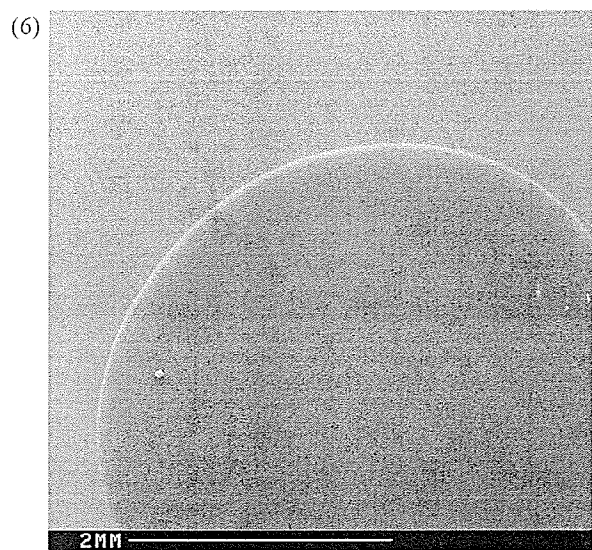
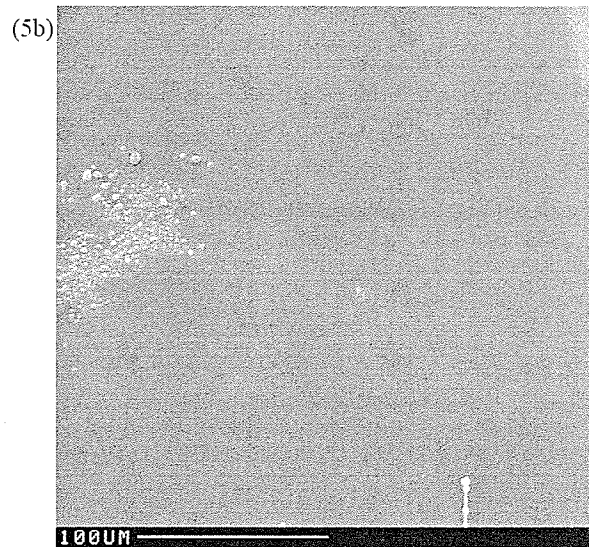
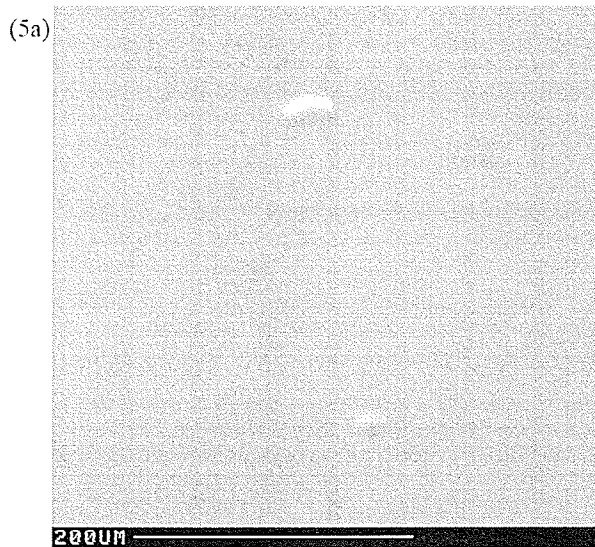


Figure 2.5: SEM of PU film cast with (a) bottled THF, showing (b) region of bubbles in film surface

Figure 2.6: SEM of PU film cast with distilled THF

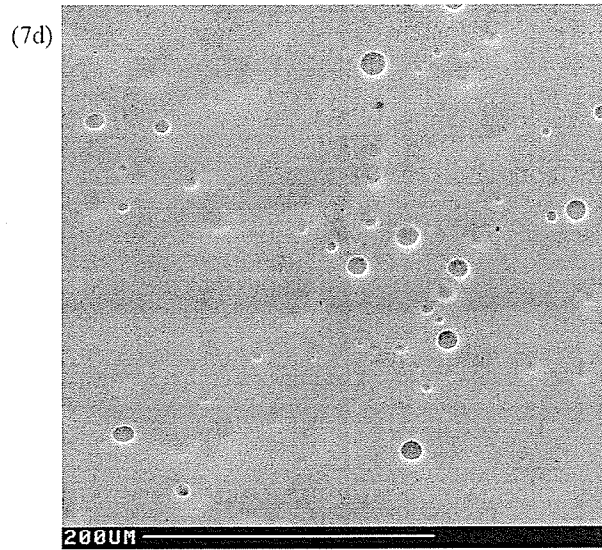
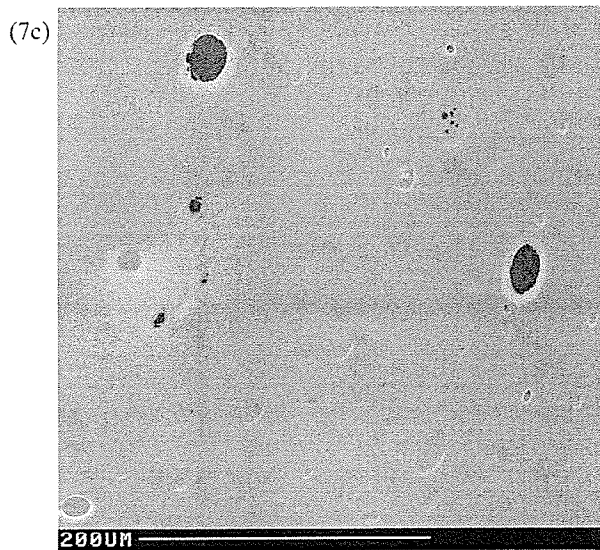
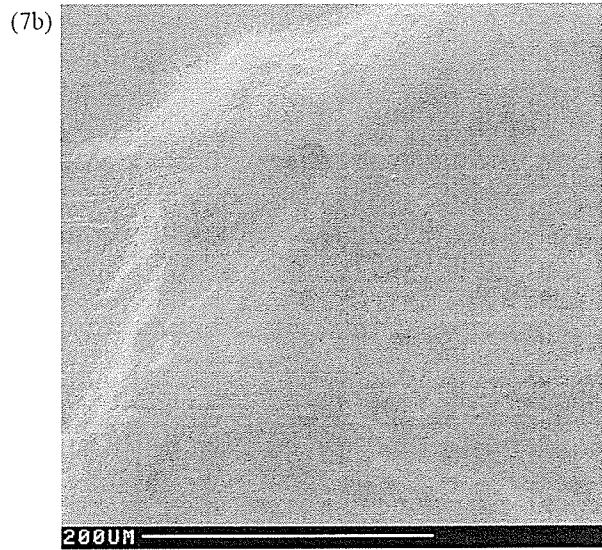
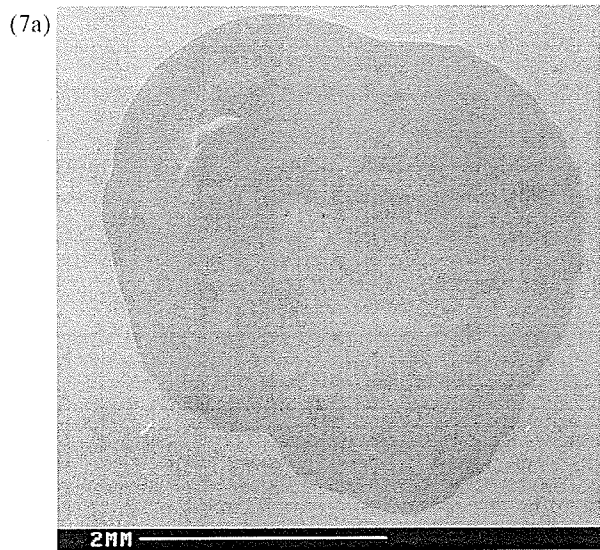


Figure 2.7: SEM of PU films cast from 10% water showing (a) irregularity of surface, (b) details of the rough textured hill, (c) deep pores in the surface, and (d) shallow pores in the surface

2.3.2 Alcohols and Chloromethanes

A series of alcohols were added to the PU film solutions to determine what effect the different solvents would have on the resulting topography. Increasing the length of the impurity solvent's carbon chain results in changes to the physical properties, such as increased boiling point, decreased polarity. However, the density remains quite consistent.

A 10% methanol PU solution showed a mostly flat topography with few defects. The edge of the film appeared jagged with only one small hole found nearby (Figure 2.8a). This hole appeared asymmetric (10 μm in length), and was positioned extremely close to the edge. As it was the only one of its kind found and at the periphery of the film, it would not likely interfere with analyses. No bubbles were observed, but an irregularly shaped bulge of considerable size ($\sim 30 \mu\text{m}$ in length) was found on its surface (Figure 2.8b).

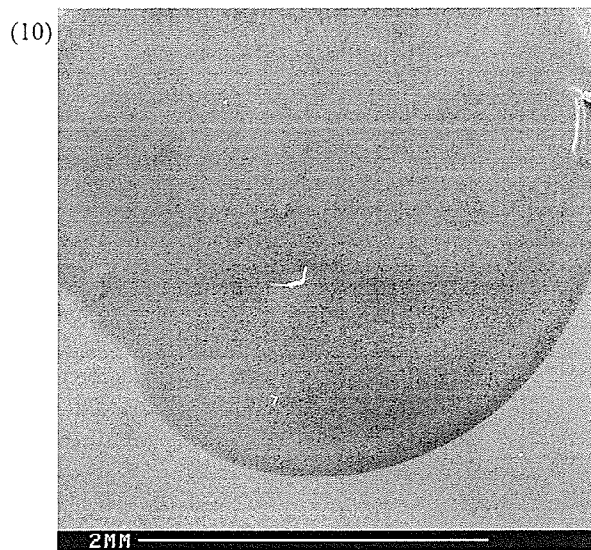
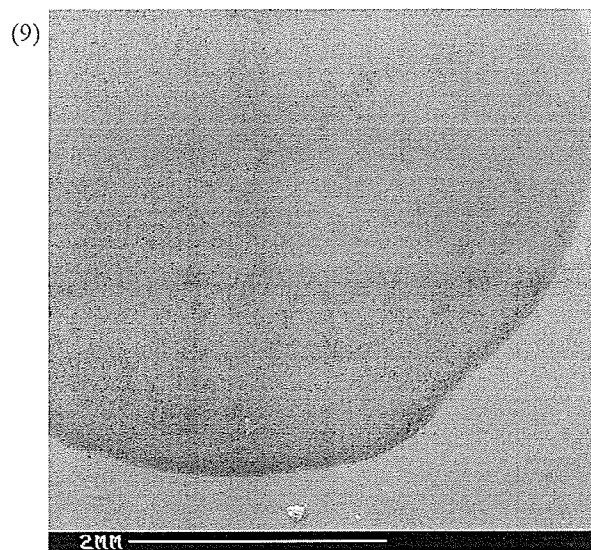
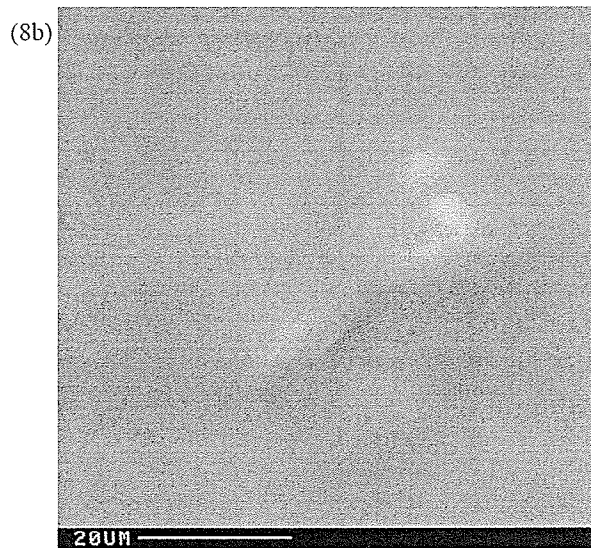
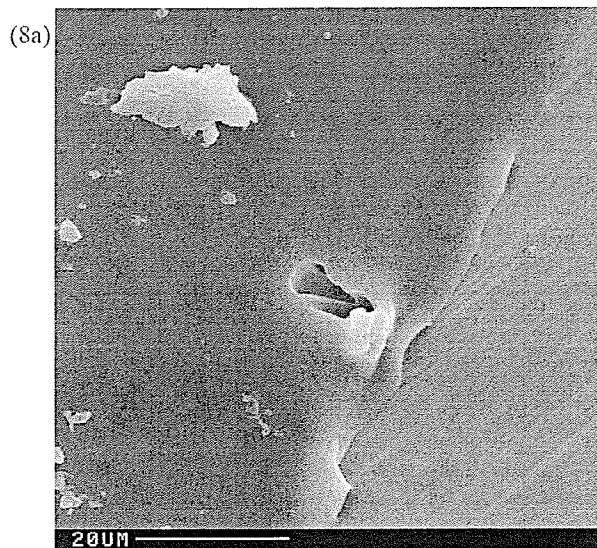


Figure 2.8: SEM of PU film cast with 10% methanol showing (a) hole in PU film at the periphery, and (b) bulge in the surface

Figure 2.9: SEM of PU film cast with 10% ethanol showing formation of a slight peripheral ring

Figure 2.10: SEM of PU film cast with 10% ethanol showing formation of a peripheral ring more defined than with ethanol

The 10% ethanol and 1-propanol PU solutions gave very similar results. The films are reasonably smooth and featureless with none of the irregularities seen in the methanol spiked solvent. Small, gradual slopes in the film are seen on the surface but no sharp changes in contour are seen. The edges of both solutions show one common feature: a ring around the entire film droplet similar to a “pie” crust is present, slightly thicker than the film in the center (Figure 2.9 and 2.10). As this change in the topography is at the center of the film, it would be acceptable for practical use and possibly desirable if one needed to constrain a droplet of solution. The thickness of the ring formed by 1-propanol is thicker and more obvious than that formed by ethanol.

For the 10% 1-butanol solution, the peripheral ring is very pronounced (Figure 11a). Radial lines from the ring can be seen aligned with the approximate center of the droplet (Figure 2.11b). In comparison to the droplet from the distilled THF, the surface is not flat, comprising of gently contoured hills and valleys which appear closer to the edge. However, the center region of the film still appears flat.

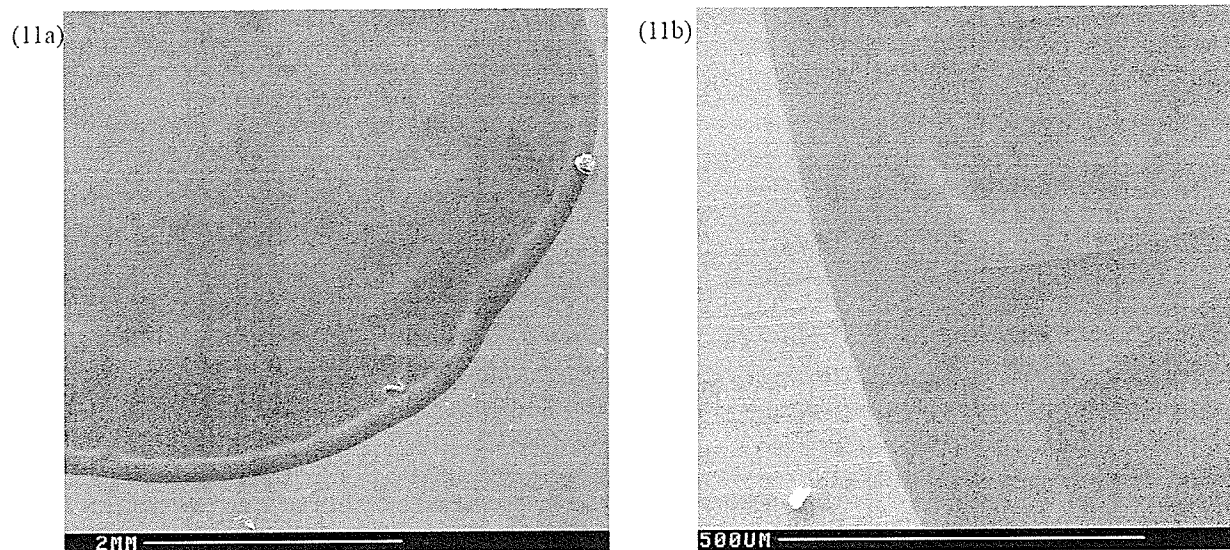


Figure 2.11: SEM of PU film cast with 10% 1-butanol showing (a) ring structure at the periphery (b) radial lines from the ring

The films from various chloromethane spiked PU solutions gave topographies much more consistent in appearance. The dichloromethane spiked solution gave a very flat surface with no surface defects, with only one small defect at the edge (Figure 2.12a and 2.12b). The trichloromethane spiked solution gave a similar flat topography but with a single large defect on the surface (~175 μm in diameter) resembling a crater (Figure 2.13a and 2.13b).

The PU film formed by the carbon tetrachloride spiked PU solution appeared very smooth at low magnification, showing no obvious features such as the previously observed rings, craters or holes (Figure 2.14a). However, one small anomaly was found. Very near the center, there appeared to be a small spot (100 μm in diameter) of a different shade of grey (as it appears in the SEM) than the rest of the PU film (Figure 2.14b). On closer examination, we see there is a distinct circular region which appears lighter in shade. At higher magnifications, we can see a single, small raised bubble in the center of the anomaly. Seen slightly further from the anomaly are small ripples in the film, indicating that it is not entirely flat.

Both alcohol and chloromethane series tested gave PU films which were reasonably free of defects. Though we cannot specifically attribute any features found in the PU films to the physical properties of the solvent spiked into the solution, some generalizations can be made.

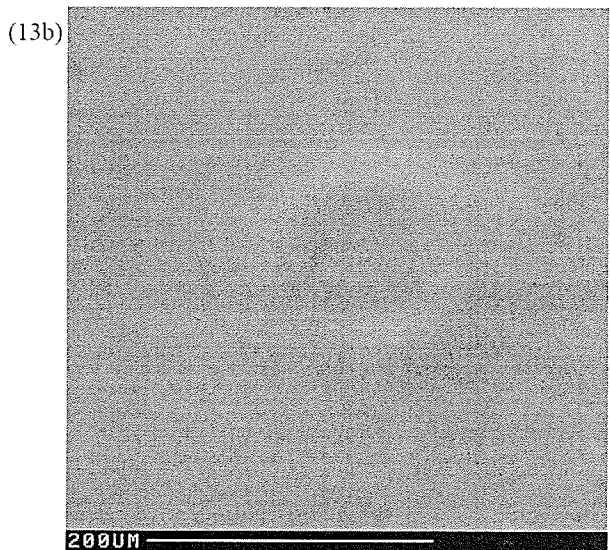
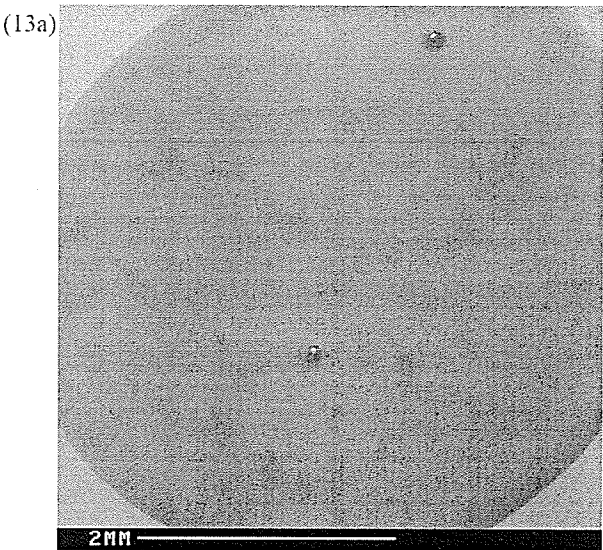
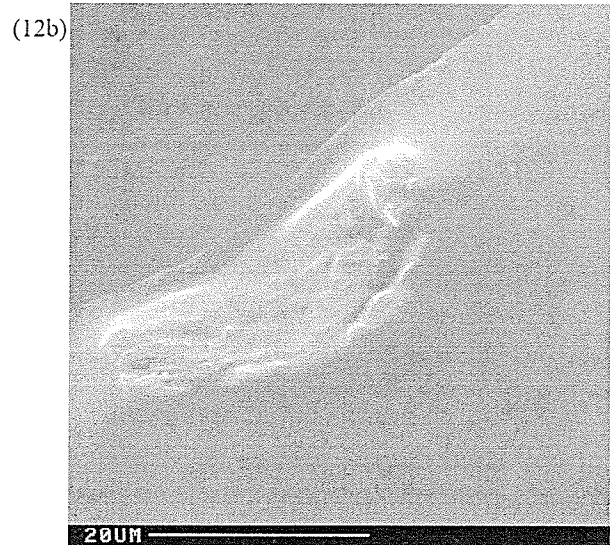
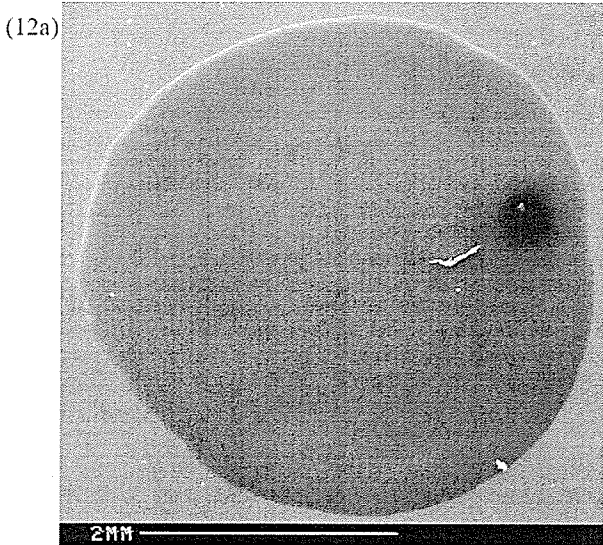


Figure 2.12: SEM of PU film cast from 10% dichloromethane showing (a) smooth surface, and (b) edge defect

Figure 2.13: SEM of PU film cast from 10% trichloromethane showing (a) smooth surface, and (b) surface crater defect

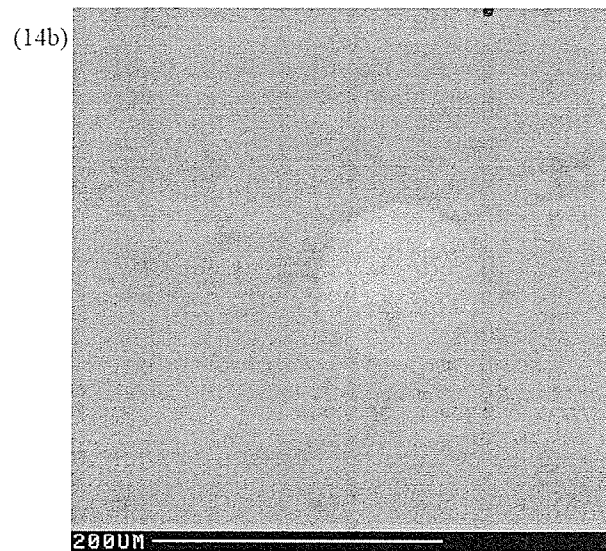
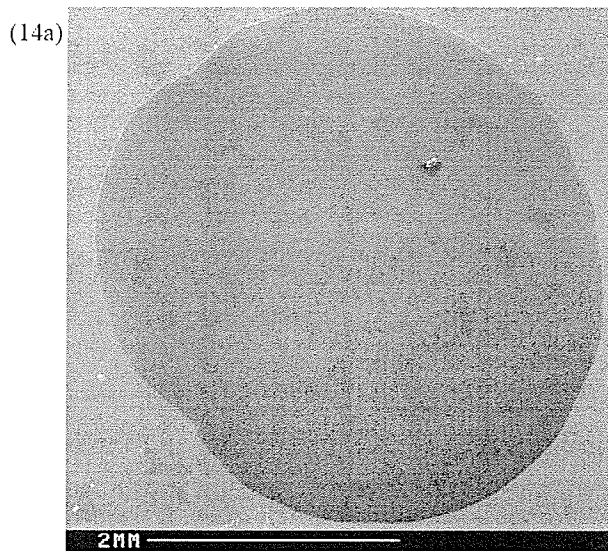


Figure 2.14: SEM of PU film cast from 10% tetrachloromethane showing (a) featureless surface, and (b) compositional defect

As the lowest boiling point solvent tested, methanol caused no major anomalies in the surface topography when added to the PU solution. With ethanol, 1-propanol, and 1-butanol, the increasing boiling point and relatively high polarity of the alcohols seem to give rise to the ring structure seen, as this feature becomes much more pronounced with the lengthening carbon chain of the solvent.

Chloromethane solutions which are more similar to THF in polarity than the alcohols tested seem to result in fairly uniform films. With increasing boiling point, there seems to be some correlation with the formation of surface defects. However, the nature of the anomaly seems to be dependent on the polarity of the spiked solvent, as boiling points similar to those of the alcohols tested give different anomalies (ring structure of alcohols compared to the flat topography of similar chloromethanes). As boiling points of the spiked solvent exceed the boiling point of THF, surface anomalies begin to form, as they did with the alcohols.

2.3.3 Other solvents

Polymer films cast with solvents with volatile solvents similar in boiling point and polarity to THF, such as ethyl acetate and hexanes give smooth films (not shown).

2.3.4 Dissimilar Solvents to THF

An acetone spiked solution gave a film with no raised features but rather small linear indentations or tears in the surface near the edge (Figures 2.15a and 2.15b). The indentations ranged in size from several microns to twenty microns. There were no indications that the marks had any pattern to their distributions. Acetone is more volatile than THF, as well as more polar.

Acetonitrile gave a film which did not show any obviously visible features, but which had gentle hills and valleys (Figure 2.16). The solvent itself is relatively similar to the alcohols tested in boiling point and polarity, but produced no features in the PU films similar to those produced by the alcohols.

As a non-polar solvent, toluene has a lower dielectric constant than THF. However its boiling point is substantially higher, which gives it a much slower rate of evaporation than THF. As expected, the toluene spiked PU solution gave a non-uniform film. The most noticeable feature was a large crater near the center of the film (~ 400 μm in diameter) (Figure 2.17a), similar to the crater seen in the trichloromethane film. In addition, the bottom of the crater showed jagged holes, measuring from 2-20 μm in diameter at the longest point (Figure 2.17b).

Except for water, DMSO was the most polar solvent tested, and had the highest boiling point. Consequently, it took a substantial amount of time to air dry in

comparison to the other solvents, despite the small droplet size used. The resulting film had several anomalies which we had previously been observed in PU films cast with other solvents.

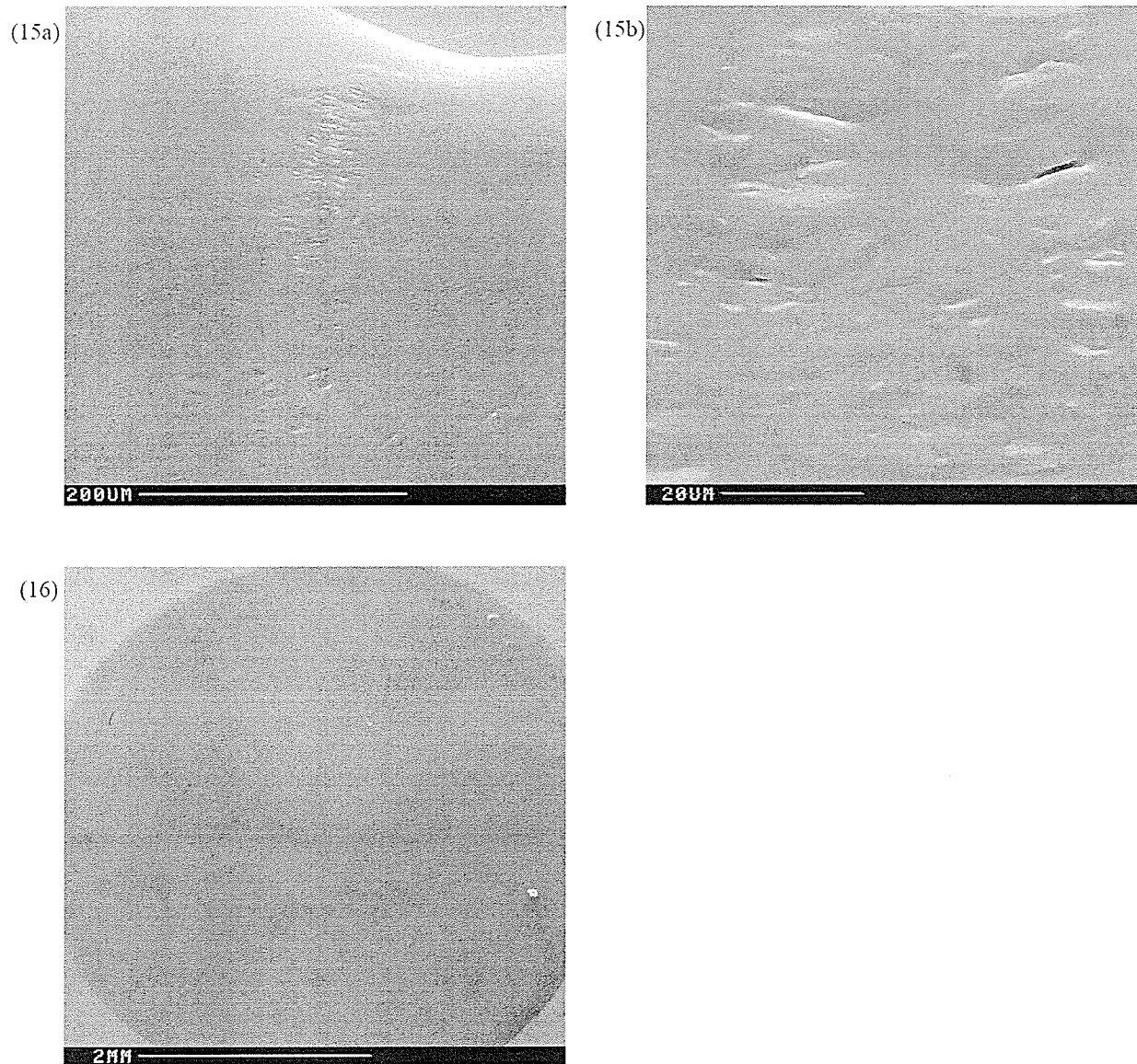


Figure 2.15: SEM of PU film cast from 10% acetone showing (a) indentations in the film surface, and (b) close-up of the indentations

Figure 2.16: SEM of PU film cast from 10% acetonitrile, showing an anomaly free surface with gentle contours

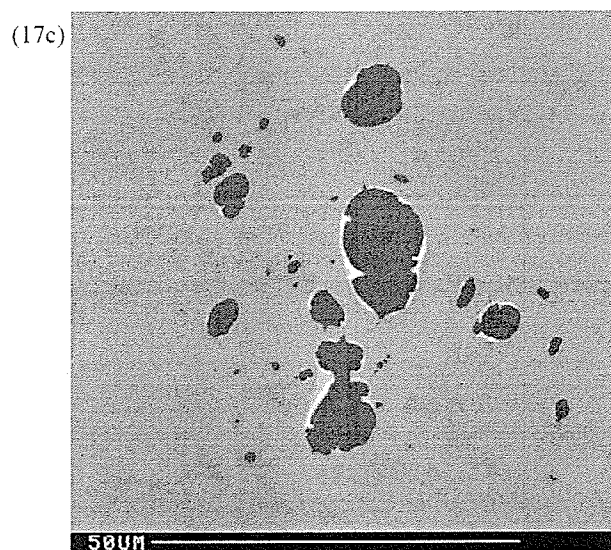
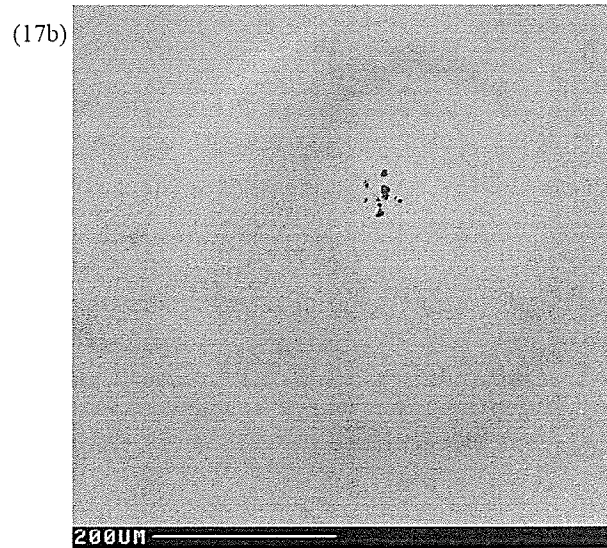
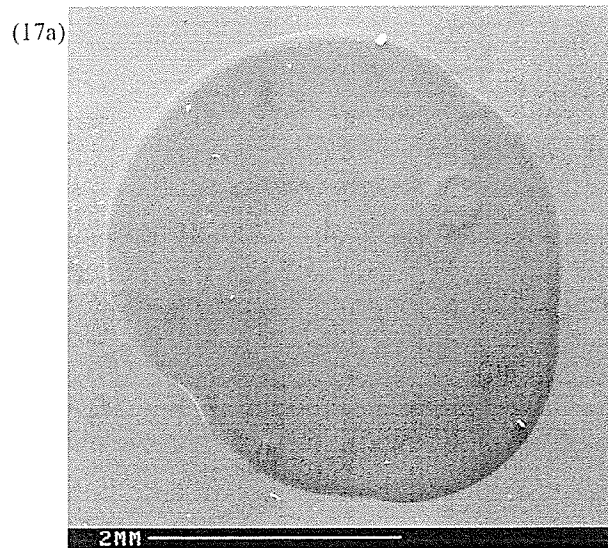


Figure 2.17: SEM of PU film cast from 10% toluene, showing (a) a smooth surface with a large surface bulge (b) close-up surface bulge, and (c) holes in the bottom of the surface bulge.

First, is the presence of a periphery ring around the PU film with radial lines pointing towards the center, similar to that seen in 1-butanol (Figure 2.18a). The second feature was a bulge in the surface of the film, similar to what was observed in the methanol spiked PU film, though the edges of the anomaly found in DMSO seem sharper and more defined (Figure 2.18b).

The last feature found in the DMSO film was what initially appeared to be a small hole in the film. The hole was initially found by detection of backscattered electrons, indicating a compositional difference. A closer scan using the backscattering detector indicated that the spot was not a hole, but in fact a crystal (Figure 2.18c and 2.18d). Determination of the composition of the crystal by energy dispersive x-ray emission showed the crystal to be comprised of potassium and chlorine. Logically, we can conclude that the crystal was KCl, likely formed as an impurity from the DMSO.

It is difficult to predict what kind of polymer morphology will arise when PU is cast with a binary solvent system. Though specific features cannot be predicted, some correlations can be made. The parameters of boiling point and polarity seem to be the most influential in the final product formed. Generally, non-polar solvents generate flat films, and polar solvents producing surface irregularities in the form of peaks, craters, and holes. However, when pairing a non-polar solvent with THF, if the boiling point of the second solvent exceeds the boiling point of THF substantially, surface anomalies are formed. Though the observed anomalies are specific to each solvent, polar solvents produce more unpredictable features. Solvents with a high boiling point and a high dielectric constant appear to form the ring structure or crater.

As THF is quite volatile, solvents with lower boiling points are uncommon. Acetone and dichloromethane both have significantly lower boiling points, and form films with only minor surface anomalies.

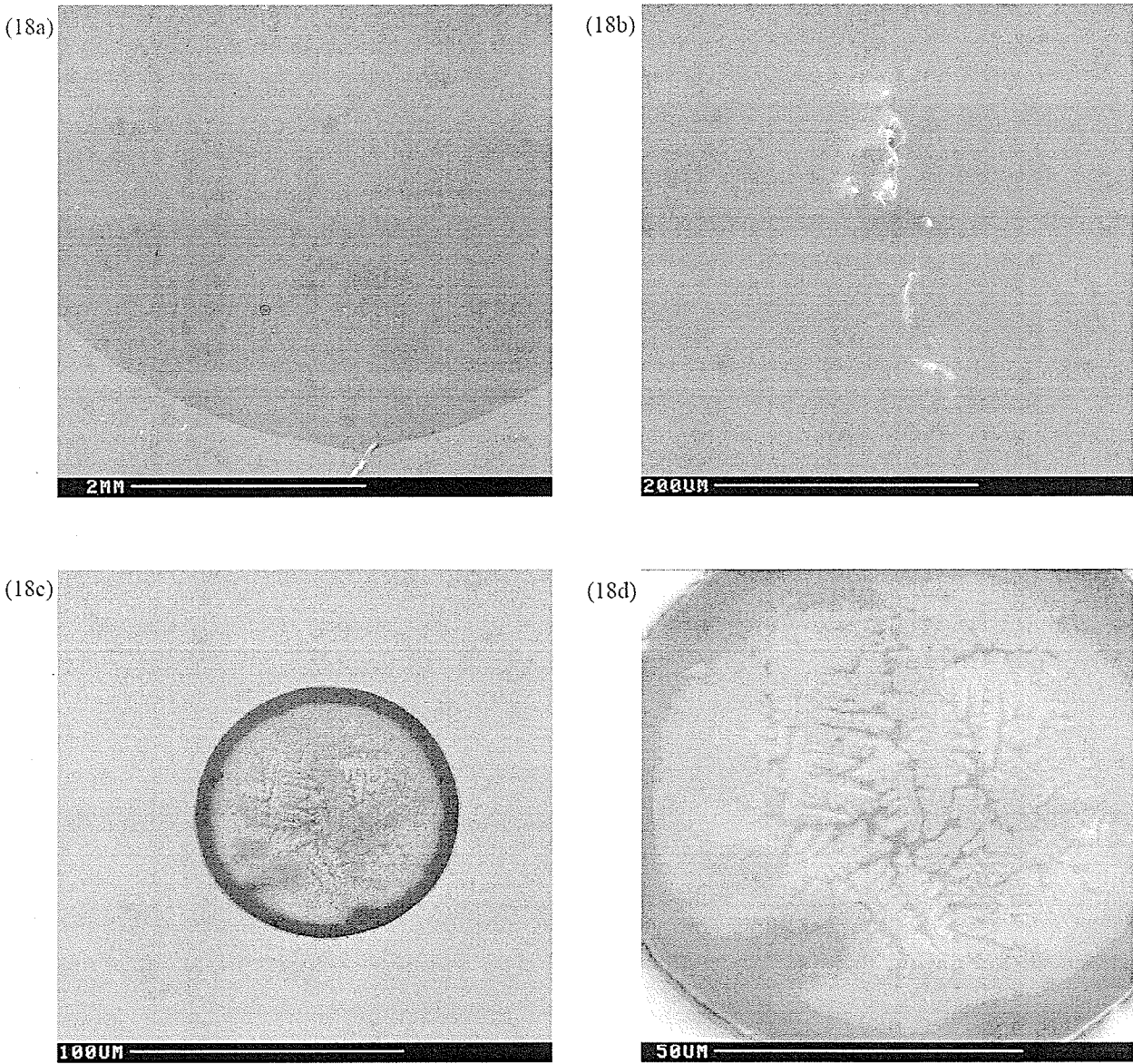


Figure 2.18: SEM of PU film cast from 10% DMSO showing (a) periphery ring, (b) anomaly in surface texture, (c) KCl embedded in film surface, and (d) close-up of KCl

2.3.5 Spin Coating

By use of spin coating in the formation of films, it is possible to achieve a uniform thickness on a flat substrate. As a materials ability to electrically insulate is dependent on thickness, the thinner the resulting PU membrane, the better will be the charge dissipation. As we only use the surface of the membrane for interaction with the sample, almost any thickness will suffice if the film is robust enough for handling during the sample deposition and washing steps.

Spin coating consists of four distinct steps. Initially, the substrate is applied to the surface to be coated. Secondly, the surface is spun, and accelerated to the final angular velocity. Thirdly, the target is held at constant angular velocity while the film thins as determined by the viscosity of the fluid. Fourthly, the solvent evaporates while spinning at constant velocity.

It was found that the PU film solution was sufficiently viscous that following the application of a drop of PU to a target, the droplet was pulled off the side of the target during the acceleration stage due to the droplet not being placed perfectly symmetrically over the center of the target. For this reason, the PU films were applied to the target after they reached maximum rotational velocity.

For our application, rotational velocity of the centrifuge was indirectly determined. As velocity control is defined by a variable autotransformer, the rotational velocity is expressed as a percentage of the power allowed for the centrifuge. Given that the centrifuge has a capacity of ~ 1500 rpm, we will assume that the centrifuge can attain this speed at 100% power, and the proportional velocity at lower voltages.

As one can logically surmise, the fastest rotational speed will give the thinnest PU film. At 100% speed, a PU film cast from distilled THF gave a very uniform, featureless topography (Figure 2.19a). A cross section of the film shows a thickness of 1.5 μm (Figure 2.19b). Though the PU film is featureless in itself, it coats the steel target evenly, taking on the topography of the target itself. Given that the surface of the brushed steel has features larger than 2 μm , the PU film shows some small irregularities in the surface as it coats the steel.

When PU films were formed at 80% speed, some differences were noted. Though similar in smoothness and thickness (2 μm) (Figure 2.20a) as the film formed at 100% speed, some irregularities were found in the surface. There appear to be several cracks (~50 μm long) on the surface of the film (Figure 2.20b). Likely, these are formed due to a combination of the rotational speed of the spin coating causing strain on the polymer, and slower evaporation of the solvent at the lower rotational speed, which keeps the polymer soft for an extended period of time.

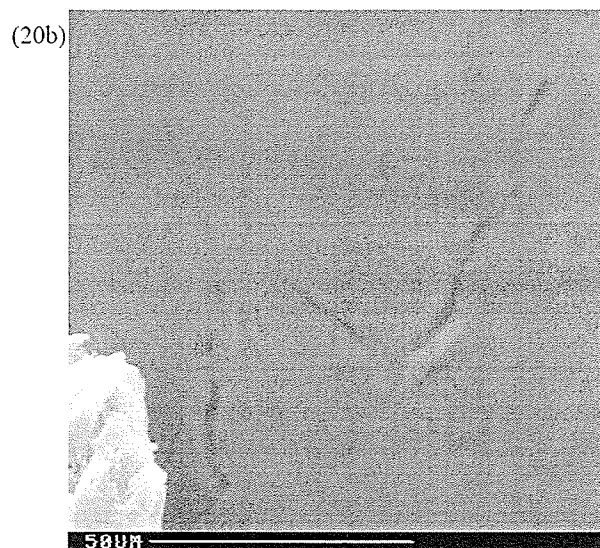
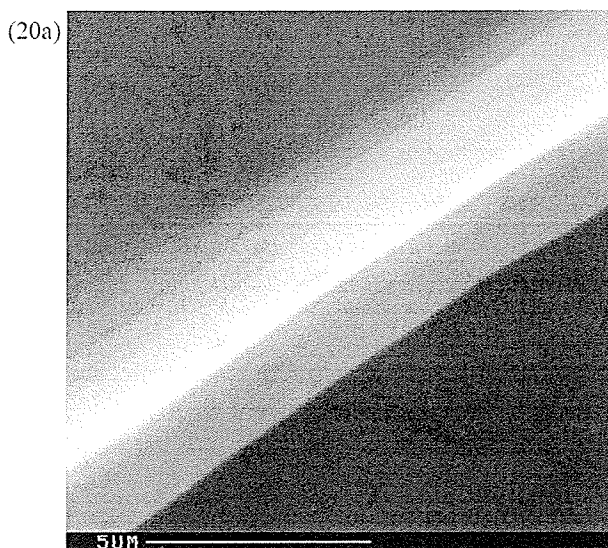
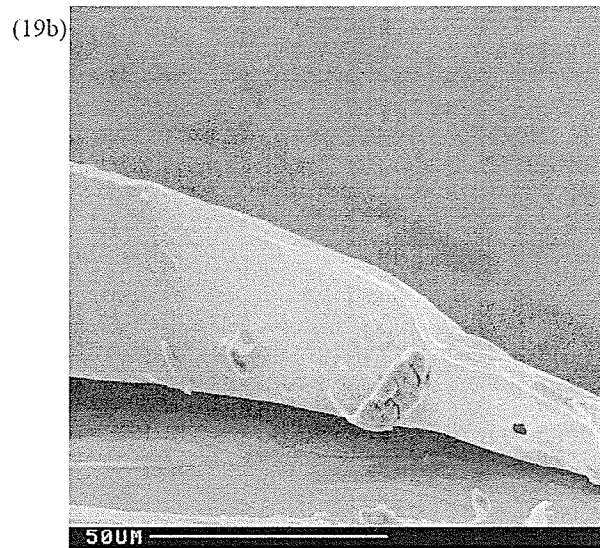
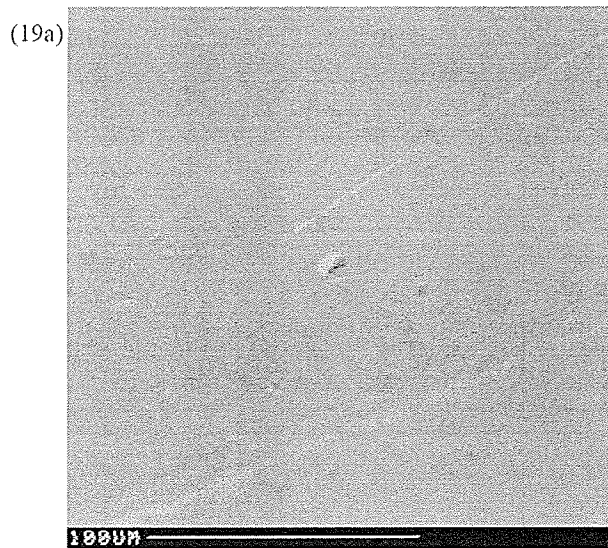


Figure 2.19: SEM of PU film spincoated at 100% speed onto a steel MALDI probe showing (a) PU film taking on surface features of the steel target, and (b) cross section of PU film edge

Figure 2.20: SEM of PU film formed at 80% speed onto a steel MALDI probe showing (a) cross section of PU film edge, and (b) cracks found in PU film surface

Secondly, the target shows a peripheral ring around the PU film, though it is different from the similar structure formed by the addition of 1-butanol (Figure 2.20c). The ring appears much less smooth, and shows none of the previously seen radial lines reaching towards the center of the film. As the ring is not present at higher rotational speeds, it is also likely that this structure is the result of slower rotational speeds with slow evaporation of the THF solvent. The polymer becomes quite viscous when nearly dry, and will not spread any further, causing excess PU to accumulate at the limit of the periphery formed by centrifugal force.

At 60% rotational speed, an increase in film thickness was seen ($5\ \mu\text{m}$) as well as the formation of the peripheral ring (Figures 2.21a and 2.21b). However, the edge of the film (which had been cut and lifted to evaluate thickness) shows a series of fine concentric lines in the surface texture (Figure 2.21c). As this is an artifact of spin coating at relatively low rotational speeds, it is likely caused by the inconsistent velocity of the rotor under low velocity, as each induction coil waits a substantial period of time before being accelerated again.

There also appears to be a concentric region on the film where several clusters of polymer strands were found, anchored to the polymer surface (Figures 2.21d-2.21f). The droplet shaped clusters and their direction of motion indicate that their formation is consistent with the clockwise direction of travel of the centrifuge. The slow drying of the polymer under rotation likely allowed the clusters to pull free and form strands as they dried. The clusters further from the center are larger due to the greater centrifugal force pulling on them.

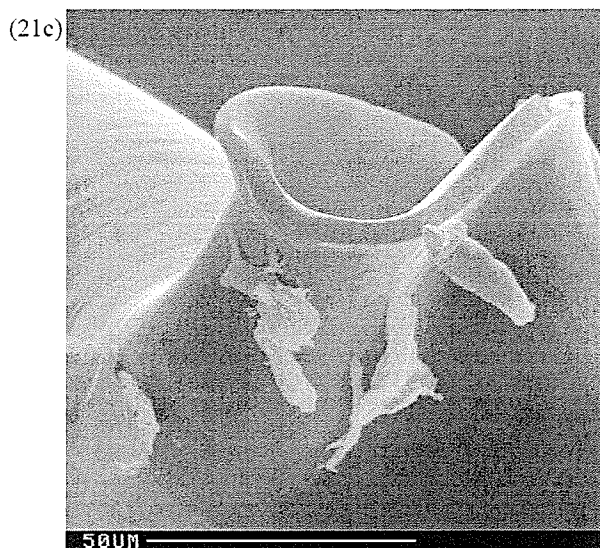
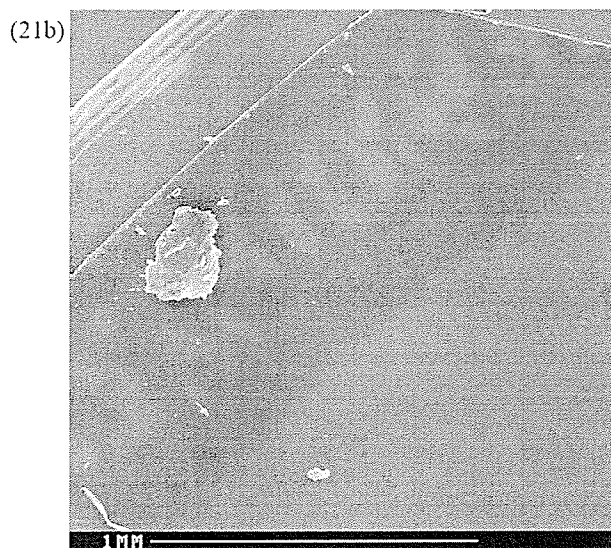
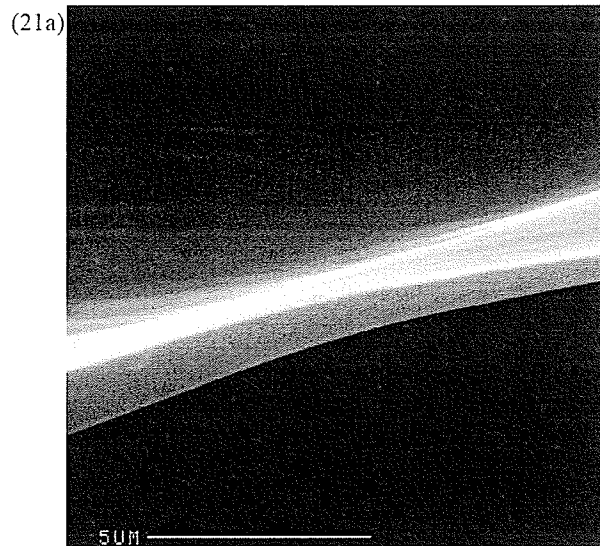
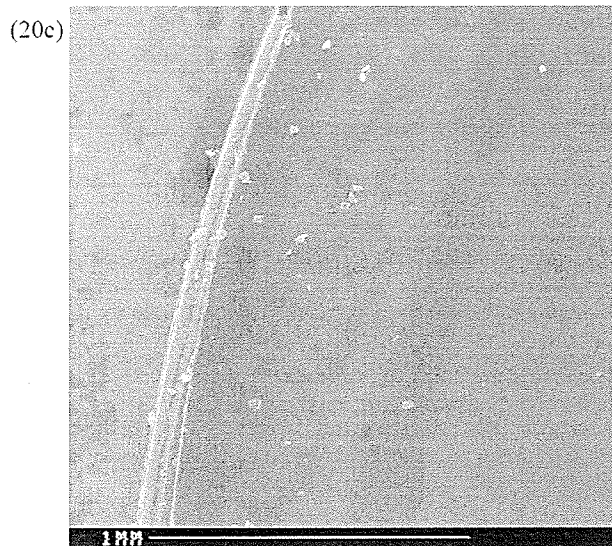


Figure 2.20c: SEM of peripheral ring of PU film formed by spin coating at 80% speed

Figure 2.21a: SEM of PU film formed by spin coating at 60% speed showing (a) cross section of edge, (b) peripheral ring formed at 80% speed, and (c) concentric lines formed by spin coating

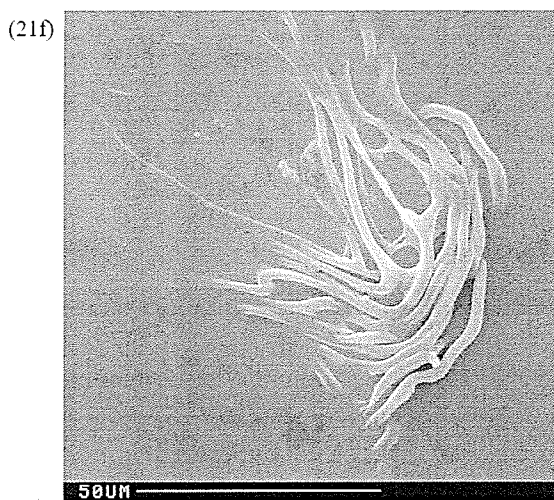
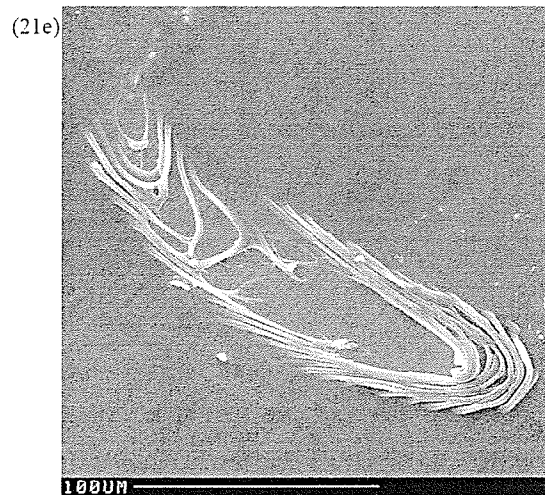
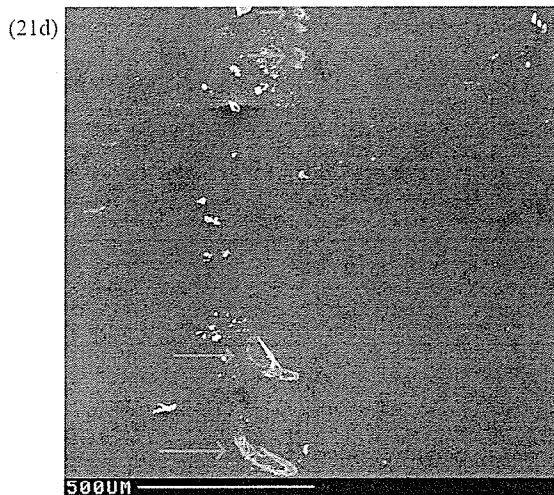


Figure 2.21b: SEM of PU film formed by spin coating at 60% speed showing (d) location of polymer strands formed (indicated by red arrows), (e) polymer strands located furthest from the center of rotation, and (d) polymer strands located closest to the center of rotation

At 40% rotational speed, the film formed had observable flaws, even without a SEM. There appear to be ridges radiating from the center of the film, giving the surface a rippled appearance (Figure 2.22a). The SEM showed a gently contoured surface (Figure 2.22b) though when tilted at an oblique angle to reflect light, the surface defects were very apparent to the naked eye. A cross section of the resulting membrane was 10 μm thick, making it substantially thicker than any of the other membranes previously formed. The cross section also showed that the film did not have a uniform composition. The edge showed an almost foam type structure which was very different from the previously formed membranes (Figure 2.22c) but which more closely resembled the PU membrane that McComb et al fashioned.

Spin coating of water spiked PU film solutions was also performed to determine if the centrifugal force changed any of the surface features previously caused by the dried drop method. A PU film solution spiked with 10A% water, spinning at 100% speed resulted in a film which appeared slightly cloudy to the naked eye. Examination by SEM showed the cloudiness to be the result of small regions of heterogeneity radiating from the center of the target (Figure 2.23a). The light grey regions seen appear to be comprised of many small, roughly circular regions (~ 150 μm diameter), closely spaced, though many of them are overlapping at the edges (Figure 2.23b). Closer examination of one of the circular regions shows the circle itself to have a heterogeneous topography. The center area of the circle shows a region covered with small surface pores, approximately 2 μm in diameter, with the light grey regions comprising larger pores of varying diameter (Figure 2.23c).

Surrounding the center appears to be a ring shaped area, with a similar pore size distribution.

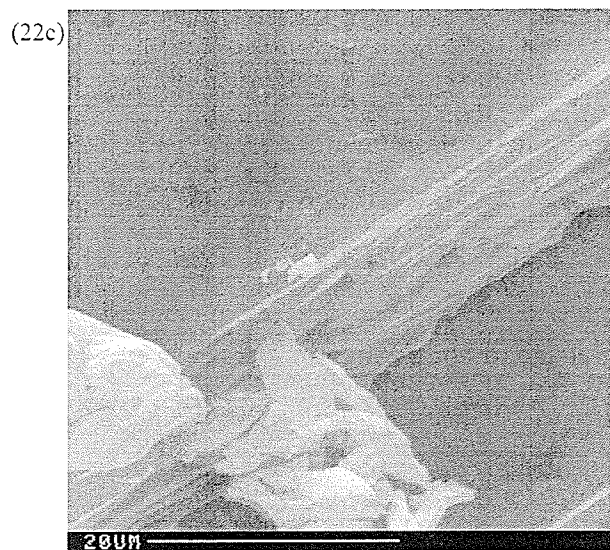
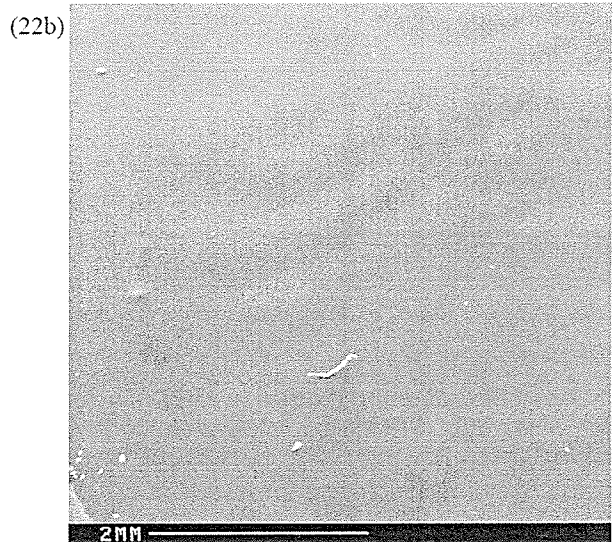
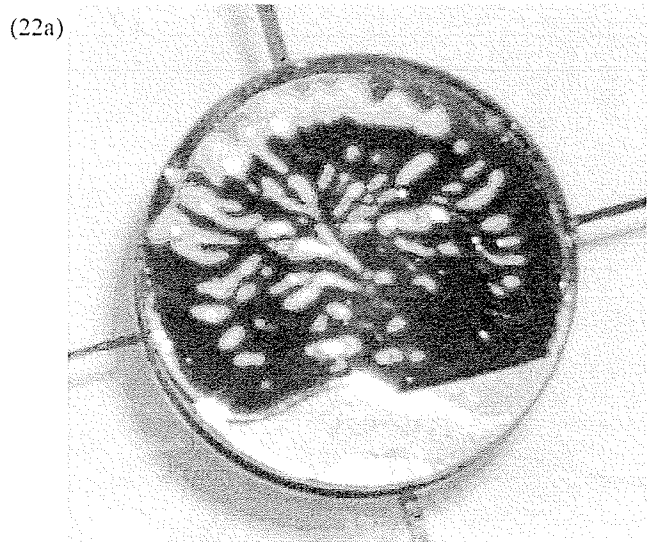


Figure 2.22: Images of PU film formed by spin coating at 40% speed showing (a) digital camera capture of Au-Pd coated PU film showing contoured surface, (b) SEM of contoured surface, and (c) cross section of film edge showing foam like structure

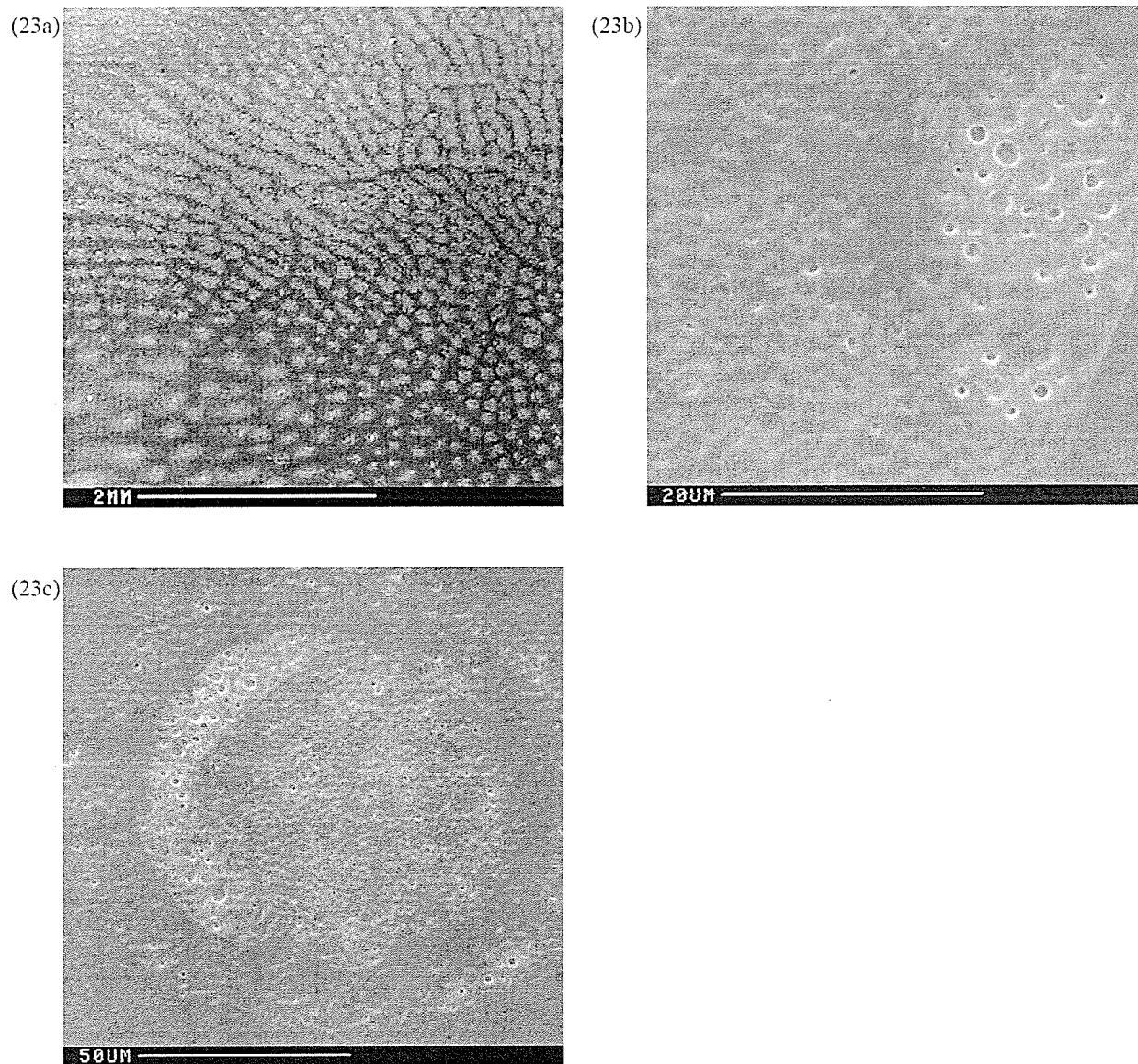


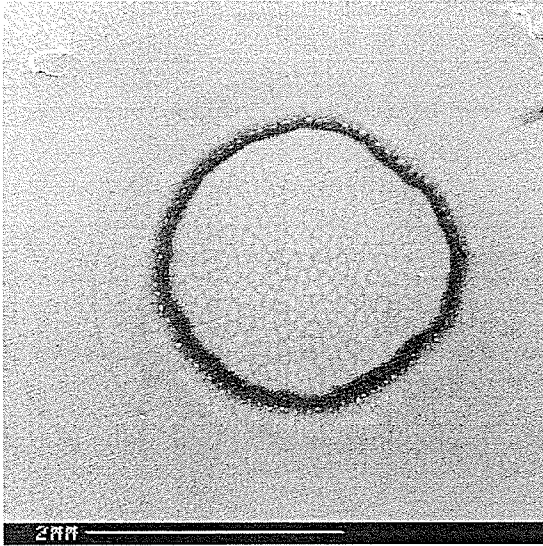
Figure 2.23: SEM of PU films from spin coating a 10% water spiked solution spun at 100% speed showing (a) surface heterogeneity composed of small regions of pores, (b) surface pores in film, (c) localized pore region.

Though similar in topography, but highly different in luminosity from electron bombardment, it is possible that the light grey regions of the circles are compositionally different because of formation of Auger electrons which are then captured by the Faraday cage and detected.

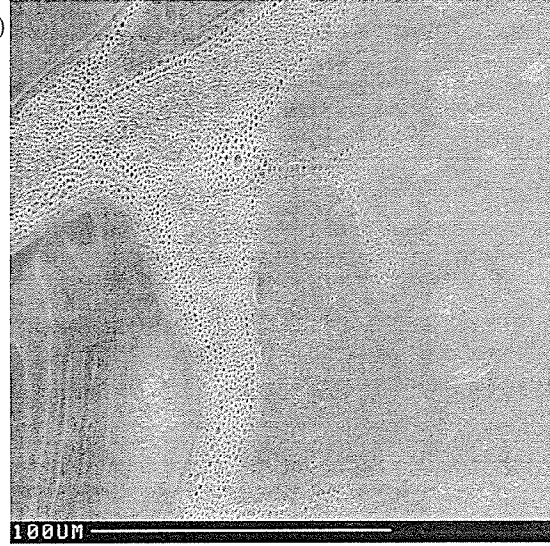
At lower speeds, the water spiked solutions gave similar but slightly more uniform topographies. Spinning at 80% speed, the resulting film also appeared cloudy as before. However, the center of the film is clearly defined, showing a dark ring structure (~2mm diameter) surrounding a center composed of tiny porous circles (Figure 2.24a). Though much larger, the center of the film strongly resembles the much smaller circles which comprise the cloudiness of the film itself. Towards the outer edges, the film shows regions of heterogeneity, where there are regions of smooth film surface without any pores (Figure 2.24b). In addition, the film shows regions of different thicknesses at the edges, separated by a sharp cliff (Figure 2.24c).

Given that the heterogeneity of the film mostly occurs at the edges, the differences are likely formed due to the differing densities of the solvents present. The system is homogeneous at the center when first applied. Centrifugal force acting upon the solvents draws the solution out towards from the center. Since water is denser than THF, the centrifugal force exerted more strongly on the water molecules. The strong hydrogen bonding of water likely means that this solvent likely moves with other molecules, forming localized regions of high water content (surface pores) and regions of low water content (smooth film).

(24a)



(24b)



(24c)

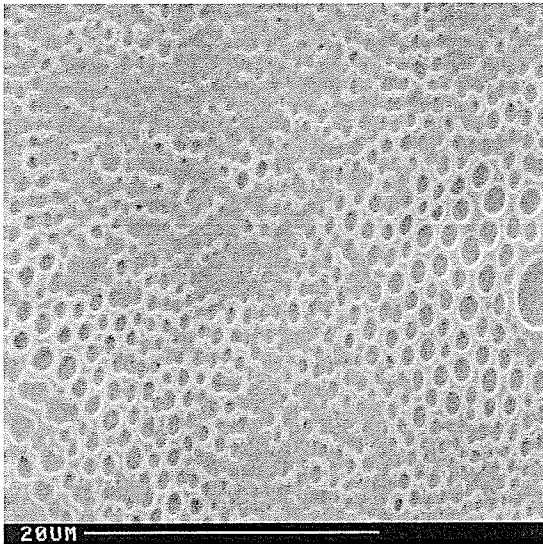
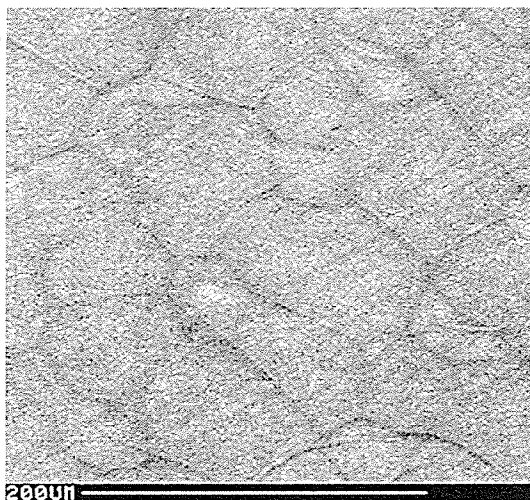


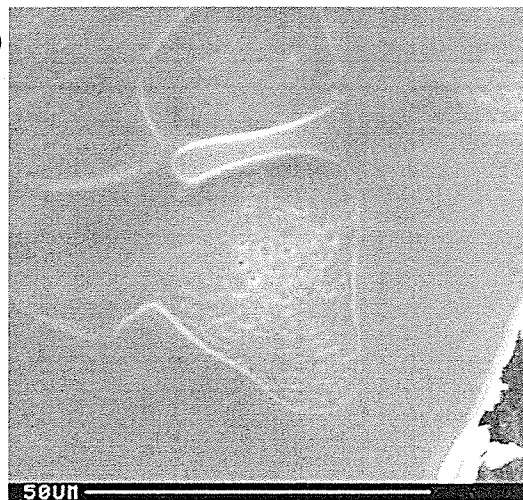
Figure 2.24: SEM of PU film formed from a 10% water solution spin coated at 80% speed showing (a) center of film with heterogeneity, (b) porous region with hills, valleys and flat regions, and (c) pores formed at different heights

Lower speeds such as 60% and 40% produced important defects such as cracks, large craters and valleys in the surface of the films (Figure 2.25a, 2.25b), rendering them unusable for MALDI. As expected, when spun at low speeds, the water has a much stronger tendency to pool as the THF evaporates. At 40% speed, there appears to be a pattern of large circles, radiating from the center of the film (Figure 2.26a, 2.26b). It is likely that these were formed by large water droplets traveling from the center of the film towards the periphery.

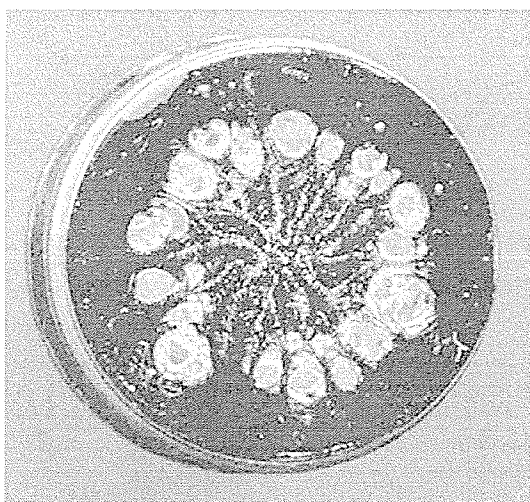
(25a)



(25b)



(26a)



(26b)

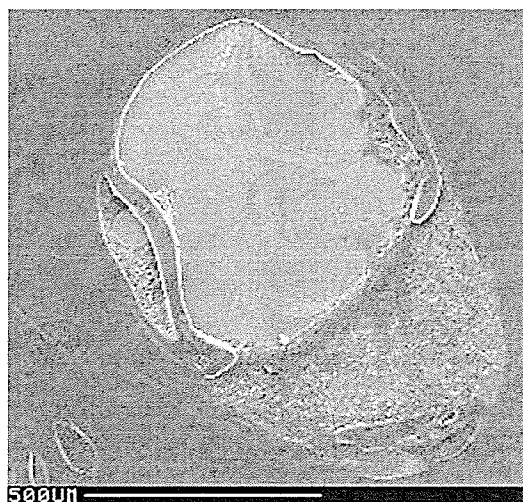


Figure 2.25: SEM of PU film formed from 10% water spike spun at 60% speed showing (a) cracks and pores in PU film surface, and (b) valley in film surface near the periphery

Figure 2.26: PU film formed from 10% water spike spun at 40% speed showing (a) digital camera capture of PU film surface showing large circular defects, and (b) SEM of circular defect

2.4 Conclusion

We were able to identify trace solvent impurities as the causes of the pores in PU films. The presence of water and BHT stabilizer in ACS grade THF causes pores to form as the PU solution dries. A solvent with very different boiling point, polarity, and density relative to THF, water would not evaporate at the same rate, or dissolve in solution. It would thus pool into localized areas as the THF dissolved. This would create pockets of heterogeneity in which the PU would not be soluble.

Through a series of tests with solvent spiked PU film solutions, the critical parameters of polarity and boiling point were identified as the most crucial with respect to the spiked contaminant solvent in determining the aspect of the film. Even if both parameters are not similar to those of THF, in some cases, reasonable quality films were obtained.

Testing a series of alcohols (from methanol to 1-butanol) as contaminants, it was found that despite the slightly higher polarities of the alcohols relative to THF, their substantially higher boiling points caused the formation of a large ring structure at the periphery, with a center mostly free of artifacts. While not an ideal surface for MALDI, the peripheral ring may be useful for physically constraining liquids applied to the surface of the target, as the outer ring functions as a “lip” for holding liquids in.

In comparison, a series of chloromethanes were spiked into the PU film solution. Lower in polarity than the alcohols, and much more similar in polarity to THF than alcohols, the resulting films were all smooth and largely featureless with the exception of very minor blemishes in the polymer surface in spite of differences

in boiling points. Based upon this, we conclude that the difference in polarity between THF and the contaminant solvent is the most important parameter to consider when trying producing a featureless film.

Though a variety of solvents were tested, no defining characteristics could be attributed to the physical features of the film produced. For example, acetonitrile has a similar polarity to methanol, and a boiling point similar to that of 1-propanol. However, it did not produce a film resembling those obtained when either alcohol was spiked.

Spin coating of PU films has a variety of effects. Even for single solvent solutions, it is possible to produce a film with flaws. At 1500 rpm, a pure THF solution produced a thin, featureless film. At lower speeds, the resulting film had flaws such as cracks which likely resulted from a combination of slow drying and centrifugal forces exerted by spin coating. This implies that there is a critical balance between dilution of the PU film solution and the rotational speed which determines rate of drying. At higher dilutions, the film will dry more slowly, and likely exhibit cracks from the exerted force of rotation.

Spin coating of a binary solvent system, containing THF and water, shows a number of effects. It is apparent that higher the rotational speed, the more homogeneous the film. However, the defects resulting from the dried drop method are manifested much differently. Instead of forming a large surface defect, the film is much more uniform with many small defects, most commonly showing as surface pores. At slower speeds, some evidence of surface bound polymer strands were seen which may be useful in increasing the surface area of PU available for binding. In

general, slow speeds produced larger artifacts, making the film completely unsuitable for MALDI applications.

With current technologies, the use of orthogonal MALDI-TOF renders many film surfaces useable as the decoupled nature of the source eliminates the need for a uniform surface. However, the flattest film surface is still the most ideal with respect to performing on-target sample preparation. Non-uniform surface characteristics may limit the ability to extract analyte from the surface.

2.5 References

- [1] Liu, Y., Bai, J., Lubman, D.M., Anal Chem. 67, 3482 (1995)
- [2] Bai, J., Liu, Y., Cain, T.C., Lubman, D.M., Anal. Chem. 66, 3423 (1994)
- [3] Vestling, M.M., Fenselau, C., Anal. Chem. 66, 4371 (1994)
- [4] Strupat, K., Eckerskorn, C., Karas, M., Hillenkamp, F., Mass Spectrometry in the Biological Sciences, A.L. Burlingame, S.A. Carr (Editors) Humana Press, Totowa NJ, p.203 (1996)
- [5] Vestling, M.M., Fenselau, C., Mass Spectrom. Rev. 14, 169 (1995)
- [6] Strupat, K., Karas, M., Hillenkamp, F., Anal. Chem. 66, 464, (1994)
- [7] Blackledge, J.A., Alexander, A.J., Anal Chem. 67, 843 (1995)
- [8] Hutchens, T.W., Yip, T. Rapid Commun. Mass Spectrom. 7, 576 (1993)
- [9] Oleschuk, R.D., Chow, A., Talanta 43, 1545 (1996)
- [10] Rzeszutek, K., Chow, A. Talanta 46, 507 (1998)
- [11] Rzeszutek, K., Chow, A. Talanta 47, 697 (1998)
- [12] Rzeszutek, K., Chow, A. Talanta 49, 757 (1999)
- [13] Muffazal Saeed, M., Moosa Hasany, S., Ahmed, M., Talanta 50, 625 (1999)
- [14] McComb, M.E., Oleschuk, R.D., Manley, D.M., Donald, L., Chow, A., O'Neil, J.D.J., Ens, W., Standing, K.G., Perreault, H., Rapid Commun. Mass Spectrom. 11, 1716 (1997)
- [15] Sreenivasan, K., Jayabalan, M., Rao, KV.C., J. Appl. Polym. Sci. 45, 2105 (1992)
- [16] Petrovic, Z.S., Fergenson, J., Prog Polym. Sci 16, 695 (1991)
- [17] Zaluzek, E.J., Gage, D.A., Allison, J., Watson, J.T., J. Am. Soc. Mass Spectrom. 5, 230 (1994)
- [18] McComb, M.E., *Characterization of Biological Compounds by Mass Spectrometry*, Doctoral Dissertation, University of Manitoba, Canada
- [19] Blackledge, J.A., Alexander, J., Anal Chem. 67, 843 (1995)

[20] Tang, X., Beavis, R.C., Ens, W., Lafortune, F., Schueler, B., Standing, K.G., Int. J. Mass Spectrom. Ion Processes 85, 43 (1988)

3 Determination of Protein Phosphorylation Sites by MALDI-QqTOF MS

3.1 Introduction

Reversible protein phosphorylation has been found to be one of the most important intracellular events in living organisms. It plays key roles in numerous intracellular communication mechanisms by using protein kinases and phosphatases to reversibly add and remove phosphate moieties to regulate protein activity [1-6]. Transduction pathways, hormones, ion channels, and nerve impulses are all examples of cell processes regulated by reversible protein phosphorylation. An estimated 30% of all intracellular proteins are possible targets for protein phosphorylation, with higher eukaryotes having an estimated 2-3% of the genome encoding for kinases and phosphatases [7-9]. In vertebrate cells, the most commonly phosphorylated residues are phosphoserine, phosphothreonine, and phosphotyrosine, with experimental quantitation showing an approximate 1800/200/1 ratio respectively, making phosphoserine the most frequently found [10].

The use of mass spectrometry for peptide sequencing has become common, since the polymeric structure of a protein yields a regular ion series upon fragmentation in tandem MS. However, the structural elucidation of sites of post-translational modifications has proven comparably more difficult due to the variety of structures present [11-13].

Determination of phosphorylation sites on proteins by mass spectrometry [14-15] has proven difficult due to a number of biological factors such as low stoichiometry, heterogeneous phosphorylation composition, and low abundance of

signaling molecules [16-19]. From an analytical perspective, the analysis of phosphorylated proteins is difficult because of the reduced ionization efficiencies of phosphorylated samples. Both MALDI and ESI exhibit lower sensitivities in positive mode for phosphorylated peptides than their non-phosphorylated counterparts. This is due to the negatively charged nature of the phosphate moiety, which reduces the ionization efficiency [20-23]. The more phosphate groups present, the lower the ionization efficiency, resulting in lower sensitivity and poor detection limits. In addition, the presence of strongly ionizing peptides suppresses ionization of the phosphopeptides, reducing sensitivity [24].

Previous research has shown the usefulness of nanospray-ESI in structural studies of phosphopeptides [24-26]. Though MALDI-TOF has had limited success obtaining structural information from phosphopeptides from PSD, the use of a custom built MALDI-ion trap instrument has shown some promise with the ionization and detection of a tetra-phosphorylated peptide [27,28].

In this work, I evaluate the MS data of a phosphorylated peptide from β -casein, analyzed with an in-house built MALDI-QqTOF instrument. Coupled with the advantages of a MALDI source, the QqTOF analyzer offers exceptional MS/MS abilities in comparison to PSD methods.

3.2 Experimental

3.2.1 Materials and Methods

Non-porous polyurethane membrane samples were provided by JPS Elastomerics (Northhampton, MA) and washed prior to use [29]. Diammonium citrate, ammonium acetate, bovine β -casein, dephosphorylated β -casein, and TPCK treated trypsin were purchased from Sigma Chemical Co. (St. Louis, MO, USA)

De-ionized water was obtained from a Barnstead NanoPure filtration system supplied by a reverse osmosis feedstock. MALDI matrices, sinapinic acid, and 2,5-dihydroxybenzoic acid were purchased from Sigma.

Polyurethane membranes were prepared by soaking in methanol and sonicating for several minutes, repeating once more, and allowed to air dry. Membranes were mounted to MALDI targets by SprayMount adhesive (3M Canada, London, Ontario) and allowed to dry.

Samples of β -casein and dephosphorylated β -casein were spotted onto polyurethane films and digested under a variety of conditions, including variations in time, temperature, buffer type and buffer concentration to determine optimal on-membrane digestion conditions. Droplets of the sample (3 μ l, 60 pmol) were applied to the polyurethane membranes and allowed to dry. Samples were digested by applying 5 μ l of trypsin (\sim 0.01mg/ml) to the dried samples and allowing to digest for the desired amount of time. Proteolytic digestion was halted by addition of 1 ul of glacial acetic acid and samples were allowed to go to dry. Prior to a washing step, 2 ul of methanol was added to increase affinity for the substrate and allowed to dry. Samples were washed with 5 ul of de-ionized water and allowed to dry. A saturated

sinapinic acid matrix solution was added to the dried sample spot and aspirated several times over the sample region to extract the purified peptides from the membrane surface for incorporation into the matrix crystals.

Sample preparation for MS/MS was done in similar fashion once the optimum conditions were determined from the on-membrane digestion, except for the choice of matrix solution. A solution of 50mg of DHB in 200 μ l of 50:50 acetonitrile/25mM diammonium citrate was determined to be the most suitable.

Profiling of the results of varying on-membrane digestion conditions were performed on Manitoba TOF-II [30], an in-house built linear TOF instrument (Department of Physics, University of Manitoba). Samples were irradiated with a nitrogen laser (337 nm, VSL337ND, Laser Science Inc.). Manitoba TOF-II is configured with a 1.2 meter flight tube, and a two grid extraction system, using a 25 kV accelerating potential on the target and first grid, and a 1200 ns delayed extraction before a 3 kV pulse is applied to the target again. Each spectrum consisted of ca. 100 laser shots.

Samples requiring MS/MS were analyzed on Manitoba TOF-IV, a prototype MALDI-QqTOF instrument built in-house (Department of Physics, University of Manitoba, and Sciex Canada In., Thornhill, ON, Canada). The instrument design and function are described elsewhere [31].

3.3 Results and Discussion

3.3.1 MS of β -casein and dephosphorylated β -casein

Buffer conditions strongly influence digestion efficacy. Initially, the choice of buffer must logically be restricted to those buffers which do not suppress ionization in mass spectrometric analysis. Though digestion with commonly used buffers such as EDTA or TRIS qualitatively results in the same tryptic fragments, the presence of the residual buffers following a wash step results in suppression of signal, thereby reducing sensitivity. Volatile buffers, though compatible by nature with mass spectrometric ionization methods, are often incompatible with the required pH range for protease digestion.

It has been shown that the presence of small amounts of ammonium salts aids the MALDI of phosphorylated peptides [22,32]. Residual amounts of these buffer salts should be conducive with the goal of the experiment. However, it was found that excessive concentrations of any buffer results in the formation of buffer crystals deposited on the surface of the polyurethane membrane following the halting of proteolysis and drying. While excessive crystals could be removed in the wash step, and did not interfere with ionization of the sample in MALDI, the crystals reduced the affinity of the polyurethane membrane for the sample. By occupying space on the surface of the membrane, they reduce adsorption of the analyte, resulting in sample loss during the washing step. To limit the effects of this phenomenon concentrations of ammonium buffers were limited to 50mM.

Though increased digestion times would theoretically give a more complete digestion of the sample, they were found to yield only minor spectral differences in

the samples. In addition, the idea of performing on-membrane digestions within only a drop of sample material was guided by the idea of very rapid sample analysis. Though the sample droplets could be maintained in volume indefinitely by further addition of buffer and/or enzyme, this concept is not consistent with the goal of the experiment. Ultimately, it was found that a 10-15 minute tryptic digestion yielded sufficient fragments for analysis.

Typically, trypsin is incubated at approximately 37 °C for proteolysis. For sufficiently short incubation periods, as in our methods in development, it was found that increased incubation temperatures were not useful in improving sample digestion. High digestion temperatures were found to cause rapid evaporation of the droplet to dryness, resulting in the halting of the proteolysis. In addition, the high temperatures caused rapid evaporation of volatile buffer components, thus altering digestion conditions as well as being undesirable for any thermally unstable compounds. Attempts to prevent evaporation of the droplets by sealing the droplet with a small container showed no improvements to the digestion. Optimally useful conditions were found to be 15 minutes digestion using 50 mM ammonium acetate at room temperature.

When applied to β -casein, the optimized digestion protocol gave rise to incomplete digestion, though coverage of all tryptic fragments of β -casein was found (Table 3.1).

Table 3.1: Measured m/z values of $[M+H]^+$ ion of on-membrane tryptic digestion products of bovine β -casein

Tryptic Fragment	Calculated m/z**	Measured m/z	Accuracy (%)
T1-2	3124	3120.3	-0.11
T1-3	3479.4	3476.2	-0.09
T3-12 ²⁺	8207	8209.9	0.04
T4-7 ²⁺	3931.9	3931.3	-0.02
T4-12	16057.5	16066.8	0.06
T5-14 ²⁺	8752.1	8754.9	0.03
T7-9	6175.3	6176.9	0.03
T9-12	7986.3	7987.9	0.02
T9-13	8748.3	8745.2	-0.04
T9-16	12452.7	12458.1	0.04
T10-12	7358.6	7358	-0.01
T10-16	11825	11826.2	0.01
T11-12	7093.2	7090.7	-0.04
T11-13	7855.2	7852.7	-0.03
T11-16*	11559.65	Internal Calibrant	
T12	6363.4	6361.2	-0.03
T13-16	4485.4	4483.5	-0.04
T14-16	3723.5	3721.4	-0.06
T16-16*	2911.53	Internal Calibrant	
* Indicates internal calibration points		** Average Mass	

The fragment of interest, which has four phosphate moieties consists of two undetached tryptic fragments and corresponds to T1-2 (Figure 3.1). However, given that the C-terminus of T1-2 is an arginine residue, it is highly unlikely that trypsin would be able to cleave here since trypsin would have a limited peptide region to bind and cleave the single arginine residue. Comparison to digestion in solution revealed no evidence of T2 indicating that the T1 theoretical cleavage point is a false cleavage point for trypsin in β -casein.

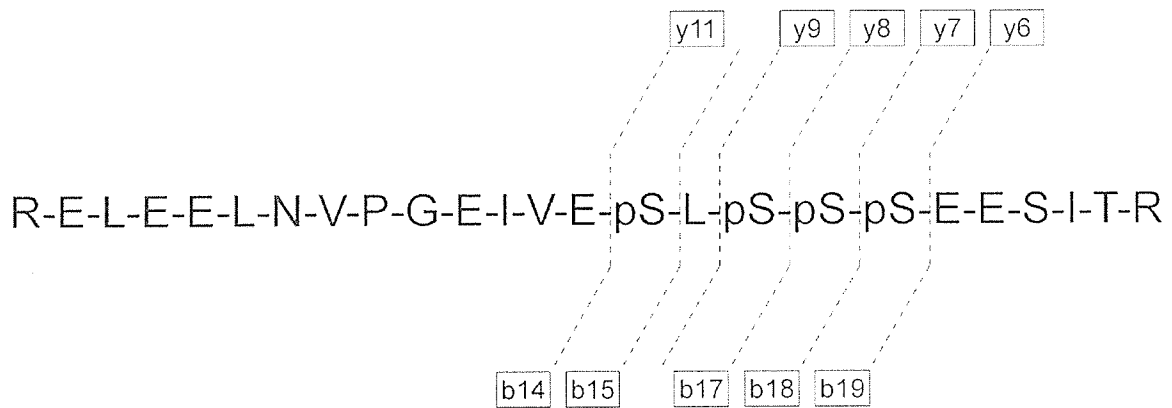


Figure 3.1: Peptide sequence of T1-2 tryptic fragment of bovine β -casein with schematic fragmentation pattern

3.3.2 MS/MS of [M+H]⁺ dephosphorylated T1-2

The MS/MS spectrum showed mainly b- and y-ions, with some a-ions present (Figure 3.2). The b-ions showed strong signals over the low mass range of the spectrum from b2 to b8. Fragments b9 and b10 were not found, though this is not surprising as they would require fragmentation at a proline residue. Remaining b-ions (b11-b24) were detected, though with much lower abundance. Similar traits were found for the a-ion series, though not nearly as complete a spectrum was found.

The y-ion peak series was found to have varying heights throughout the spectra. As expected, the fragment corresponding to the proline residue (y17) was not found, with the omission of an additional fragment at y9. Overall, sufficient information was available to elucidate the whole sequence of the dephosphorylated T1-2 unambiguously.

In comparison, MS/MS data from [M+H]²⁺ showed an incomplete b-ion series with many omissions in the larger mass range (b16-b19, b22-b24) in addition to the missing b9 ion. The corresponding y-ion series was nearly complete, with omissions at y22 and y23.

3.3.3 MS of [M+H]⁺ of phosphorylated T1-2

Initial QqTOF-MS spectra of the tryptic digest showed some anomalies not seen during the digestion profiling by axial MALDI-TOF. Specifically, peaks located near T1-2 were observed, spaced at regular intervals (Figure 3.3). The extraneous peaks were measured to differ in mass from T1-2 in increments of m/z 98. Given that the peaks were related to T1-2, it was surmised that the peaks were resulting from metastable artifacts of the collisional damping interface, as they were previously undetected by linear MALDI-TOF. Based solely on peak intensity, H_3PO_4 is preferentially eliminated from phosphorylated peptides when using the MALDI-QqTOF source [33]. This indicates that the sensitivity of the QqTOF arrangement for phosphorylated peptides may be reduced due to the fragmentation.

The successive losses of 98 m/z were also observed by DeGnore and Qin [26] in their analysis of T1-2 using an ESI ion trap, as well as by Annan using MALDI-TOF [28]. In fragmenting T1-2, it has been previously observed that the β -elimination of H_3PO_4 from phosphoserine was possible in MS/MS, forming dehydroalanine residues [26]. Using a collisional damping interface, our spectra revealed that the elimination of HPO_3 (mz 80) was also occurring. Given the possible permutations of losses of HPO_3 and H_3PO_4 , the spectrum becomes quite complicated. Metastable artifact peaks will undoubtedly be composed of combinations of possible mass losses from each phosphorylation site, with no possibility of distinguishing between them.

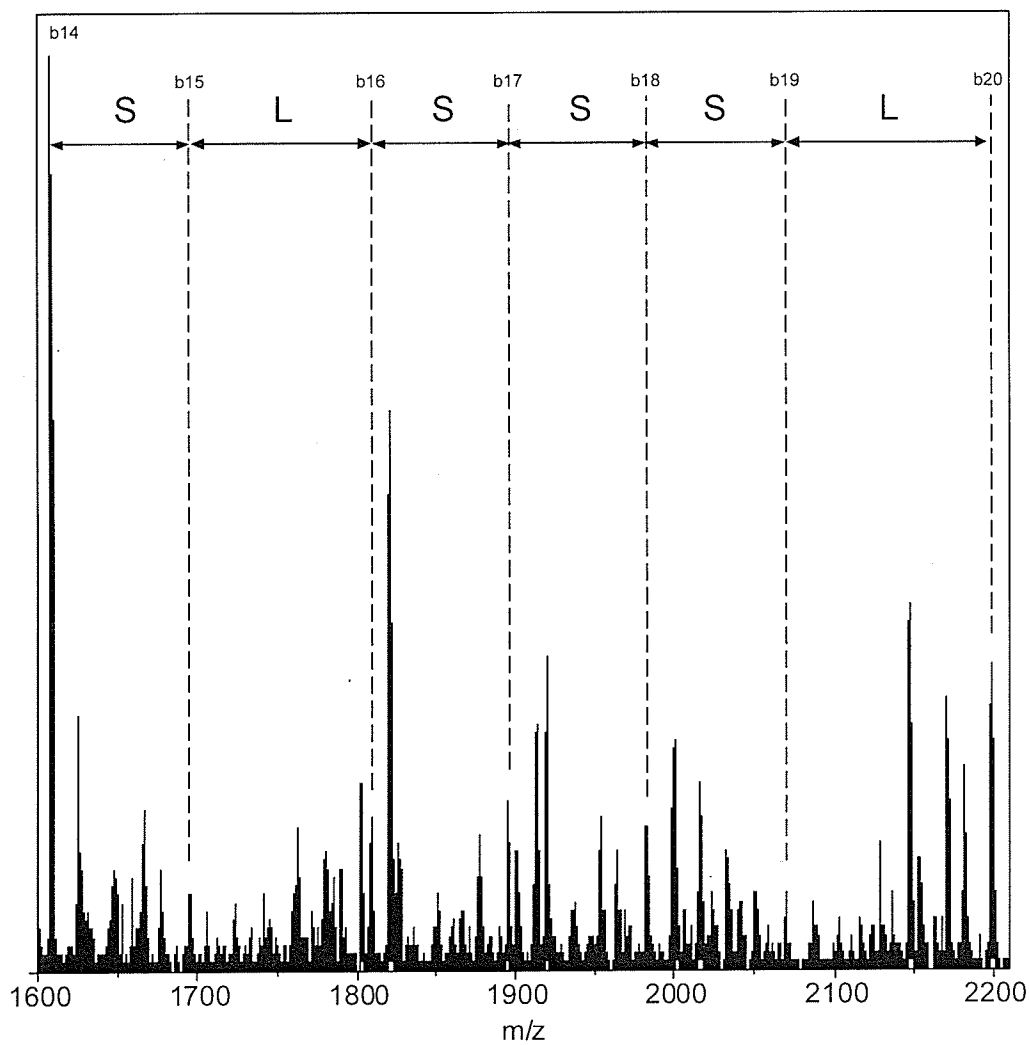


Figure 3.2a: MALDI QqTOF MS/MS spectrum of $[M+H]^+$ ions of dephosphorylated T1-2 digestion products of β -casein showing range of b-ions containing serine residues targeted for phosphorylation

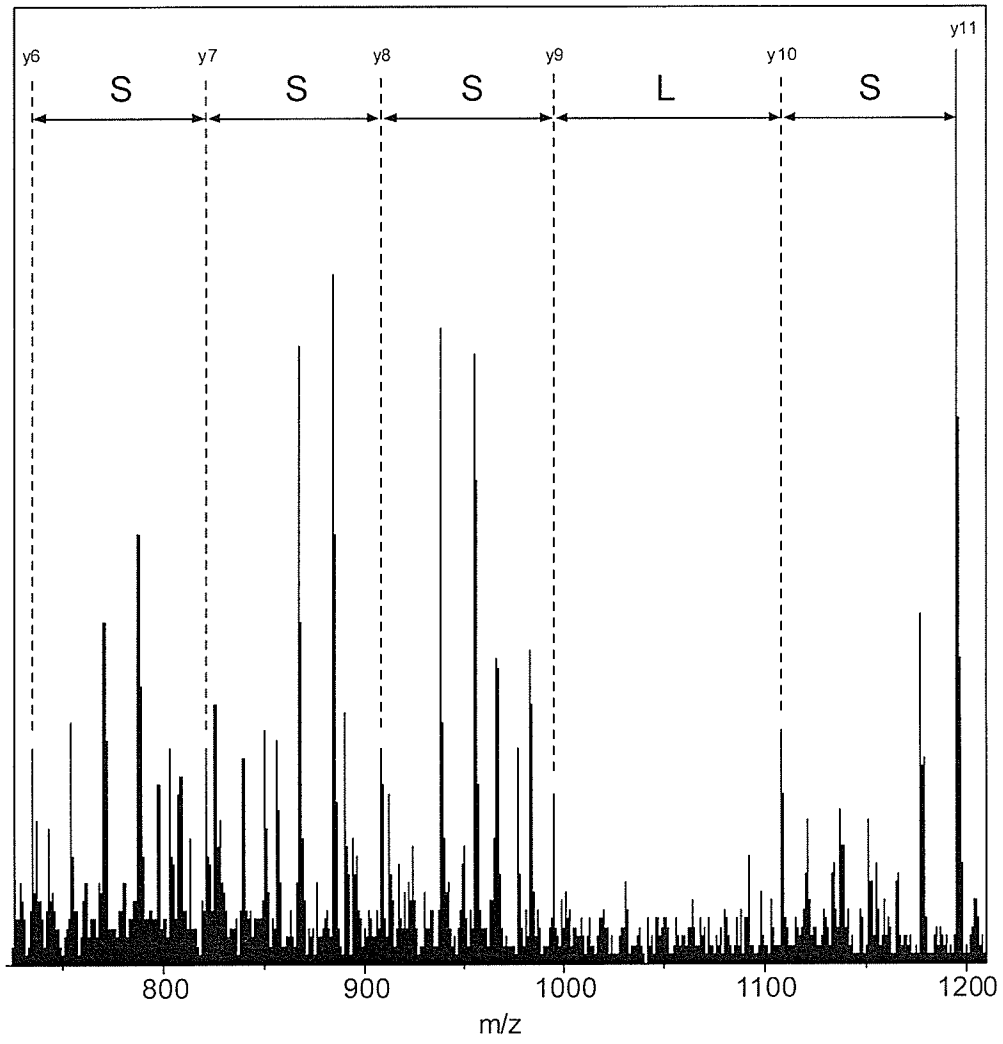


Figure 3.2b: MALDI QqTOF MS/MS spectrum of $[M+H]^+$ ions of dephosphorylated T1-2 digestion products of β -casein, showing range of y-ions containing serine residues targeted for phosphorylation

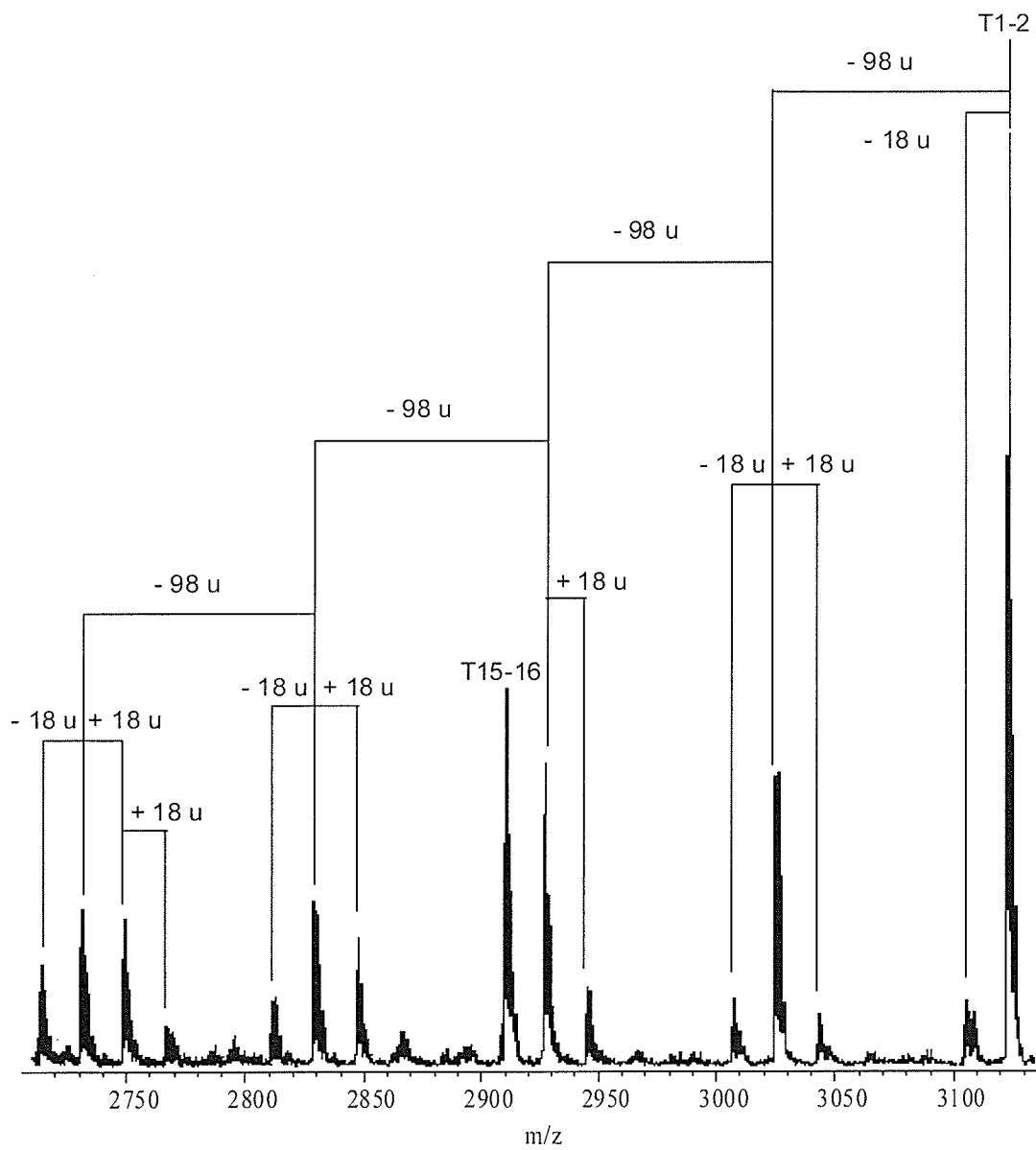


Figure 3.3: Portion of MALDI MS spectrum of β -casein digest products showing prompt decay loss of H_3PO_4 moieties from phosphorylated fragment T1-2

Also observed in the QqTOF MS spectrum were the $[M+H]^{2+}$ ions of T1-2 (m/z 1561), as well as their counterparts in the dephosphorylated sample, though they were much less abundant. However, they were still suitable for MS/MS.

The phosphorylated T1-2 fragment (m/z 3122) was initially too large for the mass range allowed for MS/MS. Modifications were made to the instrument to allow it to operate up to m/z 6000 for MS/MS making possible the analysis of T1-2.

3.3.4 MS/MS of $[M+H]^+$ of phosphorylated T1-2 by QqTOF

The high mass region of the MS/MS spectrum of tetraphosphorylated T1-2 is dominated by the fragmentation and loss of the phosphate moieties, as observed in the MS spectrum $[M+H-n H_3PO_4]^+$ ions, with $1 \leq n \leq 4$ were observed, (strongly resembling the MS spectrum prompt decay losses of H_3PO_4) resulting in the formation of dehydroalanine residues.

Losses of $nHPO_3$ were also featured in the MS/MS spectrum. Consequently, the resulting ion series contains fragments differing in mass from the ion series corresponding to the loss of H_3PO_4 (by 18 Da). Given the number of phosphate moieties present, as well as the different combinations of losses, there are likely numerous ion series present, corresponding to the various losses of phosphate moieties in their different forms from different sites in the peptide. We cannot differentiate between ions of equal m/z with differing sites of phosphate elimination, and so we cannot determine which (if any) phosphoserine in the peptide undergoes a preferential loss of HPO_3 versus H_3PO_4 .

From the large number of different ion series which are possibly formed, only one ion series is seen, corresponding to the loss of a single HPO_3 . This indicates that the loss of H_3PO_4 is much more prevalent than the loss of HPO_3 . Accompanying the b- and y-ion series, are peaks corresponding to the loss of a single HPO_3 , and three losses of H_3PO_4 . Based upon the relative peak heights, it appears that the loss of a single HPO_3 out of the four phosphate moieties present is a very common event, as the peaks in the b- and y-ion series are very often accompanied by a corresponding peak of $[\text{M}+\text{H}+18]^+$ of relatively strong intensity.

By comparison of the MS/MS spectra of the phosphorylated and dephosphorylated T1-2, we can rapidly localize the phosphorylation sites. Peaks of the b-ion series were found to match from b2 to b14, indicating that the phosphorylation sites are located in the b15-b24 segment (Figure 3.4a). Fragments b15, b17-b19 appeared at m/z differences of 69 u, indicating the presence of dehydroalanine.

From the C-terminus, matching y-ions for y1-y6 were identified by comparison with the spectrum of dephosphorylated T1-2. Fragments y7 to y11 appeared with m/z differences of 69 u, again indicating the presence of dehydroalanine (Figure 3.4b).

It should be noted that no peak m/z differences corresponding to the mass of a phosphoserine were found in the MS/MS spectrum. It appears that the β -elimination of H_3PO_4 from phosphoserine to form dehydroalanine is the dominant process in MS/MS when using this instrument design (Figure 3.5). It also appears that the

collisional damping interface acts as a collision cell, causing similar (though not nearly as extensive) fragmentation of the labile moieties.

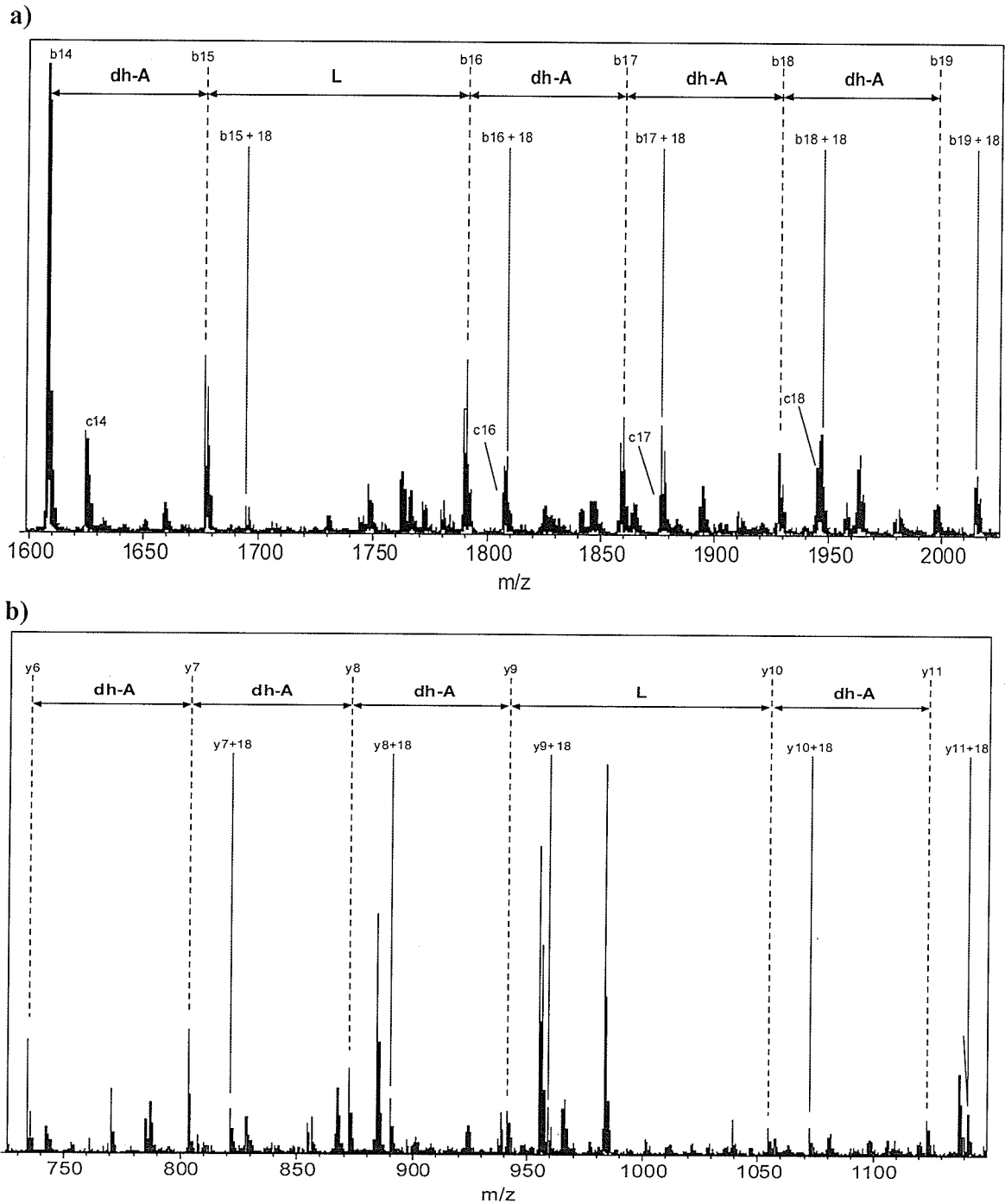


Figure 3.4: MALDI QqTOF MS/MS spectrum of $[M+H]^+$ ions of dephosphorylated T1-2 digestion product of β -casein. (a) Range of b- and c-ions containing dehydroalanine residues (dh-A) formed by loss of H_3PO_4 (b) range of y-ions containing dehydroalanine residues formed by loss of H_3PO_4

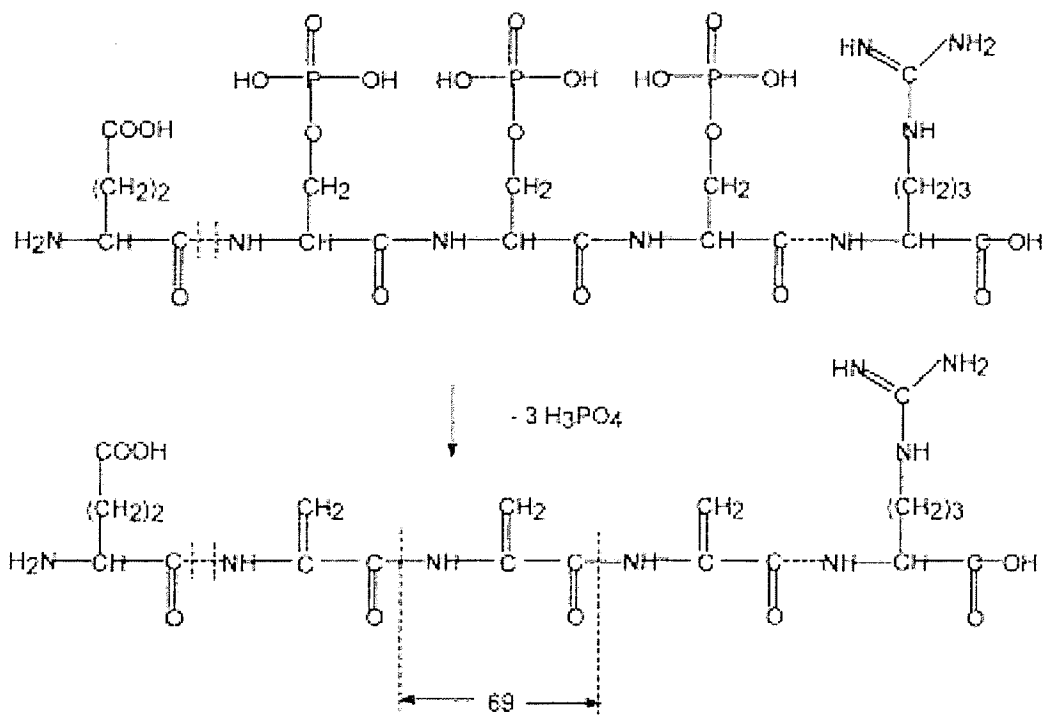


Figure 3.5: Formation of dehydroalanine residues via β -elimination of H_3PO_4

Though c-ions of the segments containing dehydroalanine were found, it was noted that the isotopic distributions were incorrect, as the monoisotopic peak was much smaller than expected (Figure 3.6). Fragment c14, which has no phosphoserine had an observed isotopic distribution which closely matched the calculated envelope. Fragment c15 contains one phosphoserine and appeared as a small peak with only a slight difference in isotopic distribution relative to the theoretical envelope. The c16 fragment also contained one phosphoserine, and was a much larger peak. It showed a drastically different isotopic distribution from the calculated distribution. For peptides of this mass (m/z 1625), monoisotopic peaks should be approximately the same intensity as the $m+1$ peak. Instead, the monoisotopic peak for c16 was found to be only half as large as the $m+1$ peak. The successive c-ions containing phosphoserine residues (c17-c19) also displayed a similar pattern.

The distorted isotopic distribution patterns were attributed to the overlap of two separate but related ion peak distributions: the c-ion series ($b_n + 17$ u) and $b_n + 18$ u ions. The $b_n + 18$ u ion series is attributed to the loss of HPO_3 instead of H_3PO_4 from a phosphoserine, resulting in a serine residue instead of a dehydroalanine. Each ion series present was thus superimposed onto a second ion series. There also exists a possibility for a maximum of four losses of HPO_3 , though as shown from the MS spectrum, the β -elimination of H_3PO_4 is much more likely. As no ions were found which correspond to two losses of HPO_3 ($b_n + 18$ u + 18 u), it is unlikely that any higher losses would be observed for a peptide unless more than four phosphate moieties were present. There were no residues corresponding to serine, as these should have been formed upon the loss of HPO_3 .

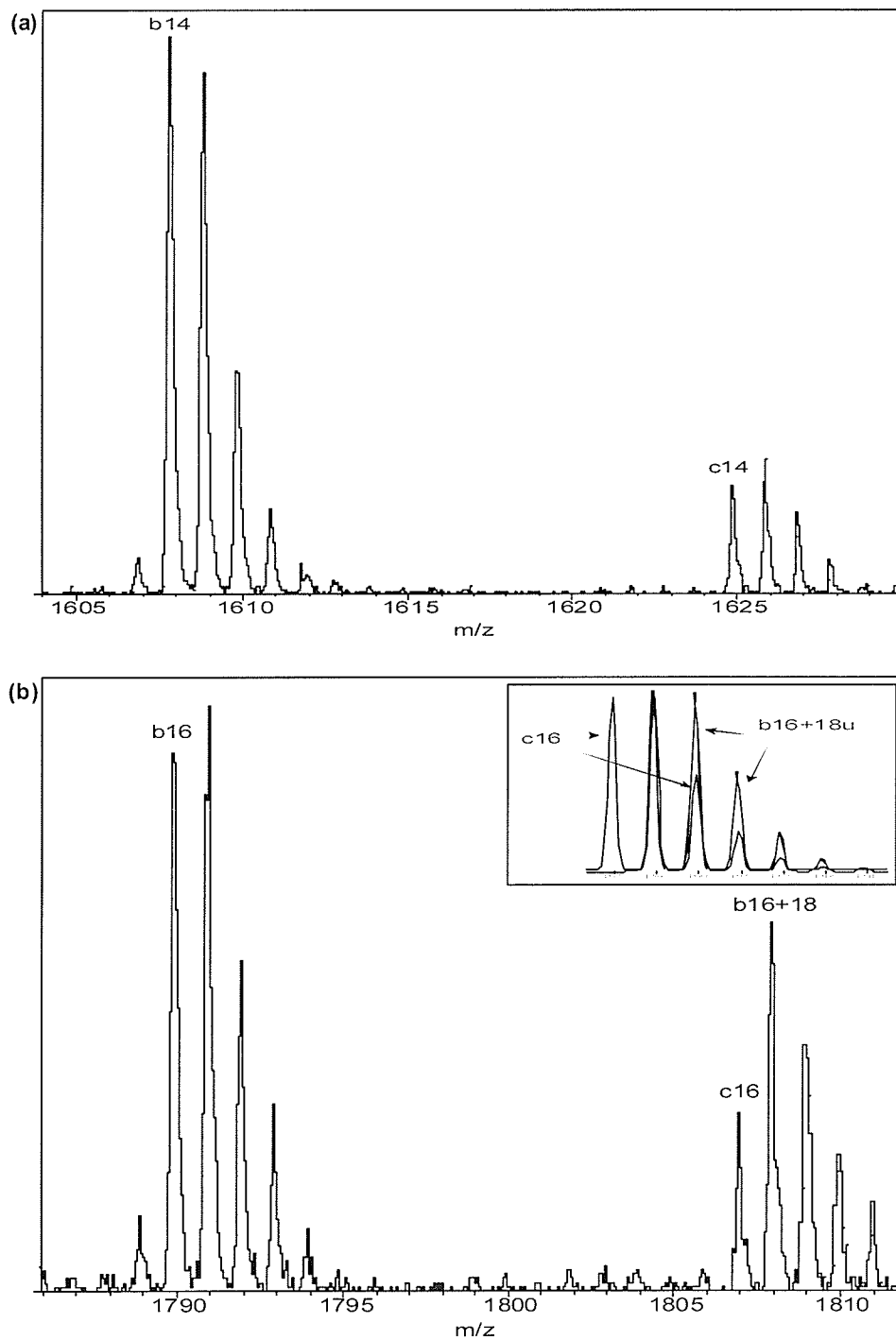


Figure 3.6: Portions of MALDI QqTOF MS/MS spectrum of T1-2 showing isotope distributions of fragments. (a) b14 and c14, containing no phosphorylation sites, and (b) b16 and c16, containing one phosphorylation site, showing b16+18u fragment. The inset shows calculated isotopic distributions and relative contribution for the corresponding c and b+18u ions

3.3.5 MS/MS of metastable decay products

The MS/MS spectrum of phosphorylated T1-2 shows limited fragmentation in the m/z range 2000-2500 as well as the domination of the fragments resulting from the loss of the phosphate groups $[M - nH_3PO_3]^+$. Given the abundance of prompt decay products, the MS/MS of a dephosphorylated prompt decay product may reveal valuable structural information. The absence of the four phosphate moieties results in an ion which is substantially smaller, fragmenting along the backbone rather than by loss of phosphate ion. There will be an expected decrease in the occurrence of b_n+18 and y_n+18 ions, as loss of HPO_3 should not occur. Lastly, if the structural information provided by the MS/MS of the prompt decay product can positively identify the phosphorylation sites, it may prove a useful alternative for future analysis for ions in this range of m/z . Typically, the MS/MS high mass limit for this type of instrument is 3000 m/z . As a result of the loss of the phosphate groups, the dephosphorylated prompt decay product (m/z 2730) falls within the useable mass selection range of the quadrupole, compared to the phosphorylated T1-2 (m/z 3122).

The MS/MS spectrum of $[M+H-4H_3PO_4]^+$ ions showed a clearer fragmentation pattern in the m/z 2000-2500 range than phosphorylated T1-2 (Figure 3.7). The observed b-ion series strongly resembled the MS/MS spectrum of T1-2, with the same omissions of b_9 and b_{23} . The resulting y-ion series was more complete, with better coverage of the high mass region. As expected, dehydroalanine residues were detected.

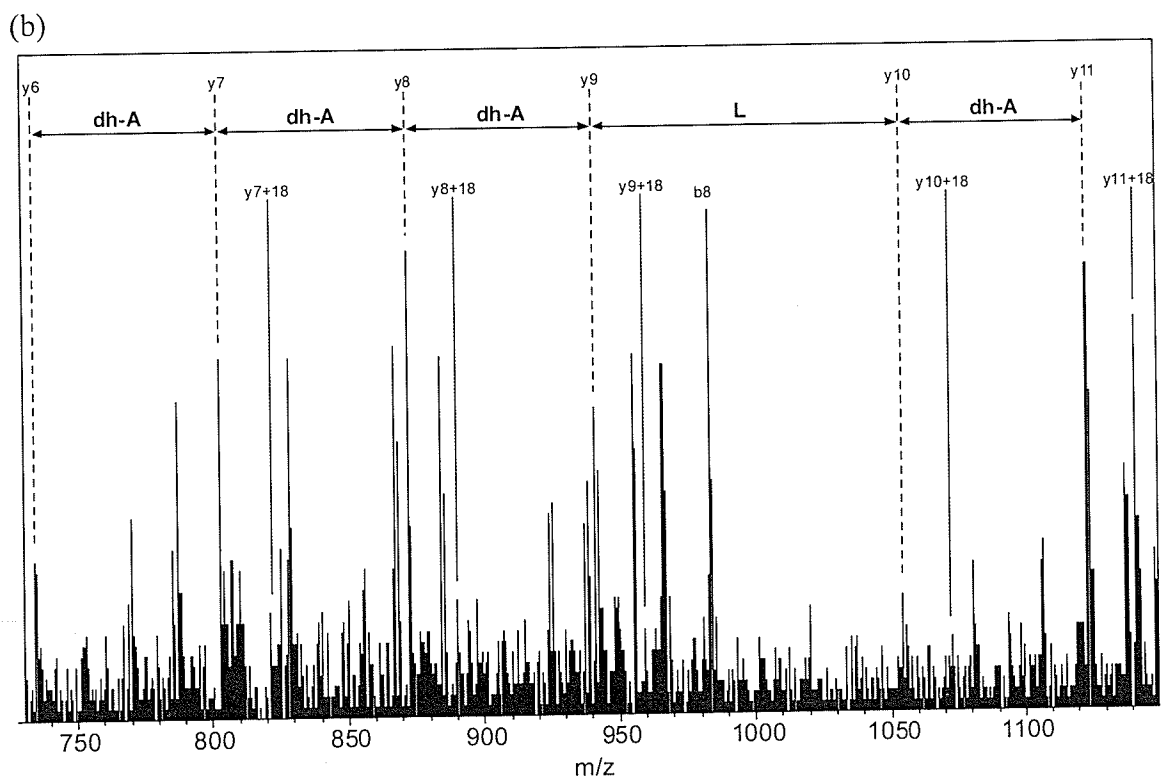
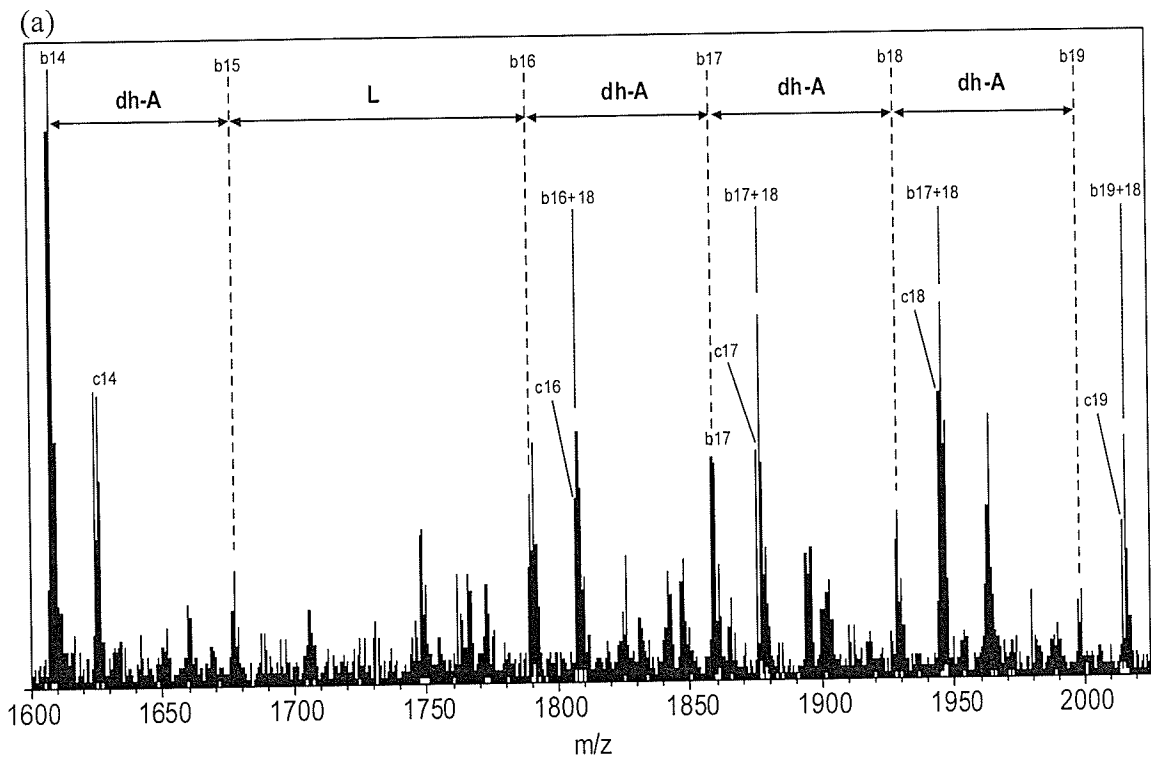


Figure 3.7: MALDI QqTOF MS/MS spectrum of prompt decay product of $[M+H-4 H_3PO_4]^+$ ions showing (a) b-ions and (b) y-ions containing phosphorylation sites

Despite the lack of phosphate residues, b_n+18 and y_n+18 ions were found, though they were present only as minor features. The continued occurrence of these peaks indicates that the observed masses resulting from prompt decay still occur to a small degree from a combination of losses (Figure 3.8) possibly involving rearrangement of the c-terminal [34]. The loss of HPO_3 (m/z 80) from phosphoserine, combined with loss of H_2O (m/z 18) would result in the combined loss of m/z 98 seen in the prompt decay process. The likelihood of this occurring in the collisional damping interface is increased with increasing number of phosphoserines. However, there was no evidence of any preferential loss of HPO_3 from a specific phosphoserine.

The MS/MS spectrum of the dephosphorylated prompt decay product of T1-2 allowed for complete sequencing of the peptide with unambiguous assignments of phosphorylation sites.

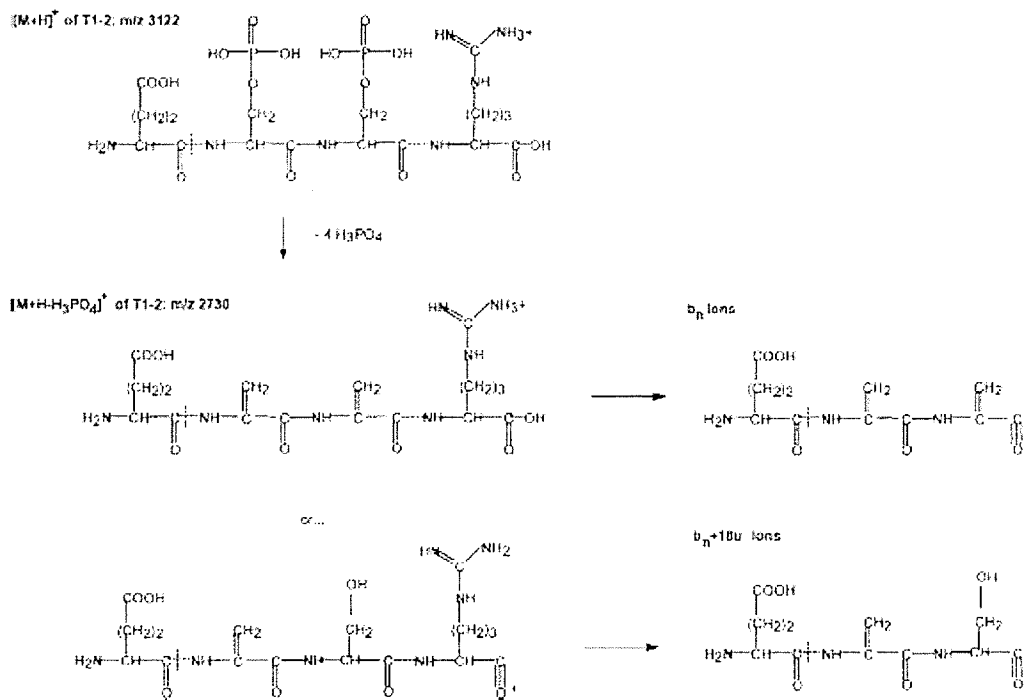


Figure 3.8: Proposed formation of b_n+18 ions in MS/MS of $[M+H-4H_3PO_4]^+$

3.3.6 MS/MS of doubly charged ions

In situations where the mass of the peptide is too large for MS/MS mass selection, the doubly charged ion is often used. The addition of ammonium salts improves the ionization efficiency of doubly charged ions of phosphorylated peptide T1-2.

In the MS/MS spectrum, a dominant peak at m/z 1365 corresponding to $[M+2H-4H_3PO_4]^{2+}$ is found, as well as doubly charged peaks at m/z 1356 and m/z 1374. The former peak correspond to $[M+H-4H_3PO_4 - 18]^{2+}$, while the latter corresponds to $[M+H-3H_3PO_4 - HPO_3]^{2+}$. No other doubly charged ions corresponding to incomplete losses of phosphate such as HPO_3 were found. Because these ions occur only under MS/MS conditions and not in the source, their presence is in agreement with observations made by others [27] stating that phosphate groups are less likely to be lost from doubly charged ions than singly charged ions.

As in the MS/MS of the singly charged T1-2, b- and y-ions dominate the spectrum, with some a- ions also present (Figure 3.9). The b-ions are present from b2 to b21, with a small but discernable peak corresponding to b-9; ions b22-b24 are absent. The y-ion series is nearly complete, with y22 as the only omission. Ion series for b_n+18 and y_n+18 are found for dehydroalanine/serine containing fragments, though they appear with much lower signals. Overall, the results are similar to those obtained by MS/MS of the $[M+H]^+$ ions of T1-2.

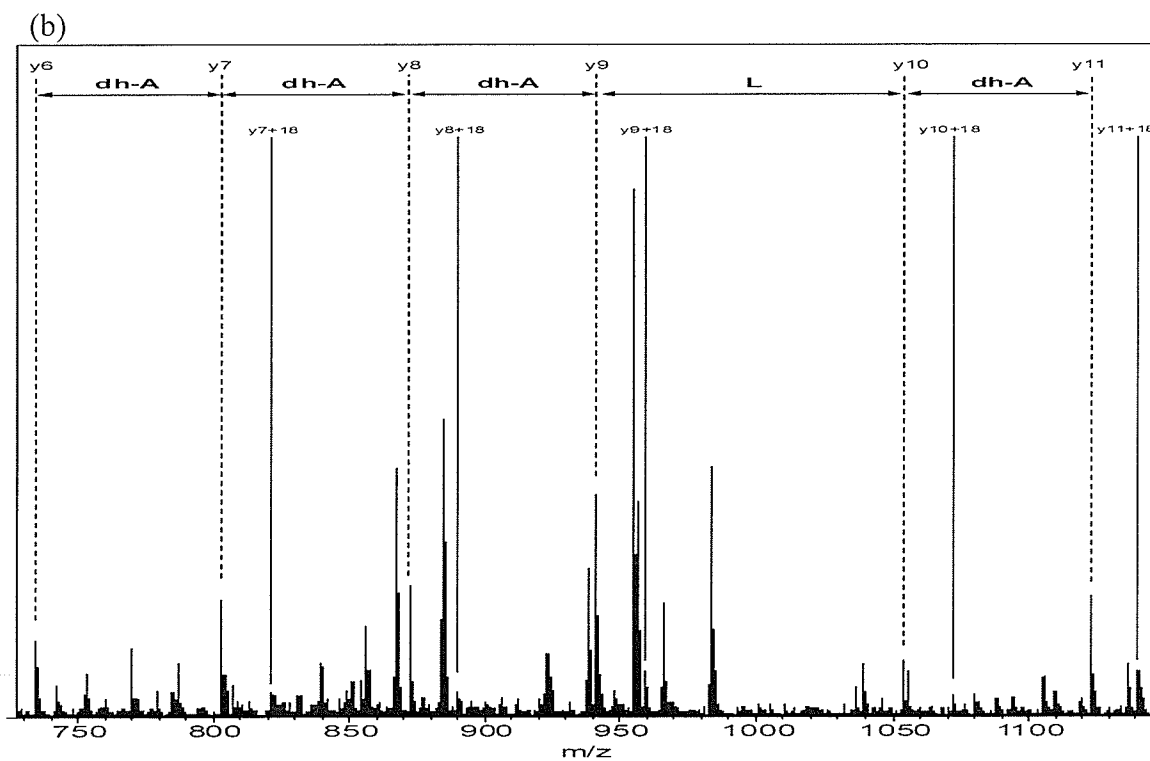
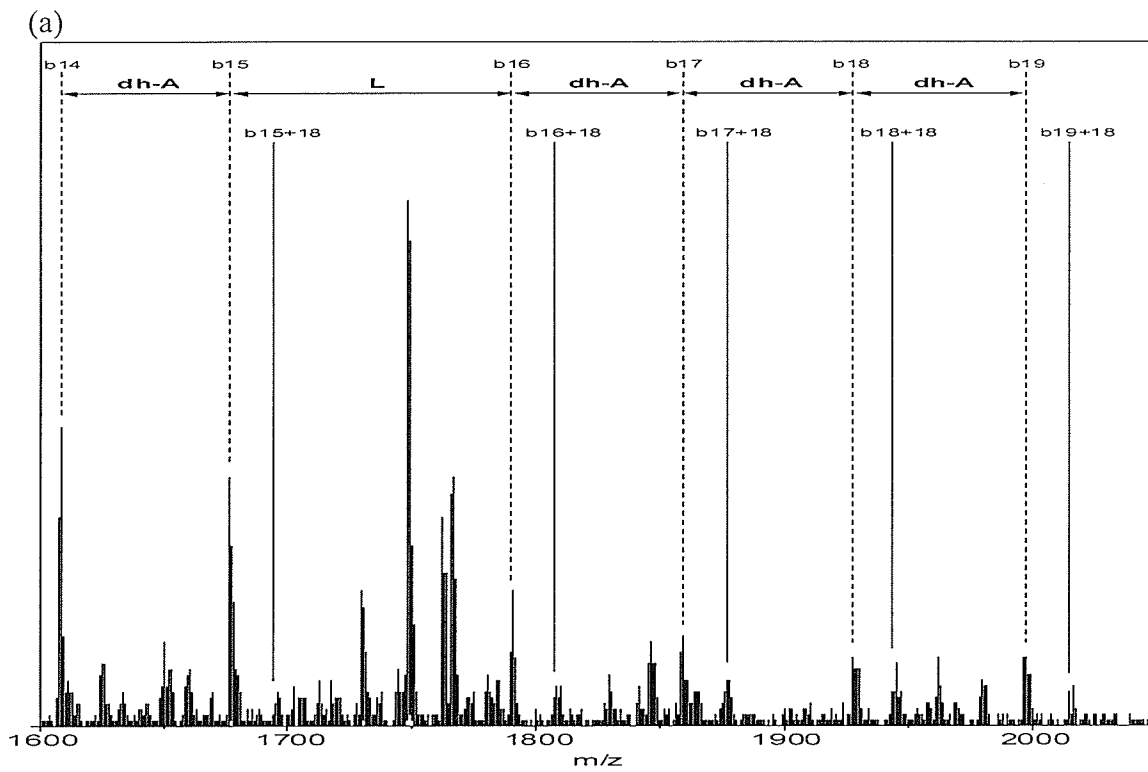


Figure 3.9: MALDI QqTOF MS/MS spectrum of $[M+H]^{2+}$ of T1-2, showing (a) b-ions and (b) y-ions containing phosphorylation sites

3.4 Conclusions

Rapid determination of phosphorylation sites (specifically phosphoserine) by MALDI-QqTOF-MS is possible. On-membrane digestion can provide sufficient digestion to provide peptides suitable for MS/MS.

With the use of ammonium salts, MALDI-QqTOF provides good sensitivity for identifying phosphorylated peptides. Both $[M+H]^+$ and $[M+H]^{2+}$ ions are found in MS spectra.

As an artifact from the collisional damping interface, in-source fragmentation of phosphopeptides may occur. MALDI-MS of tryptic fragment T1-2 of β -casein shows β -elimination of up to four H_3PO_4 groups, as well as the possible of elimination of HPO_3 from serine in source.

The MS/MS of this tryptic fragment reveals the same type of β -elimination of the phosphate residues. Elimination of H_3PO_4 from phosphoserine results in the formation of dehydroalanine residues, while the elimination of HPO_3 results in a serine residue. Consequently, there are overlapping isobaric b- and y-ion series, given the different eliminations possible for each phosphoserine residue. The elimination of H_3PO_4 is much more prevalent than the loss of HPO_3 , making the ion series with dehydroalanine much more dominant than any other ion series. While no b-ion or y-ion series is complete, there is sufficient data to determine the sites of phosphorylation.

The MS/MS spectrum of the $[M+H]^{2+}$ ions gave more complete b- and y-ion series, with a dominant peak for the elimination of all phosphate groups, $[M+H-4H_3PO_4]^+$. Tandem MS of the prompt decay product $[M+H-4H_3PO_4]^+$ proved to be

quite useful. While lower in abundance than the parent ion, the prompt decay product is considerably smaller in mass, hence is mass selectable for MS/MS by most mass spectrometers. Despite having lost all phosphate residues, the prompt decay product still shows overlapping ion series in its MS/MS spectrum. As expected, b- and y-ion series are dominant, with dehydroalanine residues showing where phosphoserine are situated, but the presence of b_n+18 and y_n+18 series is still present. This indicated that the non-specific elimination of HPO_3 from a phosphoserine was still occurring, combined with the elimination of H_2O elsewhere from the peptide. However, we are still able to make unambiguous assignment of the phosphoserine residues.

3.5 References

- [1] Venter, J.C., Adams, M.D., Myers, E/W., Li, P.W., Mural, R.J., Sutton, G.G., Smith, H.O., Yandell, M., Evans, C.A., Holt, R.A. *Science* **291**, 1304 (2001)
- [2] Hunter, T. *Cell* **80**, 225 (1995)
- [3] Krebs, E. G. *Trends Biol. Sci.* **1994**, 19, 439-439.
- [4] Sun H.; Tonka N. K. *Trends Biol. Sci.* **1996**, 19, 480-485.
- [5] Faux M. C.; Scott J. D. *Trends Biol. Sci.* **1996**
- [6] Cohen, P. *Trends Biochem. Sci.* **25**,596 (2000)
- [7] Zolnierowicz, S., Bollen, M. *Embo J* **19**, 483 (2000)
- [8] Manning, G., Whyte, D.B., Martinez, R., Hunter, T., Sudarsanam, S. *Science* **298**, 1912 (2002)
- [9] Alonso, A., Sasin, J., Bottini, N., Friedberg, I., Osterman, A., Godzik, A., Hunter, T., Dixon, J., Mustelin, T. *Cell* **117**, 699 (2004)
- [10] Ambrosio, C.D., Salzano, A.M., Arena, S., Renzone, G., Scaloni, A. *J. Chromatog. B* **849**, 163 (2007)
- [11] de Hoog, C.L., Mann, M. *Annu. Rev. Genomics Hum. Genet.* **5**, 267 (2004)
- [12] Aebersold, R., Mann, M. *Nature* **422**, 198 (2003)
- [13] Steen, H., Mann, M. *Nat. Rev. Mol. Cell Biol.* **5**, 699 (2004)
- [14] Stickmann, A., Meyer, H.E., *Proteomics* **1**, 200 (2001)
- [15] Ficarro, S.B., McClelland, M.L., Stuckenberg, P.T., Burke, D.J., Ross, M.M., Shabanowitz, J., Hunt, D.F., White, F.M. *Nature Biotechnol.* **20**, 301 (2002)
- [16] Hunter, T. *Cell* **100**, 113 (2000)
- [17] Delom, F., Chevet, E., *Proteome Science* **4**,15 (2006)
- [18] Mann, M., Ong, S.-E, Gronborg, M., Steen, H., Jensen, O.N., Pandey, A. *Trends Biotech.* **20**, 261 (2002)
- [19] Annan, R.S., Huddleston, M.J., Verma, R., Deshaies, R.J., Carr, S.A. *Anal. Chem.* **73**, 5387 (2001)

- [20] Liao, P.-C., Leykam, J., Andrews, P.C., Gage, D.A., Allison, J. *Anal. Biochem.* **219**, 9 (1994)
- [21] Craig, A.G., Hoeger, C.A., Miller, C.L., Goedken, T., Rivier, J.E., Fischer, W.H. *Biol. Mass Spectrom.* **23**, 519 (1994)
- [22] Asara, J.M., Allison, J. *J. Am. Soc. Mass Spectrom.* **10**, 35 (1999)
- [23] Ma, Y.L., Lu, Y., Zeng, H.Q., Ron, D., Mo, W.J., Neubert, T.A. *Rapid Commun. Mass Spectrom.* **15**, 1693 (2001)
- [24] Carr, S.A., Huddleston, M.J., Annan, R.S. *Anal. Biochem.* **239**, 180 (1996)
- [25] Neubauer, G., Mann, M. *Anal. Chem.* **71**, 235 (1999)
- [26] DeGnore, J.P., Qin, J. *J. Am. Soc. Mass Spectrom.* **9**, 1175 (1998)
- [27] Qin, J., Chait, B. *Anal. Chem.* **69**, 4002 (1997)
- [28] Annan, R.S., Carr, S.A. *Anal. Chem.* **68**, 3413 (1996)
- [29] McComb, M.E., Oleschuk, R.D., Manley, D.M., Donald, L.J., Chow, A., O'Neil, J.D.J., Duckworth, H.W., Ens, W., Standing, K.G., Perreault, H. *Rapid Commun. Mass Spectrom.* **11**, 1716 (1997)
- [30] Tang, X., Beavis, R.C., Ens, W., Lafortune, F., Schueler, B., Standing, K.G. *Int. J. Mass Spectrom. Ion Processes* **85**, 43 (1998)
- [31] Loboda, A.V., Krutchinsky, A.N., Bromirski, M., Ens, W., Standing, K.G. *Rapid Commun. Mass Spectrom.* **14**, 1047 (2000)
- [32] Zhu, Y.F., Taranenko, N.I., Allman, S.L., Martin, S.A., Haff, L., Chen, C.H. *Rapid Commun. Mass Spectrom.* **10**, 1591 (1996)
- [33] Tholey, A., Reed, J., Lehmann, W.D. *J. Mass Spectrom.* **34**, 117 (1999)
- [34] Thorne, G.C., Ballard, K.D., Gaskell, S.J. *J. Am. Soc. Mass Spectrom.* **1**, 249 (1990)

4 A Comparison of Sheathless Capillary Electrophoresis with LC-ESI-MS and MALDI-MS for Evaluation of Phosphoprotein Mapping

4.1 Introduction

4.1.1 Capillary Electrophoresis

For the analytical sciences, the ability to separate the individual components of a mixture is crucial, as it is very often the only way to perform a thorough and detailed analysis of each compound's structure and function. For the biochemical sciences, the separation of mixtures of biomolecules into constituent components for further analysis is often very difficult, given the complexity of living systems, the chemical similarities of many components, and their often fragile nature.

In 1909, Michaelis separated serum proteins based on their isoelectric points, and coined the term "electrophoresis" [1]. The development of electrophoresis into a separation technique was pioneered in the 1930's by Tiselius who used it to separate serum proteins albumin, and α -, β -, γ -globulins [2]. It was not until 1967 that Hjertén conducted the first separations by capillary electrophoresis, using glass capillaries with a diameter of 3 mm [3].

In capillary electrophoresis, a fused silica capillary is used as an electromigration channel. The ionized silanol groups (SiO^-) of the inner capillary wall attract ionic species from the buffer, forming what is an essentially static positive ionic layer on the capillary wall called the "Inner Helmholtz Plane". As the electrostatic attractive force of positive ions to the silanol groups decreases exponentially with distance, a second positive ionic layer (called the Outer Helmholtz Plane) is formed on top of the Inner Helmholtz Plane (Figure 4.1). Unlike the Inner

Helmholtz Plane, the Outer Helmholtz Plane is not static. Under an applied potential, the ionic layer moves towards the cathode, dragging along the water of hydration with it. Due to the strong hydrogen bonding of water, the entire volume of the capillary migrates towards the cathode, creating the electroosmotic flow (EOF) which drives the bulk movement of solution through the capillary.

One important distinction between pumped flow of a typical analytical HPLC system and the EOF of a capillary electrophoresis system is in the relative velocity of the flow at the walls of the analytical system. Because the Outer Helmholtz Plane along the walls of the capillary moves with the bulk flow of the system, the velocity of the buffer along the walls does not experience significant interaction with the silica wall itself, giving a very uniform flow between the center of the capillary and the walls (Figure 4.2a).

In comparison, traditional pumped flow systems such as in liquid chromatography experience non-uniform flow between the walls and center of any tubing used. Due to friction between liquid and tube walls, flow at the walls experiences drag, causing the formation of a parabolic flow, where analytes moving at the center of the tube flow faster than at the walls (Figure 4.2b). The result is a broadening of the analyte zone causing a loss of resolution in peaks observed.

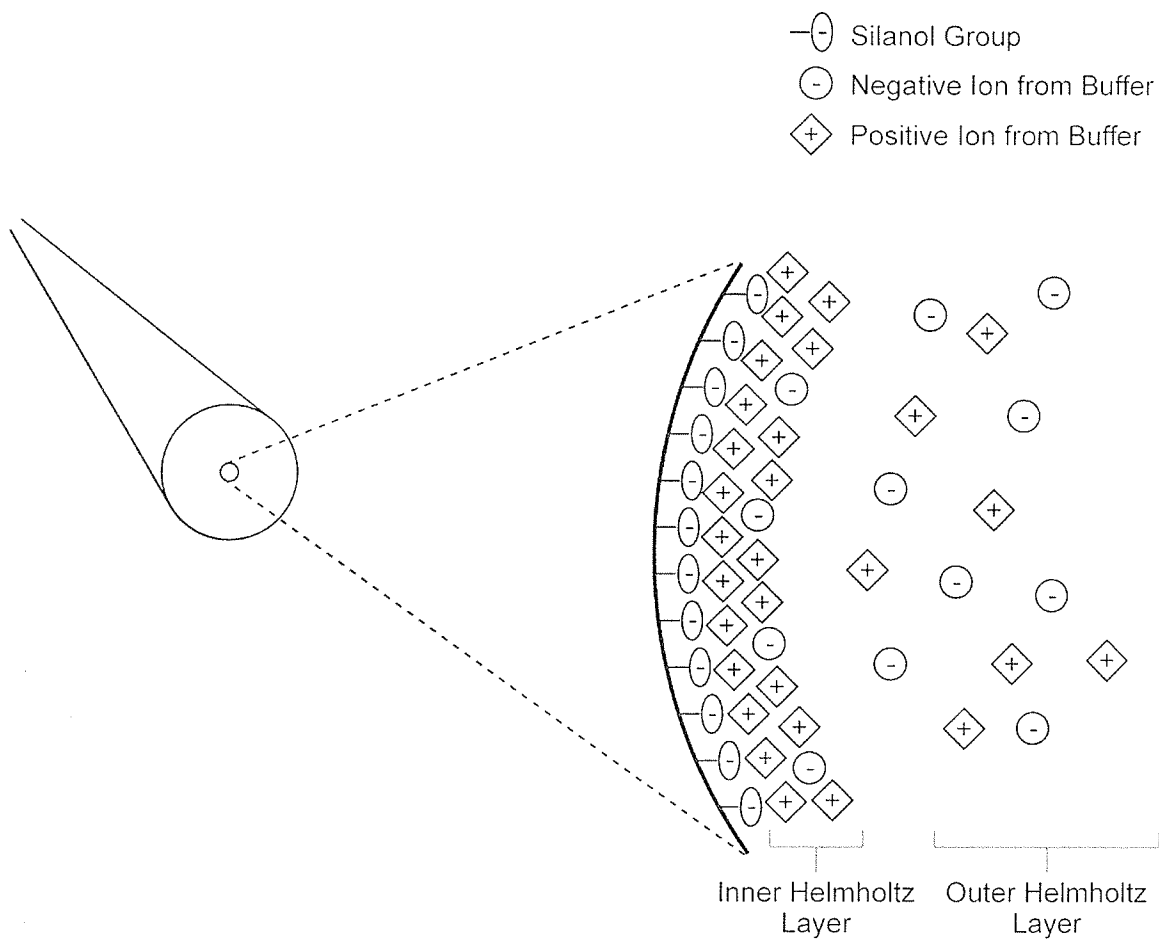
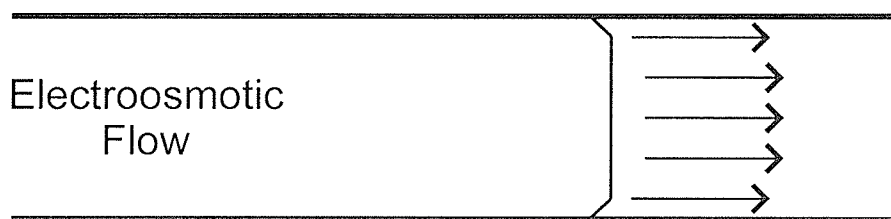


Figure 4.1: Schematic representation of the inner and outer Helmholtz layers of a CE capillary wall

a)



b)

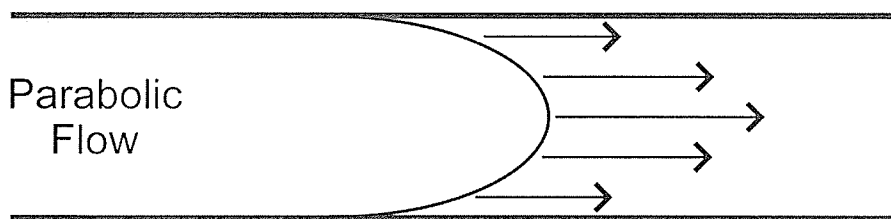


Figure 4.2: Comparison of variable flow velocities at walls and center of capillaries for (a) EOF and (b) Parabolic flow

Under an applied potential, ionic species in solution migrate towards the oppositely charged electrode based upon the electrophoretic mobility (μ) of the species:

$$\mu = q/6\pi\eta r$$

Equation 4.1: Electrophoretic mobility (μ) as a function of particle charge (q), viscosity of the buffer (η), and the Stokes radius (r).

As molecular species will likely have different mobilities due to a combination of characteristics such as charge, size, shape, mass, and presence of counter-ions, they will travel towards the opposite electrode at different velocities. Given enough time (a sufficient capillary length) and difference in electrophoretic mobility, ionic species will resolve themselves into discrete analyte zones (Figure 4.3). Due to the generated EOF moving in one direction, all species regardless if positive, neutral, or negative in charge will be swept forward towards the detector.

The simplest mode of capillary electrophoresis is capillary zone electrophoresis. The basic system is composed of inlet and outlet buffer reservoirs, a high voltage power supply, a fused silica capillary filled with buffer, and a detection system. In normal operating mode, the sample inlet of the capillary is in the same buffer reservoir as the positive electrode from the power supply (Figure 4.4)

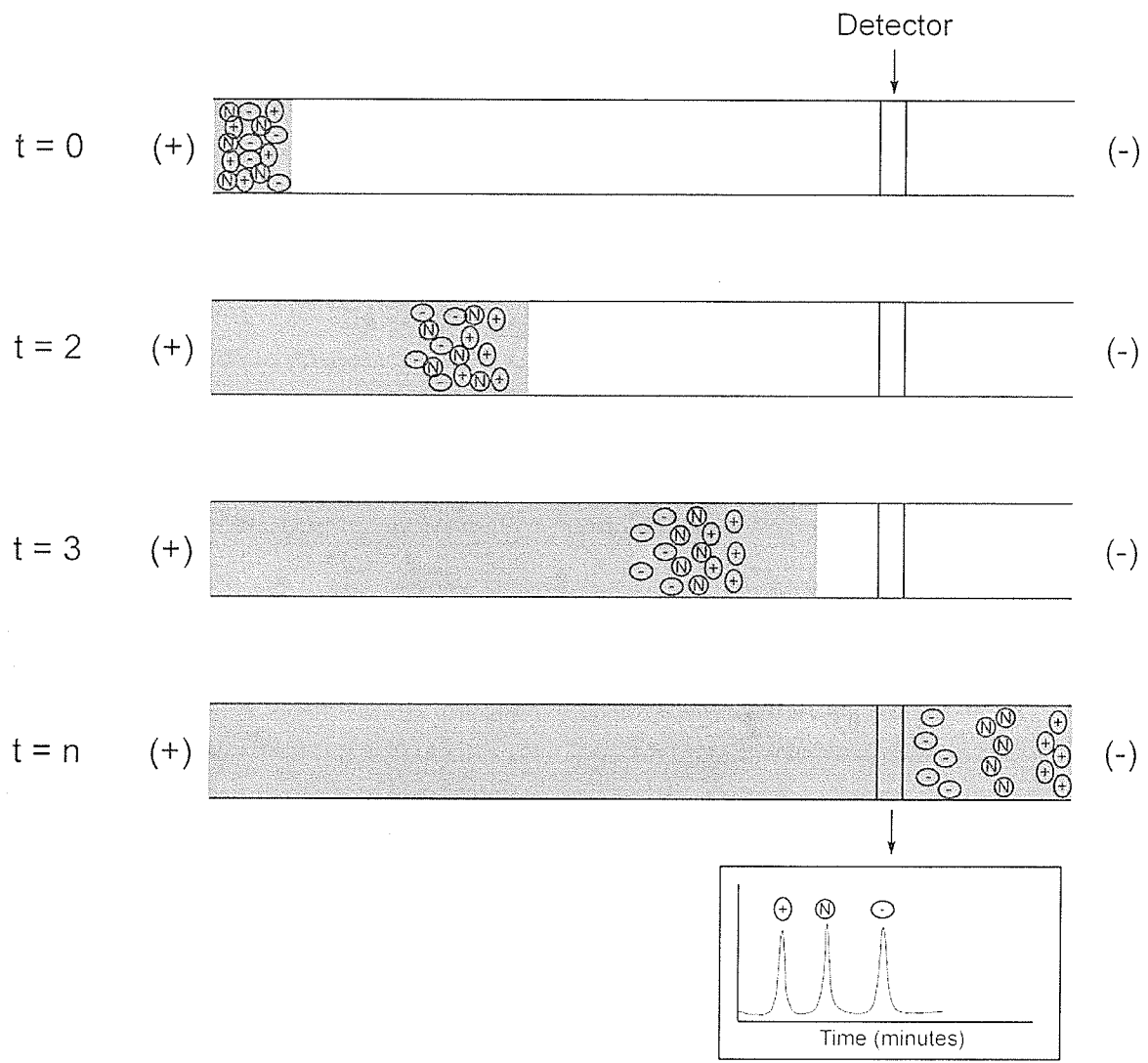


Figure 4.3: Schematic representation of separation of positive, neutral, and negatively charged species by CE

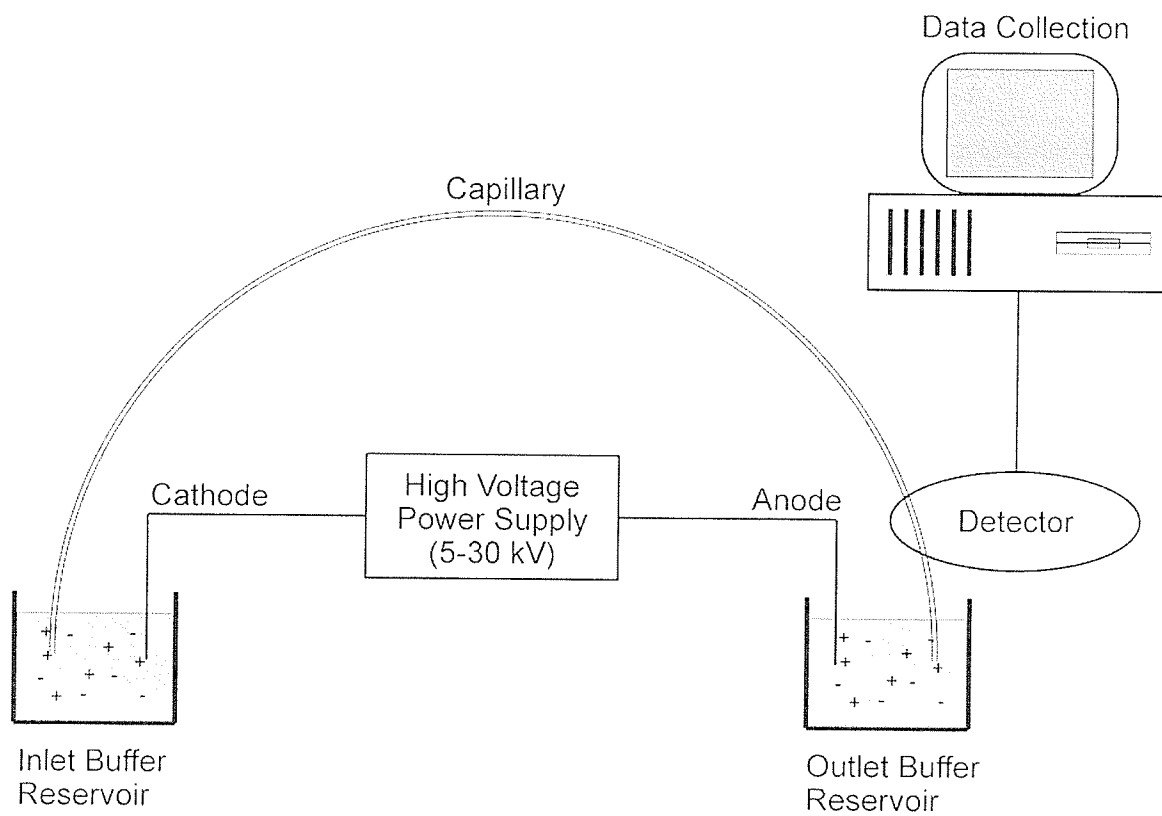


Figure 4.4: Schematic representation of a CE apparatus

As potential is applied, the EOF moves all ions towards the cathode end whereby the ions separate based on their individual mobilities before being detected near the cathode.

Capillary zone electrophoresis is unique in the field of electrophoresis, in that it does not use solid supports to prevent convectonal distortion of the analyte as it migrates. The movement of electrolytes is constrained by the walls of the capillary, though large diameter capillaries suffer from convection currents arising from joule heating.

Though it is more common as a separation method for proteins and peptides, gel electrophoresis is inherently difficult to pair with mass spectrometry. Gels must be excised, de-stained, washed free of interfering buffers, dehydrated to allow for enzymatic digestion of proteins, and finally repetitively swollen and dehydrated to allow for a moderately efficient extraction of the peptides present. In capillary zone electrophoresis, the absence of a solid support in the electrophoretic system makes the technique ideal for separation prior to mass spectrometry analysis of samples.

4.1.2 Interfacing CE to Mass spectrometry

Capillary electrophoresis has been directly interfaced to mass spectrometers via sheath-flow, liquid junction, and sheathless interfaces, all of which use ESI as an ionization method. Offline sample collection methods from CE have been described with MALDI as the mass spectrometry technique used.

4.1.2.1 Sheathless interface

Pioneered by Olivares et al in 1987 [4], the sheathless interface concept is simple. In the original design, the exiting tip of a 100 μm CE capillary was metal coated to provide electrical contact for the ESI potential to be applied (Figure 4.5). As the potential was held lower than the potential on the sample inlet, migration of the analytes still occurred though the overall potential difference from end to end was slightly reduced.

Though high resolution separations were reported by Olivares et al, their system design showed some important limitations. The stability of the electrospray was highly dependent on the buffer system used. Though a methanol/water mixture was originally chosen by Olivares et al for ion mobility of the ammonium salts chosen as test materials, the investigators recognized the unsuitability of using a volatile organic buffer system when working with some heavier compounds. The high organic content resulted in a low surface tension, allowing for lower ESI voltages, but also lowering conductivity, making electrophoresis difficult.

Research conducted by Smith [5a,5b] and Hayarti [6-8] into the parameters required to establish a stable electrospray showed the limit of surface tension and conductivity of a liquid necessary to maintain a stable electrospray. Further research by Chowdhury and Chait [9] showed that ESI of aqueous solutions made with pure water and low acid concentrations are more conducive to some protein applications. They also showed a decrease in electrospray potential when a metal tipped capillary with a sharply tapered end was used.

A variety of different coatings have been attempted to increase the robustness and lifetime of the electrospray tip, using carbon [10,11], polyaniline [12], fairy dust [13] as well as various metal coatings [14-17] though gold or silver coated tips remain the coating of choice due to longer lifetimes. Though a coated capillary end has been the predominant method for establishing electrical contact due to a combination of ease of manufacture, use, and robustness, several variations of establishing electrical contact through means such as wires [18,19], metal jacket liners [20], close proximity to the charged inlet of the mass spectrometer [21], an electrically porous junction [22] have been tested.

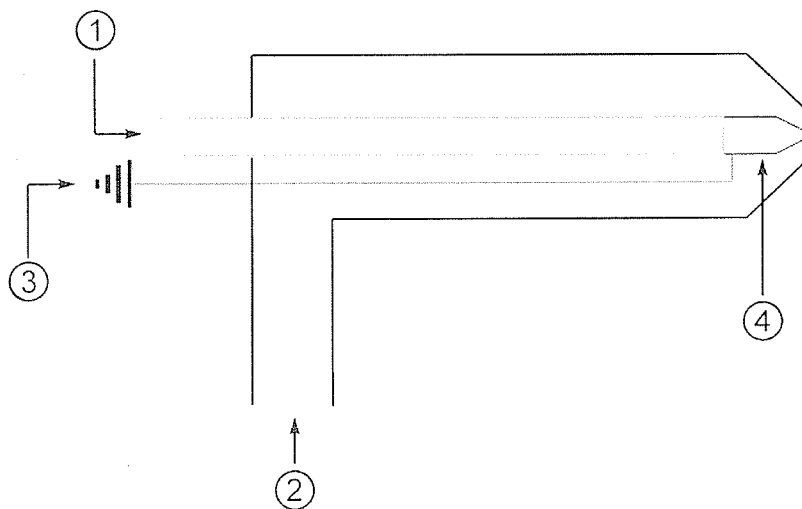


Figure 4.5: Schematic diagram of a sheathless interface, showing (1) tapered CE capillary, (2) nebulizing gas flow inlet, (3) potential applied to the capillary tip, and (4) gold coating on capillary tip to conduct current

4.1.2.2 Liquid Junction Interface

First used by Minard et al. [23] to interface CE with continuous flow fast atom bombardment (cf-FAB), the liquid junction interface has been further developed and refined by Henion et al [24,25] for CE-MS.

The CE-MS liquid junction interface is composed of a separation capillary, buffer reservoir, and a transfer capillary (Figure 4.6). The ends of the separation capillary and a conductive transfer capillary are aligned within 10-20 μm in a liquid buffer reservoir. To achieve ESI, the electrospray potential is applied to the liquid reservoir. Through a combination of mild vacuum resulting from the nebulizing gas flow around the tip of the transfer capillary, and pressure from the height of the buffer reservoir, flow is generated from the reservoir into the transfer capillary. As the ends of the capillary segments are close together, analytes elute from the separation capillary, are drawn into the transfer capillary, and electrosprayed towards the analyzer.

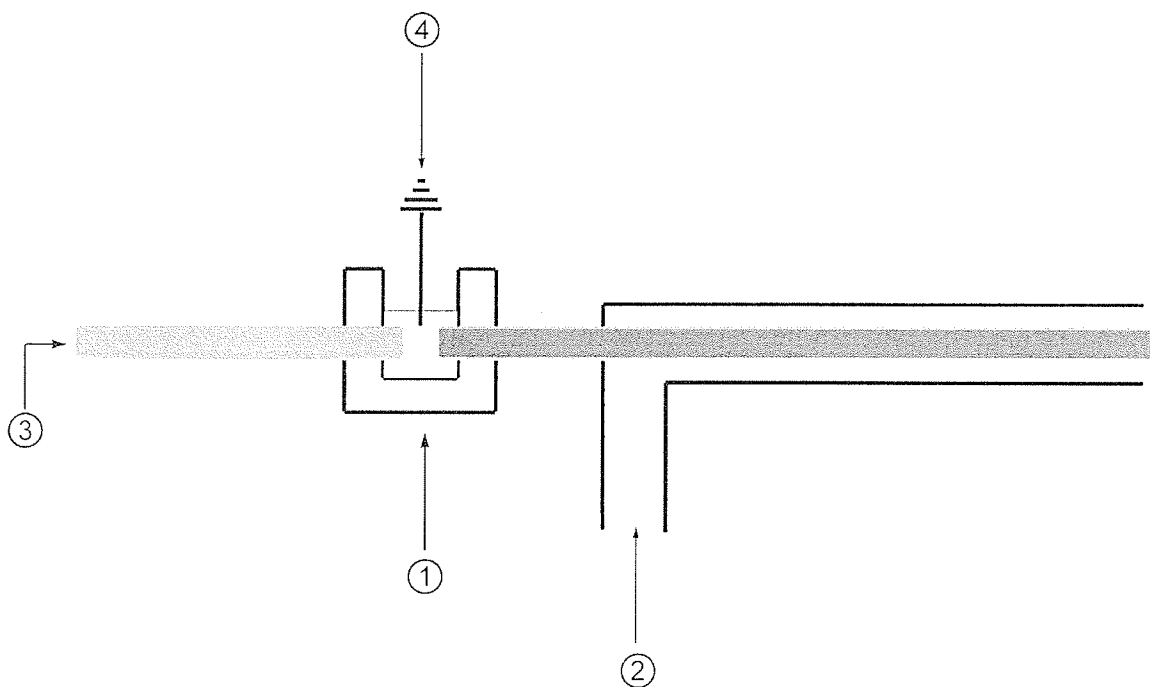


Figure 4.6: Schematic diagram of a liquid junction interface, showing (1) liquid junction interface, (2) nebulizing gas flow inlet, (3) CE capillary with buffer (4) potential applied to the liquid junction interface

4.1.2.3 Sheath-flow Interface

Originally pioneered by Smith et al [26-28], the co-axial sheath-flow interface is the most commonly used interface to date, largely due to the robustness of the design and the stable electrospray achieved.

The design consists of a sheath tube surrounding the sample outlet end of the separation capillary. A sheath liquid with electrolyte content is pumped into the sheath, surrounding the CE capillary and contacting the end of the capillary, allowing mixing with the separation buffer and enabling electrical contact (Figure 4.7). An electrospray potential is applied to the sheath tube, which conducts through the sheath liquids to allow for the formation of the Taylor cone at the end of the separation capillary. As ESI draws liquid from the capillary end, sheath liquid must be infused at a constant rate sufficient to maintain electric contact. The relative dimensions of separation to sheath capillary have been shown to affect sensitivity [29]

Sheath liquid compositions typically range from 60%-80% organic solvent such as methanol, acetonitrile, or isopropanol, with the addition of a small component of acid such as acetic acid or formic acid. Flow rates which match the electrospray requirements are typically in the 1-3 $\mu\text{L}/\text{min}$ range [30].

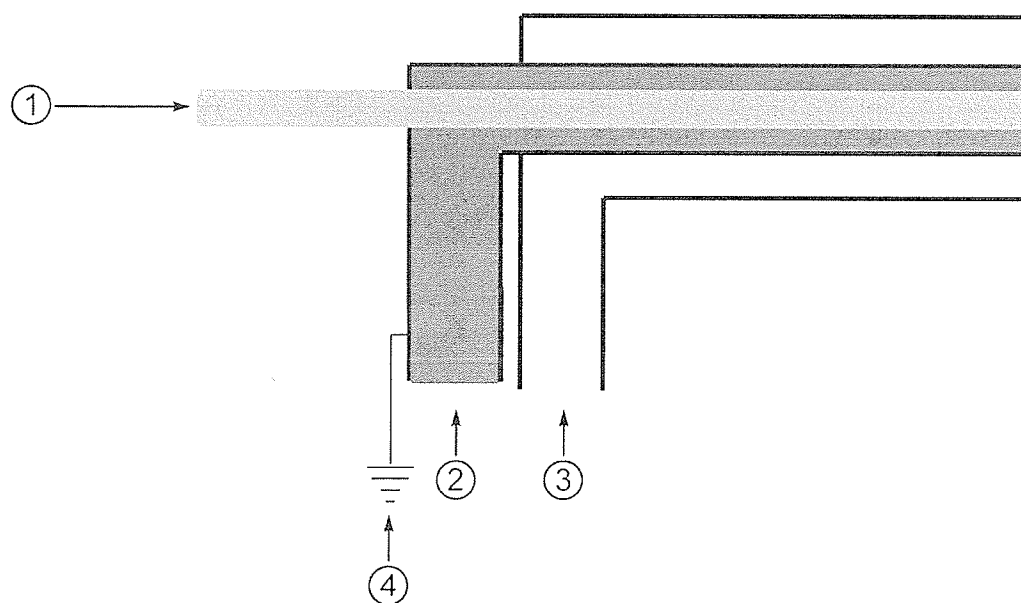


Figure 4.7: Schematic diagram of a sheathflow interface, showing (1) CE capillary, (2) conductive sheathflow liquid surrounding the CE capillary, (3) nebulizing gas (4) potential applied to the sheathflow tube

4.1.2.4 Comparison of Interface Designs

Each design presented has its own inherent strengths and weaknesses, and should be chosen to suit the user's specific needs with regards to available instrumentation, resources, and sample specific issues.

Of the interfaces described, the sheathless interface is the one leading to the highest MS sensitivity, because no external liquid is introduced to establish electrical contact and conductivity, which would dilute the sample and reduce signal [31,32]. Results reported by Kelly et al. [33] show a 10-fold increase in sensitivity of a sheathless interface over a sheathflow interface.

With a sheathless interface the difficulty lies in establishing a stable electrospray for many types of assay. In situations where the electroosmotic flow is insufficient to make up the liquid required for ESI, or if the electrolyte system requires the addition of volatile organic solvents to reduce surface tension or dilute electrolytes to achieve ESI, a sheathless system will not function. The lack of constant flow resulting from EOF can create an unstable electrospray, giving poor results.

Between the co-axial sheath-flow and liquid junction interfaces, it is generally accepted that the sheath-flow system is more reliable and convenient to use, with some evidence of slightly better signal to noise ratio as well as separation. Liquid junction interfaces have a loss of sample and dilution of peak shape during the transfer of sample from separation capillary to transfer capillary in the liquid junction reservoir.

The greatest hurdle with a sheathless interface is the reliance upon a metal coated CE tip from which to generate the electrospray. There has been no durable

method for establishing a permanent metal coating upon the tip of a fused silica capillary. The high voltages applied for ESI cause the metal to strip away, causing eventual loss of electrical contact with the sample.

Sheath-flow interfaces are the most commonly used design, largely because they are easy to use. From a hardware standpoint, it is much easier to establish a permanent sheath-flow setup than to metal-coat CE capillaries and replace them frequently. The use of a sheath liquid allows for the ESI of a wide range of buffers, with a fairly consistent electrospray voltage.

However, the sheath-flow design does have some drawbacks that users need to be aware of. The mixing of the sheath liquid with the running buffer can lead to the introduction of ions from the sheath liquid back into the separation capillary. The movement of counterions from the sheath liquid into the capillary can result in the formation of ionic boundaries which can influence analyte separation, migration times, and overall resolution. In severe cases, changes in the migration order of analytes can be observed. Therefore a choice of sheath liquid should be based on the relative ionic mobility of its components versus the ionic mobility of the separation buffer. This problem can also be solved by the addition of a small amount of hydraulic pressure from the sample inlet of the CE capillary to drive all components forward at rate faster than the ionic mobility of the sheath liquid [34].

Though the liquid junction interface has been shown to be useful, it has not been widely adopted. The primary drawback lies in the greater inconvenience of the liquid junction interface compared to the sheath-flow interface. Establishing the optimum spacing of the capillaries via a microscope is difficult. Combined with

possible loss of sensitivity, resolution and contamination of the junction buffer are all possible issues which may limit adoption of the system.

4.1.2.5 Mass spectrometers suitable for CE

Though any mass spectrometer with the ability to accept ions from an atmospheric pressure source will be able to detect ions from a CE-ESI source, there are some issues to consider with regards to sensitivity and data acquisition.

The use of micro-capillaries in CE was introduced to efficiently decrease the sample volume required, allowing the user to concentrate the sample, but also to maintain a proportionately large path length for optical detection relative to the volume. This gives micro-capillary systems an advantage in sensitivity compared to larger capillaries.

In limiting sample volumes to the nanolitre range however, the eluted peaks are also commensurately small in volume and hence short in duration as they are eluted. Capillary electrophoresis is well known for its sharp, narrow peaks eluting in time spans of only a few seconds. Though this is adequate for optical detection systems which commonly measure at 0.10 second intervals, when coupled to a mass spectrometer via a continuous flow ionization source, it may become problematic.

Mass spectrometers can be classified into two distinct categories based upon how the ions are detected: scanning type mass spectrometers and pulsed mass spectrometers. Scanning mass spectrometer designs include ion traps, magnetic sector, and quadrupole mass spectrometers. Pulsed mass spectrometers include time-

of-flight and fourier transform ion cyclootron resonance (FT-ICR) instruments, detect ions in parallel.

Pulsed mass spectrometers determine the m/z values of all ions within a short time frame, giving almost simultaneous detection of all ions. Most commonly seen in TOF instruments, the time frame between the accelerating potential pulse and detection is conveniently measured in milliseconds. For all practical purposes, this gives the analyst immediate and simultaneous detection of all ions present before the next portion of sample from a continuous ionization source is introduced into the modulating region [35-38].

In contrast, scanning mass spectrometers scan through peaks in the desired m/z range within a desired period of time which will affect the resolution of the spectra. For adequate quality data for biological applications, scans covering a range of 2000 m/z in 6 seconds on a quadrupole instrument generally provide isotopic resolution.

A comparison of CE elution time spans with scan times of a scanning mass spectrometer illustrates the potential difficulties in interfacing CE with a mass spectrometer [39,40]. During the scan time over a relatively small mass range, it is possible that narrow peaks of interest may elute without being detected. It is also possible that minor components will only be partially detected and characterized, showing a truncation of the peak. Interfacing CE with scanning mass spectrometers is more practical for applications with small m/z ranges or when high resolution spectra or electropherograms are not required.

The goal of our research was to evaluate a CE-MS system for the identification of phosphorylated peptides from a proteolytic digestion. Phosphorylated peptides exhibit reduced sensitivity in comparison to their non-phosphorylated counterparts in positive electrospray ionization mode, due to the negative charging of the phosphate moieties. For this reason, I decided to fabricate a sheathless CZE-ESI emitter for interfacing with a prototype orthogonal acceleration (oa) TOF instrument to exploit the full potential of both separation and detection systems [41]. The second part of the research was to evaluate the efficacy of CZE-ESI-*oa*-TOF in the separation and detection of a proteolytic digest in comparison with a commercially available LC-MS system for the detection of the phosphopeptide of interest. Also compared were the contents of on-membrane digests [42] of protein on polyurethane membrane (PU) which had been profiled by MALDI-TOF shown to be a reliable method for detecting phosphopeptides [43].

4.2 Experimental

4.2.1 Materials and Method

A non-porous ether type polyurethane membrane, 25 μm thickness, was used as sample substrate for on-membrane digestion, having been washed with methanol prior to use. Samples of β -casein were dissolved in 10 mM ammonium bicarbonate and deposited onto the membrane surface with a Pipetteman and allowed to dry. Approximately 50 pmol of β -casein was deposited onto the PU surface.

To digest the protein, 5 μl of trypsin solution (~ 0.01 mg/ml) was applied to the dried sample spot and digestion was allowed to take place for 15 minutes. Digestion was stopped by the addition of 1 μl of glacial acetic acid, and the sample was allowed to dry. Digested samples were washed twice to remove salts and allowed to dry before the addition of matrix.

Digests of β -casein for CE-MS and HPLC-MS were prepared by digestion of 0.4 mg/ml of β -casein in ammonium acetate buffer with ~ 0.01 mg/ml trypsin solution for 24 hours at 37° C. HPLC-MS analysis of digestion products was performed on a Hewlett Packard Series 1100 HPLC interfaced with a Micromass Quattro LC triple quadrupole mass spectrometer using a 20 μl injection. Since the flow rate of the HPLC was not compatible with the ESI interface of the mass spectrometer, a split-flow was placed between the HPLC and mass spectrometer, giving a flow rate of 50 $\mu\text{l}/\text{min}$ (1:19 flow ratio) reducing the effective sample injection to 1 μl of protein digest. Scans ranged from 500-3500 m/z over a period of 8 seconds.

Sheathless capillary electrophoresis results were obtained on an in-house built CE system. Fused silica capillaries (Polymicro Technologies) were made using 375 μm OD, 50 μm ID, one meter lengths. Tapered capillary ends were made by hand, by pulling the end to a taper in a flame, cutting the tip to give an approximate internal diameter of 1 μm before etching in 30% hydrofluoric acid. The shaped capillaries were gold coated by vapour deposition with an in-house built vapour deposition system.

CE-MS data were acquired using a Spellman CZE power supply with 4% acetic acid as the buffer solution. Approximately 50 nl of sample was injected into the capillary before being separated and electrosprayed. Mass spectrometry data were acquired on an in-house built oa-reflecting-TOF mass spectrometer (Manitoba TOF III, Dept. of Physics, University of Manitoba).

4.3 Results and Discussion

4.3.1 MALDI-TOFMS

Optimization of on-membrane digestion conditions resulted in largely incomplete digestions, though complete coverage of the protein sequence was available (Figure 4.8). In performing the optimization of the digestion conditions, it was noted that among the most important parameters was the choice of digestion buffer. Though the use of PU membranes allows for the incorporation of subsequent wash steps to remove salt impurities from the sample, trace levels may still be left behind. In the case of TRIS buffer, it appears that despite the use of dilute buffer

solutions of 10 mM, two wash steps were inadequate to remove enough buffer to allow for MALDI-TOF, as most peptides are not detected due to the charge suppression effects (Figure 4.9).

In contrast, ammonium salts have been shown to enhance the ionization of phosphorylated peptides such as those found in β -casein digests. In addition, the presence of ammonium salts does not suppress the ionization of other peptides, making these salts ideal for use with MALDI. However, excessive concentrations of ammonium salts were found to interfere with peptide retention to the PU membrane. In situations where large amounts of ammonium salts were found remaining on the membrane surface after deposition and drying, subsequent washing removed the majority of peptides. It is believed that the excessive presence of salts in dried samples competes for space with the relatively small amounts of protein on the PU membrane surface. Salts occupying the surface of the membrane will prevent adhesion of the peptides, hence subsequent washing steps will remove most peptides.

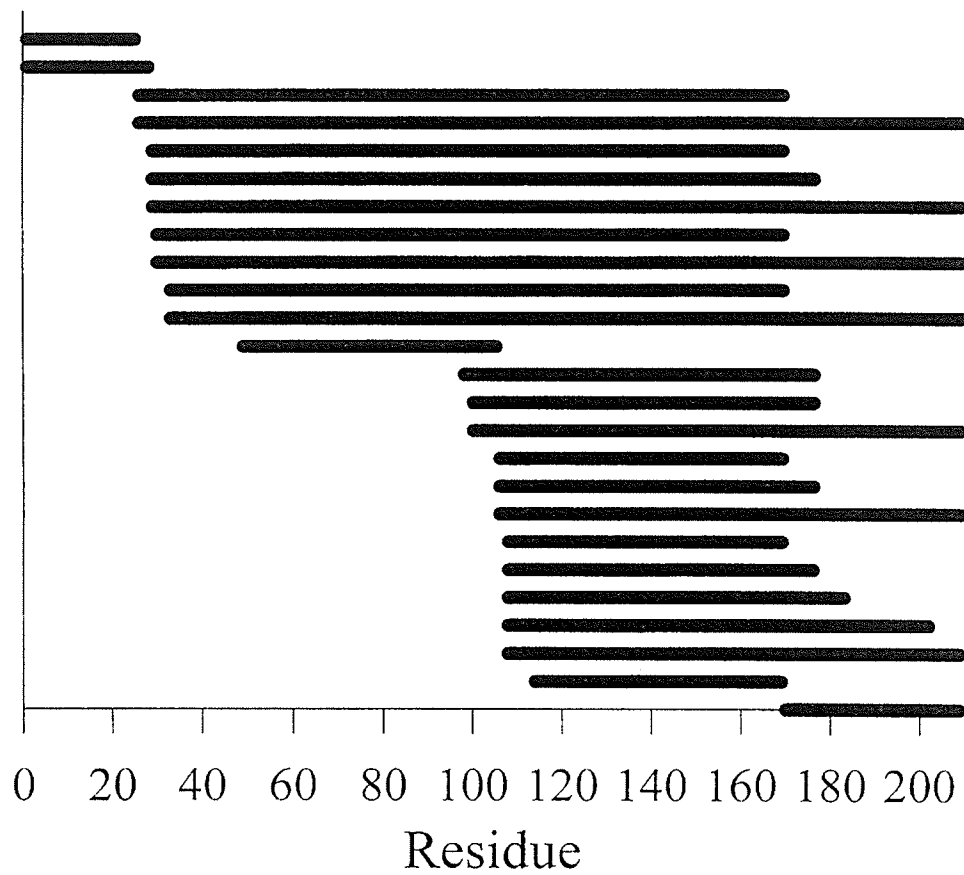


Figure 4.8: Peptide map of β -casein generated by MALDI-MS of on-membrane digestion products

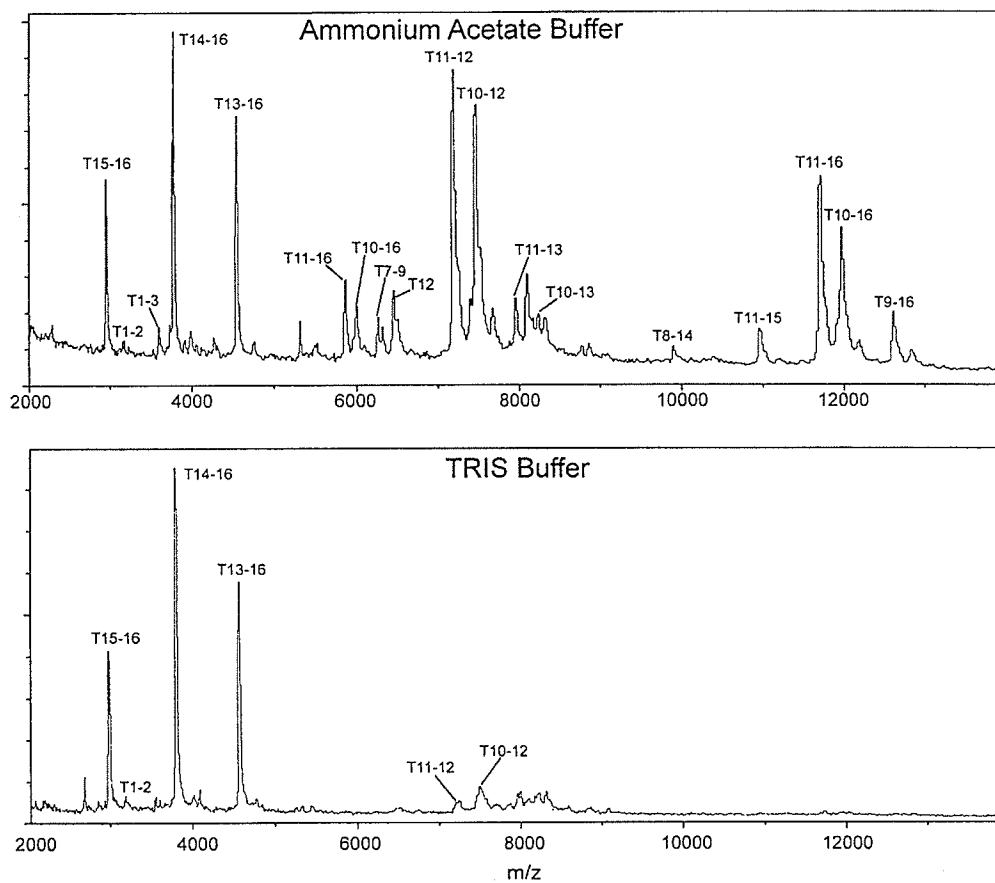


Figure 4.9: Comparison of MALDI spectra of on-membrane digestion products following ammonium acetate buffer digestion (top) and a TRIS buffer digestion (bottom). Both samples were washed as per experimental protocol

4.3.2 HPLC-MS

Data from the total ion chromatogram obtained for the β -casein digest show a number of peaks separated over the duration of the run (40 minutes) (Figure 4.10). Though elution of peptides shows some extent of separation of the components, tetraphosphorylated peptide (T1-2) was not detected. Given the negative charge associated with the phosphoserine residues, it is likely that a positively charged state could not be achieved for that peptide. The selected ion chromatograms show separation of peptides with good signal to noise ratios, as well as peak shapes. Peak widths are typically 30-45 seconds, implying that the peaks are not completely characterized due to the long scan times involved with a quadrupole instrument. The inadequate number of data points per peak gives them a very sharp appearance (Figure 4.11). More data points (i.e. scans) would be needed to define the peaks entirely.

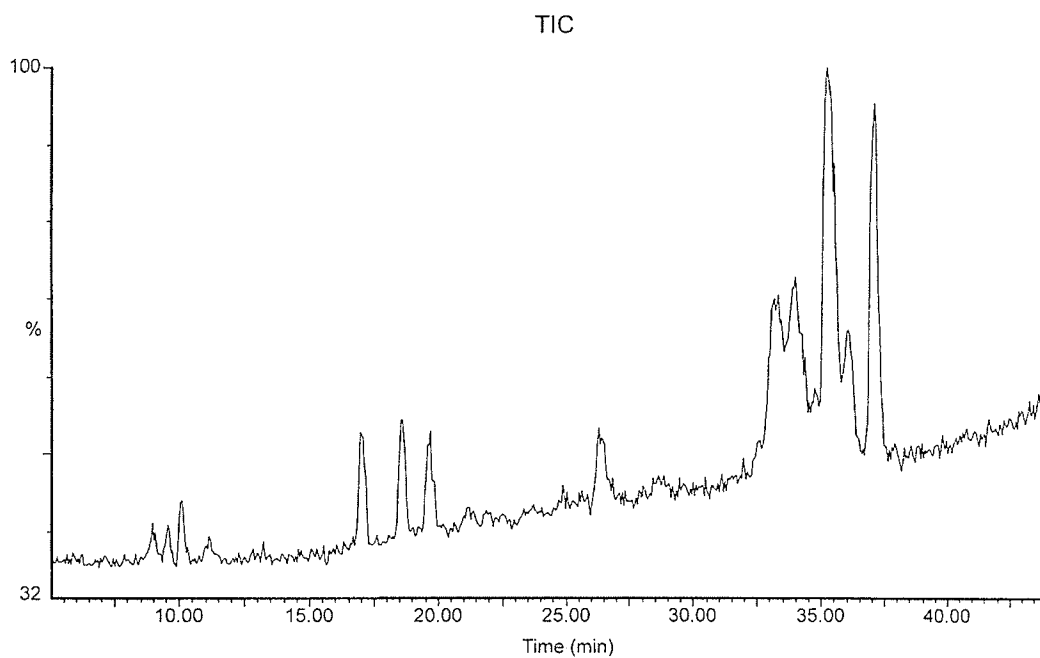


Figure 4.10: Total ion chromatogram of HPLC-MS of β -casein tryptic digest from Micromass Quattro LC triple quadrupole mass spectrometer.

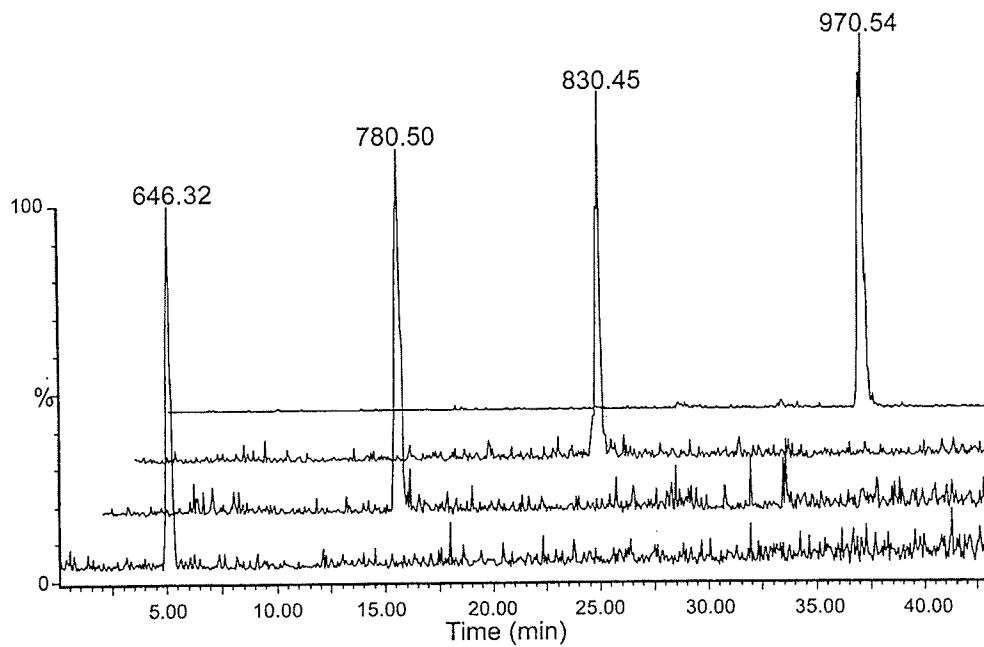


Figure 11: Selected Ion Chromatograms of HPLC-MS of β -casein digestion products from Micromass Quattro LC triple quadrupole mass spectrometer.

4.3.3 CE-TOF Compared with HPLC-MS

The total ion electropherogram was relatively short, lasting only 15 minutes until peptides were no longer detected (Figure 4.12). Most peaks were found to be eluted after 10 minutes, which was followed by a short period where electrospray was interrupted by electrical instability before resuming again. A comparison of the same selected ion electropherograms as shown in Figure 4.11 shows elution over a period of two minutes. Signal to noise ratios of selected ion electropherograms were better than in the HPLC-MS data, with the peaks better characterized (Figure 4.13) due to faster duty cycles.

The use of the oa-reTOF mass analyzer also showed better sensitivity and mass resolution than the triple quadrupole analyzer. Isotopic resolution on the triple quadrupole was possible, though unlikely in practice given the large mass range to scan, as well as the scan rate. Shown is a comparison of the signal to noise ratios of HPLC-MS and CE-TOFMS spectra obtained for the same peptide (Figure 4.14). Though the computer identifies the second isotopic peak in the HPLC-MS results, the peak is not baseline resolved. In contrast, the CE-TOFMS results show full baseline resolution of the isotopic peaks for the same peptide, with a much better signal to noise ratio. This is due to the sensitive TOF instrument, as well as efficient ionization at the sheathless interface. The CE-TOF combination allowed for the detection of sufficient peptides for a nearly complete peptide map, with only one tryptic peptide undetected (Figure 4.15).

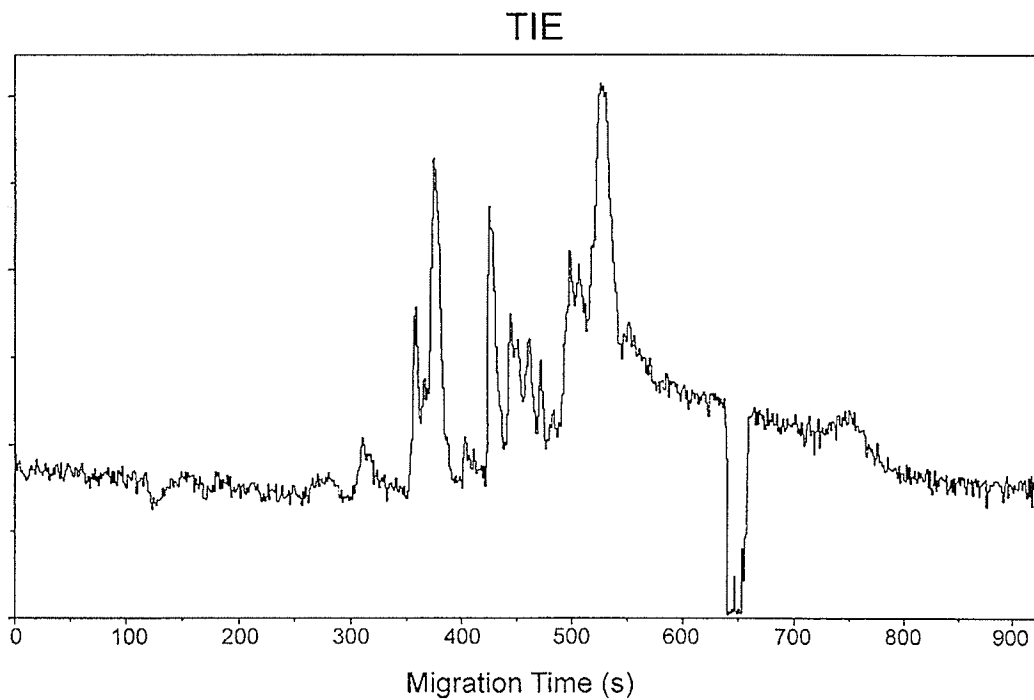


Figure 4.12: Total ion electropherogram of sheathless electrospray CE of β -casein digest obtained on an oa-re-TOF

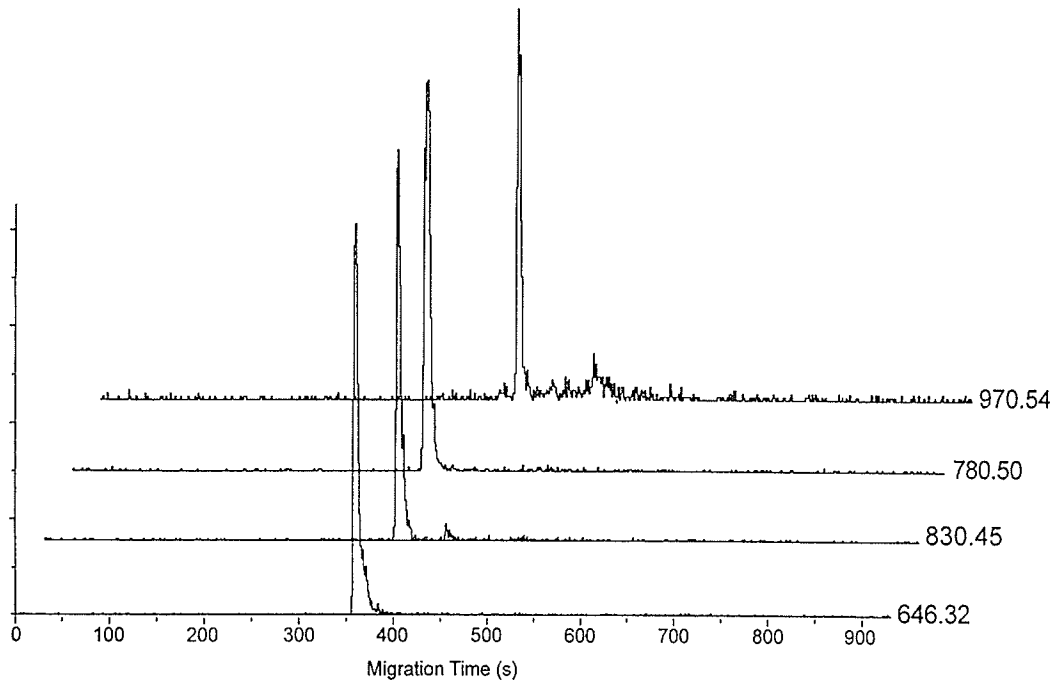


Figure 4.13: Selected ion electropherograms obtained from CE-TOFMS of β -casein digestion products obtained on an oa-re-TOF

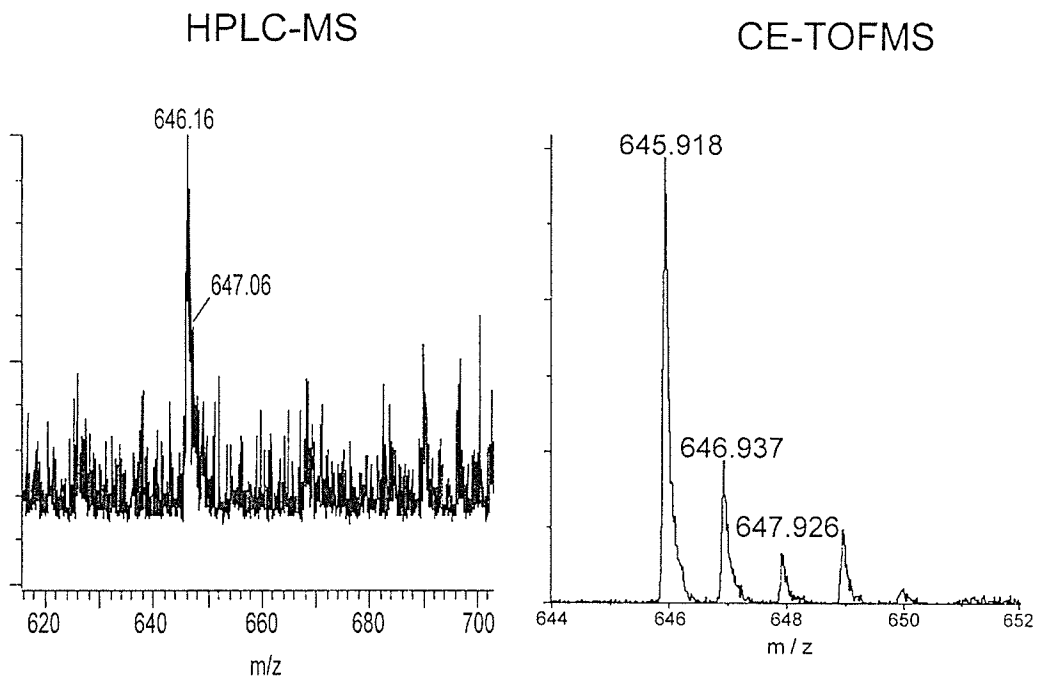


Figure 4.14: Comparison of sensitivity and resolution of HPLC-ESI-MS and CE-TOFMS

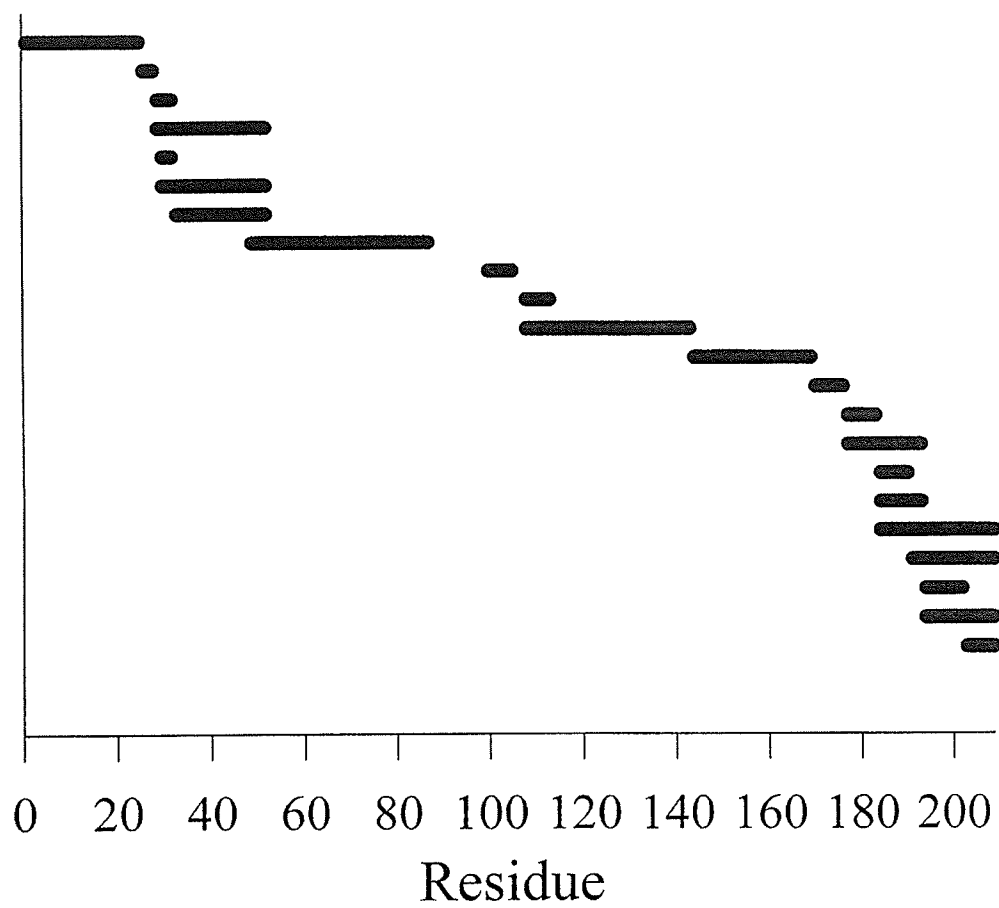


Figure 4.15: Peptide map of β -casein generated by CE-TOFMS of in-solution digestion products

The drawback to the sheathless system was the reliability of the fabrication process as well as the short durability of the metal coated tip. The tapering of the fused silica by hand yielded very few tips meeting the criteria for taper and inner diameter, as well as the cutting of the tip to give the correct internal diameter to the capillary opening. The vapour deposited gold layer was not sufficiently durable for critical analysis. Over the period of time an assay could be expected to take, the gold coating often peeled from the capillary, resulting in loss of electrical contact, rendering the capillary unusable.

4.4 Conclusion

Rapid on-membrane digestion of β -casein shows incomplete digestion of the protein, but complete sequence coverage is seen. In solution digests yielded smaller peptides, but yielded incomplete sequence coverage. Some peptides from the on-membrane digestion were sufficiently small to be sequenced by MS/MS. Though the use of ammonium salts can aid in the ionization of peptides, high concentration of salts reduces the binding of proteins to the PU membrane surface, causing loss of peptides during the washing stages.

As a single use device, the fused silica capillary cannot be used in any high throughput application, nor does it have sufficient reliability for the analysis of critical samples. But when properly functioning and paired with an appropriate mass spectrometer, the results are orders of magnitude more sensitive than the results produced from the HPLC-MS system using approximately 1% of the same sample. The assay also required much less time than with HPLC-MS assay, and smaller quantities of reagents as well. The method is sufficiently sensitive to detect a tetra-phosphorylated peptide in positive mode.

4.5 References

- [1] Michaelis, L. *Biochem. Z.* **16**, 81 (1909)
- [2] Tiselius, A., *Trans. Faraday Soc.* **33**, 524 (1937)
- [3] Hjertén, S., *Chromatogr. Rev.*, **9**, 122 (1967)
- [4] Olivares, J.A., Nguyen, N.T., Yonker, C.R., Smith, R.D., *Anal. Chem.* **59**, 1230 (1987)
- [5a] Smith, D. P. H. *IEEE Trans. Ind. Appl.* **IA-22**, 527 (1986)
- [5b] Wahl, J.H., Gale, D.C., Smith, R.D., *J. Chromatogr. A* **659**, 217 (1994)
- [6] Hayati, I., Balley, A.I., Tadros, Th. F. *Nature* **319**, 41 (1986)
- [7] Hayati, I., Balley, A.I., Tadros, Th.F. *J. Colloid Interface Sci.* **117**, 205 (1987)
- [8] Hayati, I., Balley, A.I., Tadros, Th.F. *J. Colloid Interface Sci.* **117**, 222 (1987)
- [9] Chowdhury, S.K., Chait, B.T. *Anal. Chem.* **63**, 15 (1991)
- [10] Chang, Y.Z., Her, G.R., *Anal. Chem.* **23**, 626 (2000)
- [11] Wetterhall, M., Nilsson, S., Markides, K.E., Bergquist, J. *Anal. Chem.* **74**, 239 (2002)
- [12] Maziarz, E.P., Lorenz, S.A., White, T.P., Wood, T.D. *J. Am. Soc. Mass Spectrom.* **11**, 659 (2000)
- [13] Barnidge, D.R., Nilsson, S., Markides, K.E., *Anal. Chem.* **71**, 4115 (1999)
- [14] Kriger, M.S., Cook, K.D., Ramsey, R.S., *Anal. Chem.* **67**, 385 (1995)
- [15] Wahl, J.H., Gale, D.C., Smith, R.D., *J. Chromatogr. A* **659**, 217 (1994)
- [16] Nilsson, S., Svedberg, T.M., Pettersson, J., Bjorefors, T.F., Markides, K., Nyholm, L. *Anal. Chem.* **73**, 4607 (2001)
- [17] Zamfir, A.D., Dinca, N., Sisu, E., Peter-Katalinić, J. *J. Sep. Sci.* **29**, 414 (2006)
- [18] Fang, L., Zhang, R., Williams, E.R., Zare, R.N., *Anal. Chem.* **66**, 3696 (1994)
- [19] Cao, P., Moini, M., *J. Am. Soc. Mass Spectrom.* **8**, 561 (1997)
- [20] Petersson, M.A., Hulthe, G., Fogelqvist, E., *J. Chromatogr. A* **854**, 141 (1999)

- [21] Mazereeuw, M., Hofte, A.J.P., Tjaden, U.R., van der Greef, J., *Rapid Commun. Mass Spectrom.* **11**, 1981 (1997)
- [22] Janini, G.M., Conrads, T.P., Wilkens, K.L., Issaq, H.J., Veenstra, T.D., *Anal. Chem.* **75**, 1615 (2003)
- [23] Minard, R.D., Chin-Fatt, D., Curry, R. Jr., Ewing, A.G., *Proc. 36th ASMS Conf. Mass Spectrometry and Allied Topics*, 950 (1988)
- [24] Johansson, I.M., Huang, E.C., Henion, J.D., Zweigenbaum, J. *J. Chromatogr.* **554**, 311 (1991)
- [25] Lee, E.D., Muchk, W., Henion, J.D., Covey, T.R. *Biomed Environ. Mass Spectrom.* **18**, 844 (1989)
- [26] Smith, R.D., Olivares, J.A., Nguyen, N.T., Udseth, H.R. *Anal. Chem.* **60**, 436 (1988)
- [27] Olivares, J.A., Nguyen, N.T., Yonker, C.R., Smith, R.D., *Anal. Chem.* **59**, 1230 (1987)
- [28] Smith, R.D., Barinaga, C.J., Udseth, H.R., *Anal. Chem.* **60**, 1948 (1988)
- [29] Tetler, L.W., Cooper, P.A., Powell, B. *J. Chromatogr. A* **700**, 21 (1995)
- [30] Foret, F., Thompson, T.J., Vouros, P., Karger, B.L., Gebauer, P., Bocek, P. *Anal. Chem.* **66**, 4450 (1994)
- [31] Oosterkamp, K.J., Gelpi, E., Abian, J., *J. A. Soc. Mass Spectrom.* **33**, 976 (1998)
- [32] Wahl, J.H., Goodlett, D.R., Udseth, Smith, R.D., *Electrophoresis*, **14**, 448 (1993)
- [33] Kelly, J.F., Ramaley, L., Thibault, P. *Anal. Chem.* **69**, 51 (1997)
- [34] Foret, F., Thompson, T.J., Vouros, P., Karger, B.L. *Anal. Chem.* **66**, 4450 (1994)
- [35] Wu, J.T., Qian, M.G., Li, M.X., Liu, L., Lubman, D.M. *Anal. Chem.* **68**, 3388 (1996)
- [36] Muddiman, D.C., Rockwook, A.L., Gao, Q., Severs, J.C., Udseth, H.R., Smith, R.D. *Anal. Chem.* **67**, 4371 (1995)
- [37] Fang, L., Zhang, R., Williams, E.R., Zare, R.N., *Anal. Chem.* **66**, 3696 (1994)
- [38] Banks Jr., J.F., Dresch, T. *Anal. Chem.* **68**, 1480 (1996)

- [39] Cai, J., Henion, J., *J. Chromatogr.* **703**, 667 (1995)
- [40] Ding, J., Vouros, P., *Anal. Chem.* **71**, 378A (1999)
- [41] McComb, M.E., Krutchinsky, A.N, Ens, W., Standing, K.G. *J. Chromatogr. A* **800**, 1 (1998)
- [42] McComb, M.E., Oleschuk, R.D., Manley, D.M., Donald, L., Chow, A., O'Neil, J.D.J., Ens, W., Standing, K.G., Perreault, H., *Rapid Commun. Mass Spectrom.* **11**, 1716 (1997)
- [43] Asara J. M.; Allison J. *J. Am. Soc. Mass Spectrom.* **10**, 35 (1999)

5 Evaluation of On-Target Electrophoresis as a Sample Preparation Method for MALDI-MS

5.1 Introduction

Through the development of analytical separation techniques coupled with mass spectrometry, automation and online analysis of samples has been greatly enhanced over the past decades. Purification of mass spectrometry samples allows for reduction of suppression effects, thereby enhancing sensitivity [1-4]. The interfacing of liquid chromatography with mass spectrometry has been the most robust and hence most common method of online purification and analysis of samples. Further miniaturization of separation systems has led to the interfacing of capillary electrophoresis to mass spectrometry [5], and to even further miniaturization such as the interfacing of the “lab on a chip” concept through different electrospray interfaces [6-8].

All these separation methods exploit the ability to interface an atmospheric pressure ionization source to the mass spectrometer. Although MALDI is a commonly used ionization source, the high vacuum nature of the source and the requirement of a solid matrix added largely remove any possibility of online purification prior to analysis.

Off-line sample treatments are required for MALDI, though some on-target treatment of samples has been performed using polyurethane films and surface enhanced laser desorption/ionization (SELDI) [9,10] which allow for some selective binding of the desired elements in a sample. Fraction collection onto MALDI targets is also common [11-15], though it does not have the convenience of online analysis.

While offline treatment of samples is common, it poses difficulties with issues such as sample loss and contamination with each step and transfer of the material during treatment as well as automation of analysis.

One of the most common off-line protein purification methods used is gel electrophoresis. However the method requires substantial sample cleanup and workup to provide useable peptides for proteomics analysis. It would be ideal if MALDI could be performed directly upon a gel, but the inherent three dimensional matrix of a gel is impossible for a laser to sample as it cannot desorb beyond the surface layer. Attempts to desorb proteins directly from gels or electroblotting from the gels using both ultra-violet (UV) and infra-red (IR) lasers have had little success [16-21].

Capillary electrophoresis is the electrophoretic method most compatible for mass spectrometry, given the lack of buffer additives such as SDS which greatly interferes with sample ionization. However, the high vacuum nature of MALDI makes it impossible to sample the liquid within a capillary. My research aim was to examine the viability of combining aspects of both gel and capillary methods to form a MALDI compatible sample purification method.

Similar research involving microfluidics applied to proteomics [22-24] has been carried out. Several online interfaces have been attempted, in which the sample is deposited on a moving system which transports the sample trace into the mass spectrometer for real-time analysis [25-27]. Attempts to use open-channel microfluidics for coupling with MALDI have been unsuccessful. Liu's first attempts showed minimal separation of cyclodextrins [28]. Further work by Brivio et al. used the vacuum of the mass spectrometer to draw reagents to an open channel where

analyte was mixed with reagents to perform chemical modifications [29]. The vacuum further then drew analytes and matrix into an open region to form a MALDI sample spot for analysis. No separations were performed by this method however. More recently, Brivio et al. extended the work with the introduction of a monitoring window for MALDI [30]. The most recent research was by Jacksén et al. [31] using an “open-closed-open” channel configuration, where a closed CE capillary pumped the buffer system through an open channel, and exited via a closed second capillary. Results showed only limited separation, possibly due to the ethanol-matrix solution pumped through the channel to add matrix.

In using an open channel configuration, my system resembles a large CE capillary, half exposed along its main axis. As with CE, no stationary phase is used, and the channel is filled with a buffer solution. Electrodes placed at both ends of the channel provide the electrical conductivity needed for electrophoresis. However, as in gel electrophoresis, no electro-osmotic flow is generated. To prevent diffusion of the analyte molecules from their relative positions after separation, the system is rapidly frozen. Removal of the liquid buffer component is achieved by lyophilization, which leaves the peptides at their positions in the channel. Addition of matrix or extraction of sample from regions for analysis can determine if any movement of the analyte has taken place.

5.2.0 Materials and Method

5.2.1 Electrophoresis Targets

Targets were manufactured from Teflon [32,33] by standard machining methods. Targets were designed to stand vertically in a target holder the same dimensions as a standard Bruker 384 polished steel plate. The channel and target holders were also fabricated by standard machining methods (Figure 5.1 and 5.2). The electric potential was supplied by a Spellman CZE power supply, from 1-5 kV. All peptide standards were purchased from American Peptide Company Inc. (San Jose, CA; www.americanpeptide.com).

5.2.2 Cooling System

A cooling heat sink was made by drilling and patching the ends of a copper rod, and further extending the chamber by the soldering of additional copper pipes (Figure 5.3) to allow liquid nitrogen to flow through the tube and gas to vent, while maintaining a reservoir for liquid nitrogen to remain. A leveling base was added to allow for the open channel to sit without the buffer pooling towards the ends.

5.2.3 Method

The Teflon channel was placed on the copper cooling unit and leveled using the leveling base. Gold electrodes were placed into the channels and connected to the power supply. The run buffer (25% methanol) was added by pipette to fill the channel and cover the electrodes (approximately 300 μ l).

A 3 μ l sample droplet was placed on a Teflon sheet and placed on top of a copper bar chilled in liquid nitrogen until frozen. The frozen droplet was put into the middle of the Teflon channel, and the electrophoresis potential was applied (500 V). The copper cooling unit was immediately filled with liquid nitrogen, and maintained so until the run buffer was frozen (approximately 2 minutes). Electrodes were removed, and the Teflon channel was transferred to a copper bar cooled in liquid nitrogen which acted as a heat sink. The bar and Teflon channel were placed in a SpeedVac and placed under vacuum until all solvents were removed (approximately 1 hour) (Figure 5.4).

To determine if separation of the components had taken place, surface extraction of the peptides and spotting onto a steel MALDI target was performed. The Teflon channel was roughly subdivided into six approximately equal regions. Each region was extracted by repeated aspiration of 10 μ l of run buffer over the surface of the area. Samples of each region were placed on a MALDI target and analyzed (Bruker Biflex IV) to determine if the peak ratio in each area is different after separation.

Matrix solutions consisting of DHB (100mg/ml) for application to Teflon surfaces were dissolved in acetone, and deposited onto the Teflon surface. The hydrophobic nature of the Teflon surface required the use of a high organic content solvent to be used which evaporated very quickly to prevent concentration of the matrix to a single point [34].

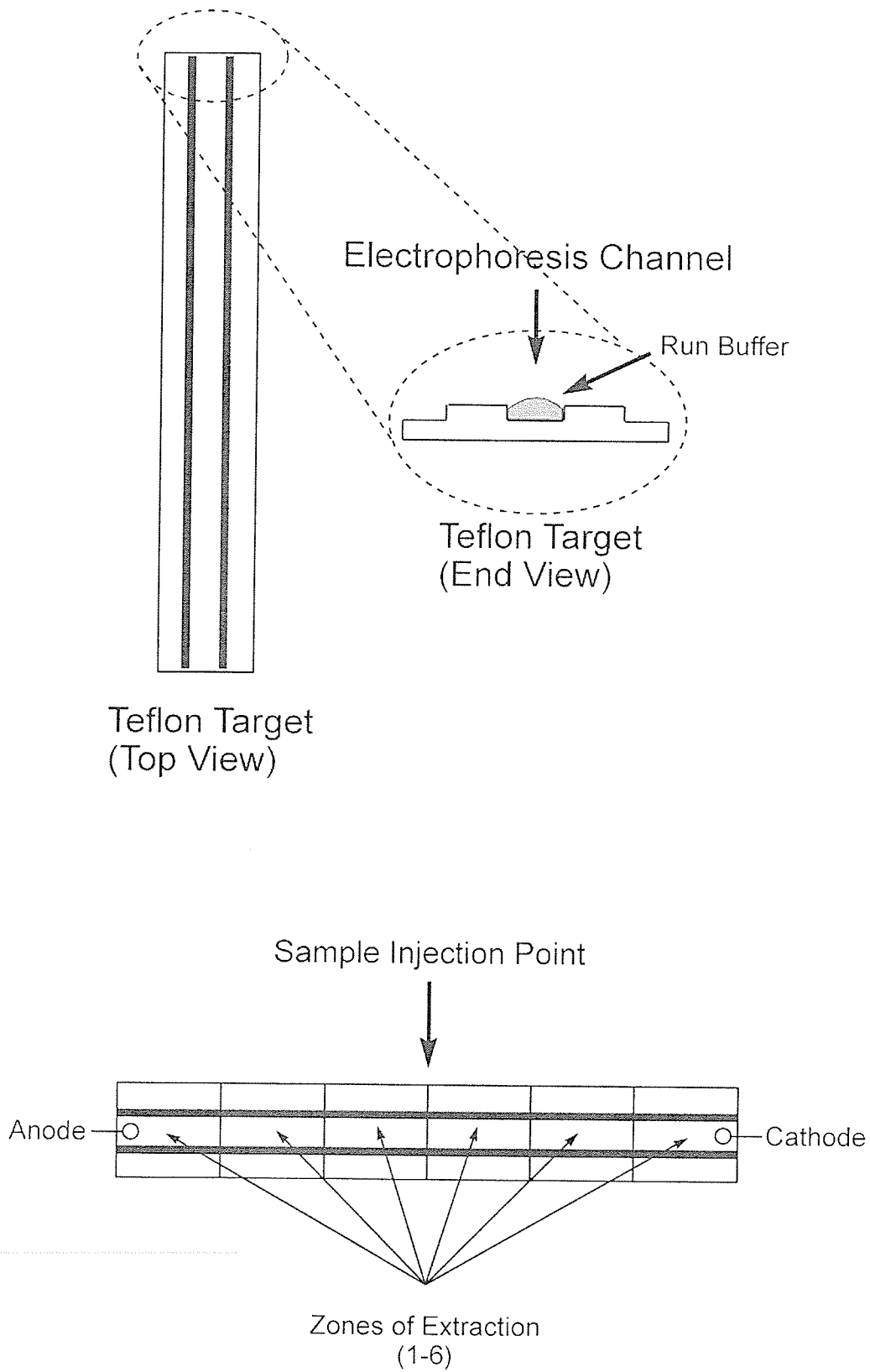
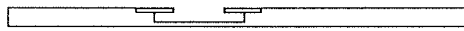
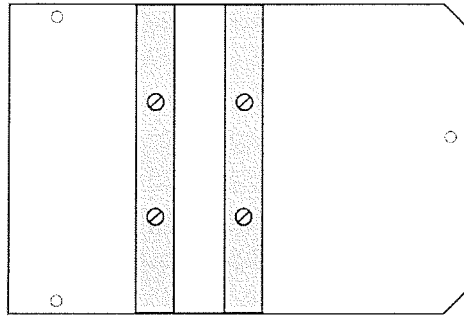


Figure 5.1: Schematic representation of Teflon Channel

Steel Target Holder
(Top View)



Steel Target Holder
(Side View)

Figure: 5.2a: Schematic of Target holder for Bruker Biflex IV

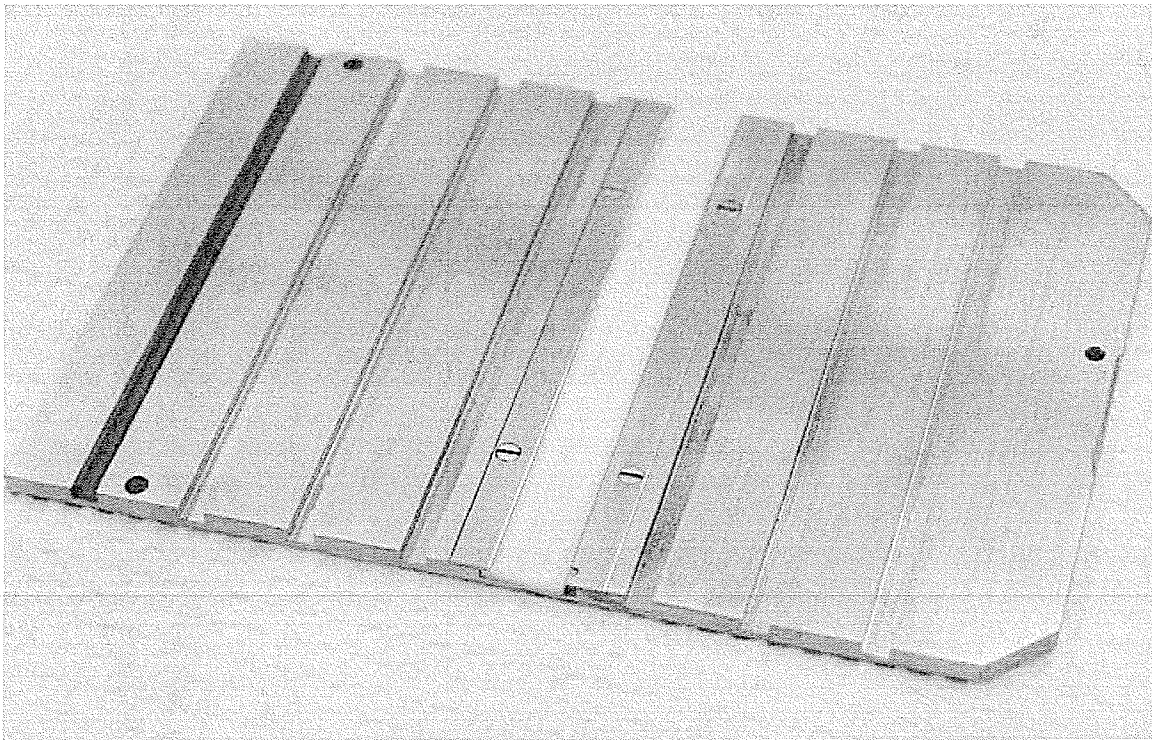


Figure 5.2b: Photo of Target holder with Teflon channel

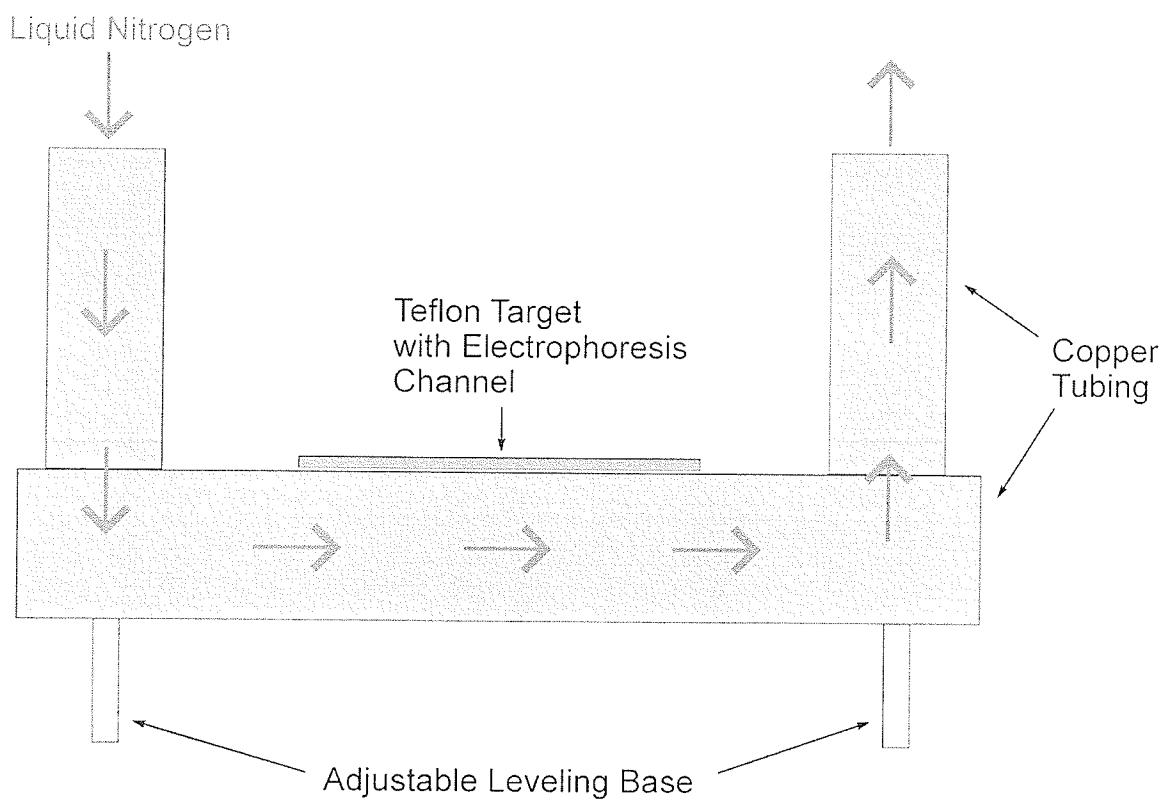


Figure 5.3: Cooling apparatus for freezing Teflon channel

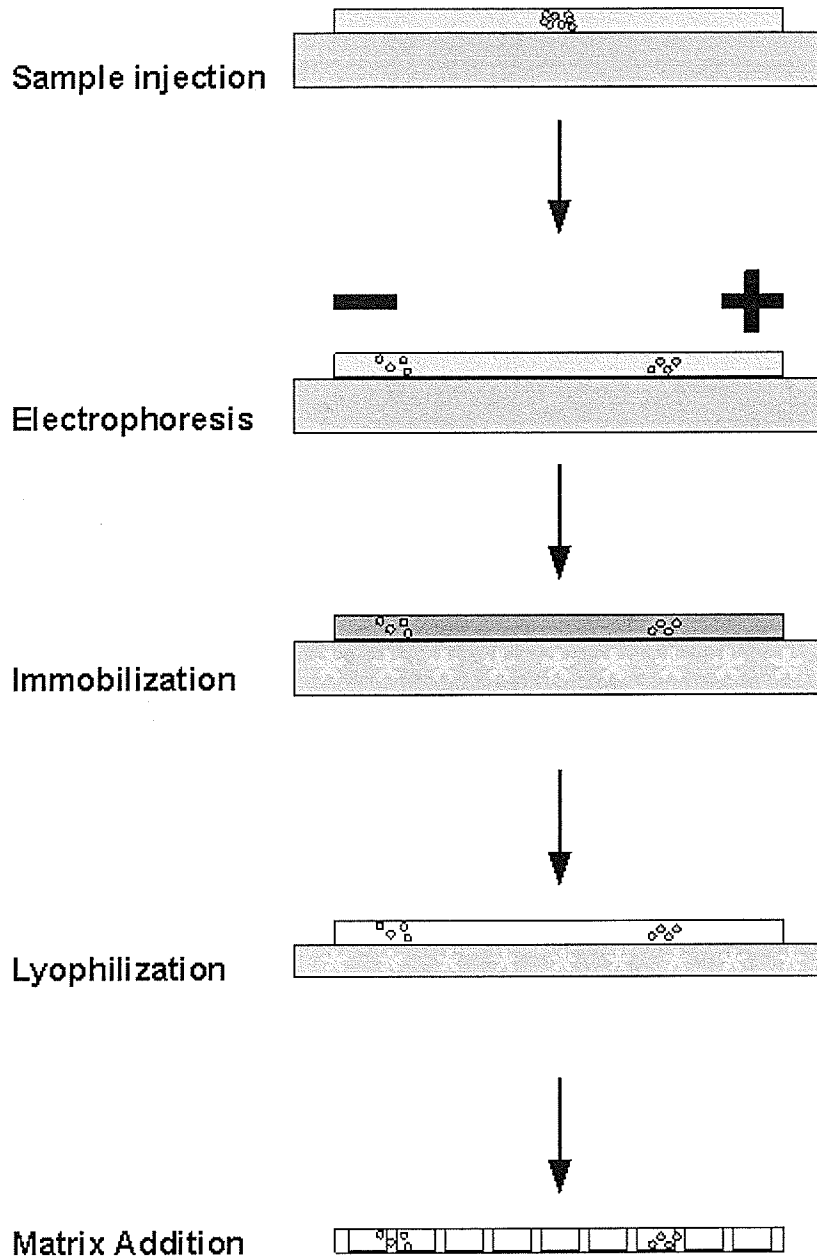


Figure 5.4: Workflow for open channel electrophoresis on a Teflon channel

5.3 Results and Discussion

5.3.1 Proof of concept

An initial demonstration of movement of analyte molecules in a Teflon channel was performed by use of coloured ionic dyes. Visible amounts of different coloured ionic dyes were deposited in the middle point of a water filled channel and a 5 kV potential was applied. Simulation of cationic and anionic molecule movement was done using Congo Red and Malachite Green, respectively (Figure 5.5).

Under a 5 kV applied potential, it can be seen that each dye moves towards a different terminal (Figure 5.6). Congo red can be seen migrating towards the anode, while Malachite Green migrates towards the cathode. In both cases, substantial streaking of each component in the channel can be seen. Though this will likely result in poor resolution in the final result, separation of oppositely charged analyte species will be possible. It is difficult to determine what differences in mobility ion species exhibit by this method, so evaluation of resolution cannot be commented on. There is obviously some diffusion of the dyes which may also be occurring with biological samples, but because peptides are substantially larger than the dyes, electrophoretic mobility will be lower and diffusion will likely be less rapid. To limit diffusion, immobilization of the components will need to be done as rapidly as possible after separation.

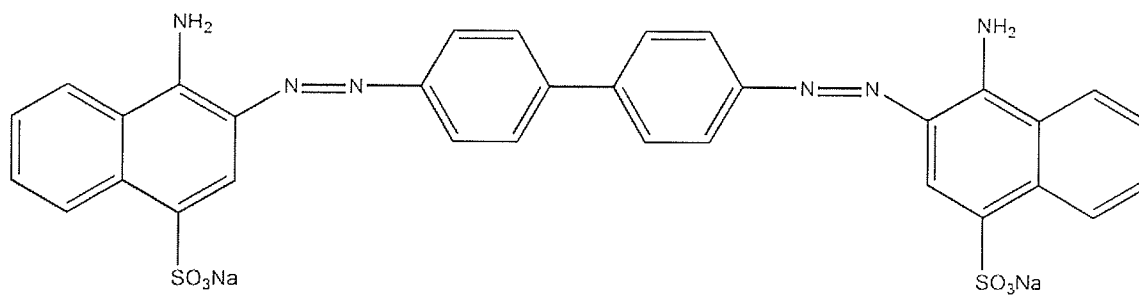


Figure 5.5a: Chemical structure of Congo Red

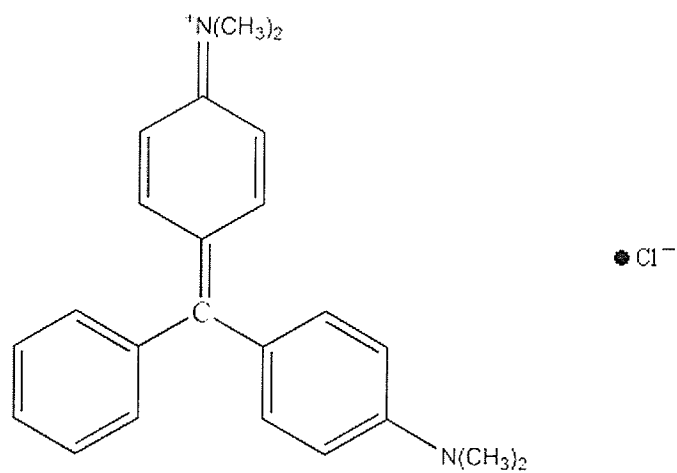


Figure 5.5b: Chemical structure of Malachite Green

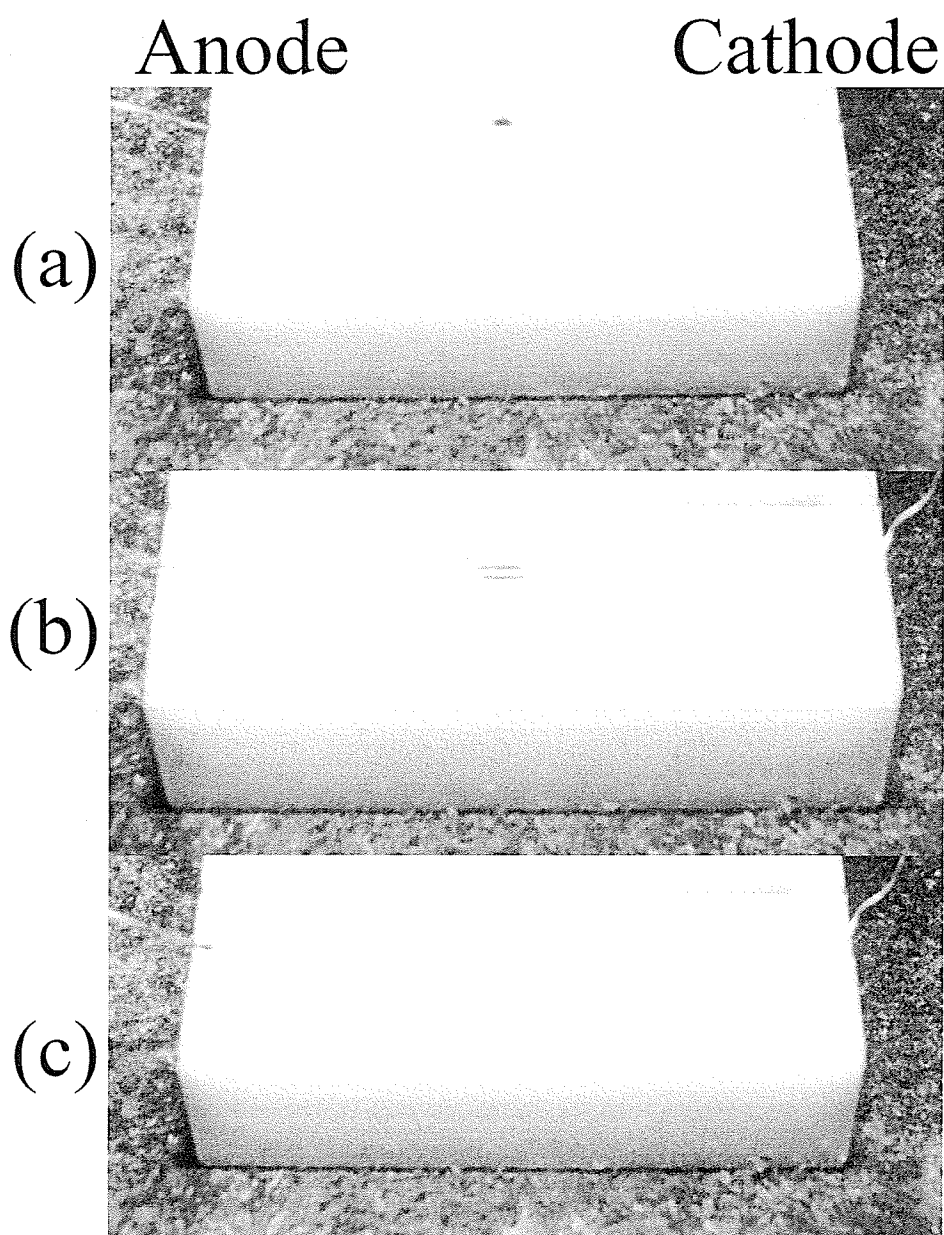


Figure 5.6: Migration of ionic dyes where (a) malachite green is injected, (b) migration of malachite green towards the cathode (c) migration of congo red towards the anode.

5.3.2 Design Considerations and Prototyping of On-target Electrophoresis

System

Initial prototyping of a Teflon insert demonstrated some design considerations of the electrophoresis channel. Initially, non-conductive epoxy was chosen as the physical support material for the electrophoretic channel, meeting the criteria of non-reactivity, non-conductivity, and no out-gassing at MALDI low pressures. The epoxy was spread into a groove cut into the MALDI target, and the target re-machined to give a narrow but deep channel for electrophoresis. The resulting target was not robust enough to withstand the freezing needed to immobilize the components. Under the strain of repeated large temperature changes, the epoxy cracked and the steel target deformed. In addition, it was difficult to electrically insulate the system in the middle of a steel target.

For these reasons, the system was redesigned to be performed off-target as a disposable insert and reloaded onto the target only when mass spectrometry results could be obtained. Teflon was the most suitable material, given its inert nature and electrically insulating properties.

Though the initial design was for a relatively narrow but deep channel, the constraint proved to be impractical for the Bruker Biflex IV instrument. The incident angle of the laser was determined to be approximately 70° , limiting accessibility of the laser to the bottom of the channel if the channel was deep. Nevertheless, a deep channel was a requirement due to the high surface tension of water. A shallow channel using water as a running buffer resulted in the water beading and not sitting

in the channel properly. The requirement of a wide but shallow channel to allow laser access necessitated a buffer solution with a substantial organic content to reduce surface tension and thus resulted in the lowering of the freezing point of the solution.

In machining the channel, it was shown that a high degree of precision was required. Ideally, the bottom of the Teflon channel should be as thin as possible to limit thermal insulation during the freezing step, as well as electrical insulation when potentials are applied inside the mass spectrometer. When extremely thin, it was found that Teflon could not maintain shape after repeated freezing/thawing.

Another consideration has been the uniformity of the Teflon channel thickness at the bottom. Non-uniform thickness caused the buffer to pool at the lower end of the target. Fabrication of the target to have uniform thickness by standard machining methods is extremely difficult. During fabrication, as the tools bite into the target and reduce the amount of material present, the stiffness of the target is reduced. The softening of the structure allows the material to flex further during cutting, creating non-uniform conditions between the starting cut and the final cut of the material. The longer the Teflon channel is, the more flex the material will exhibit as cutting is introduced. Given the soft nature of Teflon, only a short channel of uniform thickness can be made by standard machining methods.

The use of buffers in this method is prevented by the power source. Even when used in concentrations as low as 10 mM, the ionizable salts allow the buffer solution to conduct, so that the voltage dropped to zero while the current rose. The requirement of a non-conductive solution which is sufficiently volatile to be removed by lyophilization was achieved by the use of organic solvents.

Reducing the surface tension of water by the addition of methanol allows the running buffer to sit in the wide, shallow channel of the Teflon insert. A minimum of 25% methanol was needed to allow the buffer to sit correctly. Increasing the methanol content was avoided to reduce the likelihood of precipitation of biological samples from aqueous sources.

The Teflon channel was shown to have strong insulating properties in the MALDI source. When an accelerating potential was applied, no signal was seen when normal laser fluences were used. Though the channel was made as thin as possible, it was sufficient to prevent acceleration of the ions through the flight tube. Increasing laser fluence to high levels produced a signal, but at the cost of resolution. Isotopic resolution would be impossible given the geometry of the instrument, though the use of a decoupled source such as QqTOF, FT-ICR, or ion storage geometries would solve the problem.

Immobilizing the analytes following separation was difficult. Initial attempts to freeze the components while in the steel target resulted in damage to the target and channel. Freezing of the Teflon insert without disturbing the liquid in the channel necessitates an apparatus which can immediately freeze the system following electrophoresis without moving it or further contacting it. Initial attempts using a chilled glass plate placed over the channel froze the buffer quickly, but could not be used with the shallow channel since the buffer sits above the walls. In addition, the small extent or degree of contact was shown to disturb the system before freezing.

A sample preparation stage was devised which could perform the electrophoresis on, as well as enable the freezing of the buffer. A copper rod was

drilled hollow to allow liquid nitrogen to be flowed through it to reach low temperatures quickly. Part of the rod was machined flat to allow the Teflon insert to sit atop the copper stage during electrophoresis. By this method, additional contact with the channel was not required, and the target could be chilled and frozen in approximately two minutes.

Test injection of dyes into the channel by pipette led to turbulence and expansion of the sample, often occupying up to one third of the channel length. It was found by freezing the injection volume on a chilled Teflon surface and placing the solid droplet into the channel by forceps allowed the droplet to thaw in the channel with minimal diffusion. Following electrophoresis, the channel was frozen to immobilize the components, to prevent diffusion and maintain resolution.

To allow for MS analysis of the components, lyophilization of the buffer is required. When placed in the vacuum system, the sample thawed too quickly, and resolution of the components was lost. A heat sink was required to reduce the rate at which the Teflon target returned to ambient temperature. Though choice of materials for the heat sink would affect the rate of thawing, the simplest parameter remained the size of the heat sink. An excessively large heat sink resulted in an unnecessarily long lyophilization time. Optimally, a copper heat sink giving a lyophilization time of 45-60 min resulted in no excess liquid being observed during thawing.

5.3.3 Peptide Standard Results

A solution of five peptides of varying mass and pI was used to evaluate the system (Table 5.1):

Table 5.1: Peptide Standards and properties

Peptide	[M+H] ⁺	pI
Bradykinin (1-7)	757.399	11
Angiotensin II	1046.542	7.8
Angiotensin I	1296.685	7.9
Substance P	1347.735	14
Bombesin	1619.822	11
ACTH (18-39)	2465.198	4

A standard MALDI-MS spectrum of the standards was generated for comparative purposes with sample spectra from the on-target electrophoresis systems (Figure 5.7).

Analysis of each the six subdivided areas of the Teflon channel shows the presence of peptides. If no electrophoretic separation of components had taken place, movement of the analytes from the injection point would have occurred through diffusion, resulting in a spectrum from each zone with similar component and peak ratios as in the MALDI-MS of the original sample. As an indication of separation, the peak ratios were compared to the peak ratio in the standard spectra.

The spectrum of Zone 1 where the anode is located showed only small amounts of peptide present, as evidenced by the signal to noise ratio (Figure 5.8). As the electrode was positioned furthest from the injection point, the low abundance of peptides found may be the result of lack of migration during the short electrophoresis times. The peptides found were bradykinin, angiotensin II and ACTH (18-39). Of the peptides found, only ACTH (18-39) should be found in this region since its pI is lower than the buffer pH. The presence of the other components may be due to diffusion from the injection zone. On a normalized scale, ACTH (18-39) was enriched in the zone over the other peptides relative to the original sample mixture. Angiotensin II was found reduced amounts relative to bradykinin.

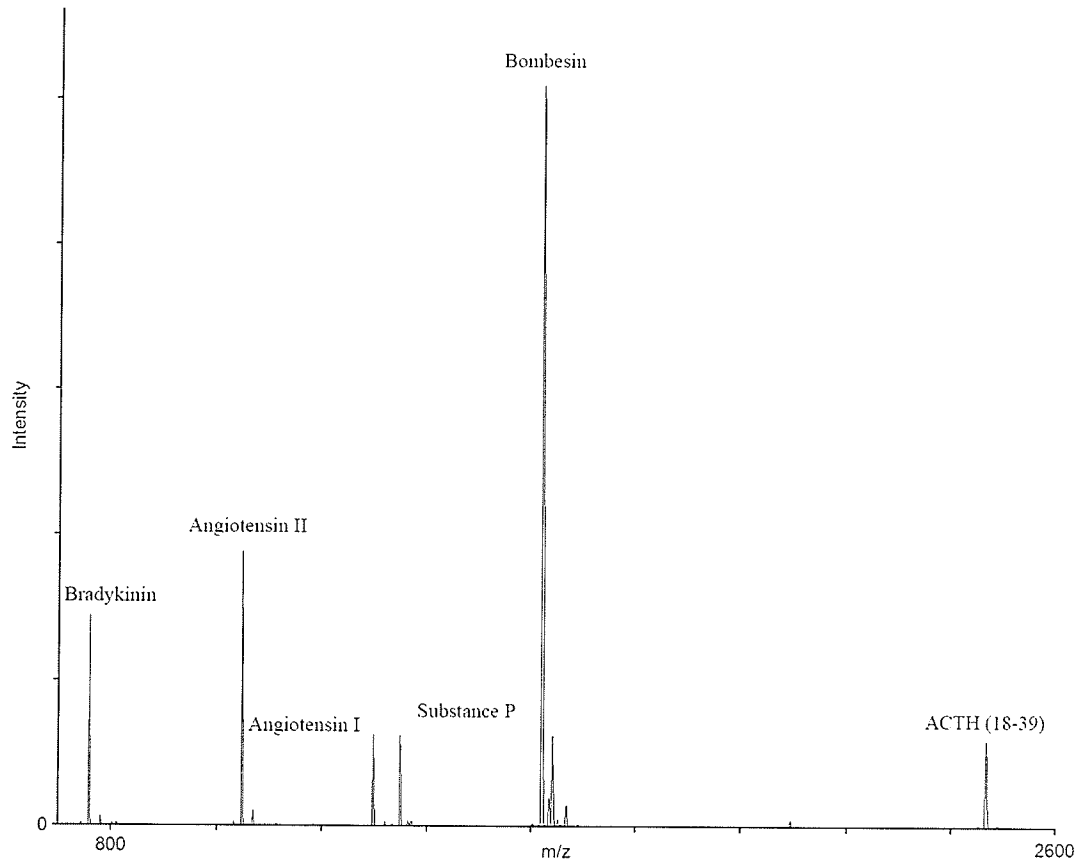


Figure 5.7: MALDI-MS of peptide standard mixture

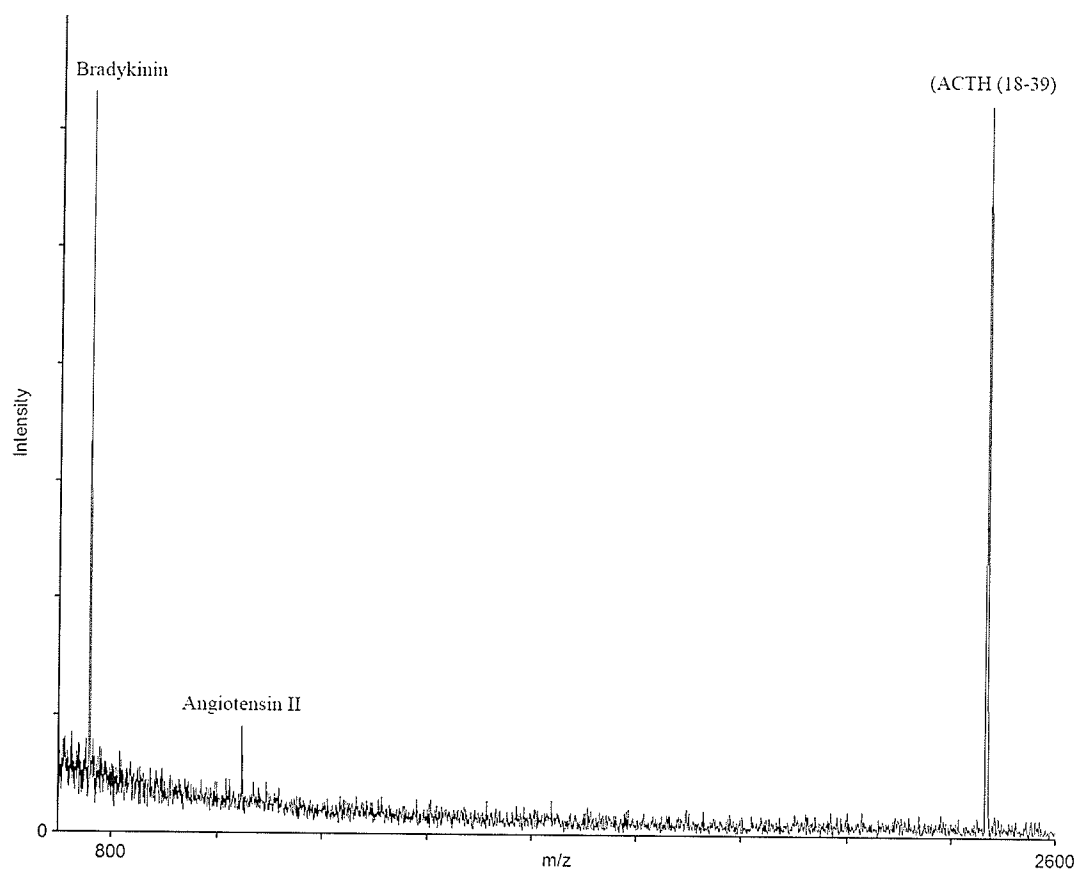


Figure 5.8: MALDI-MS of surface extract from Zone 1

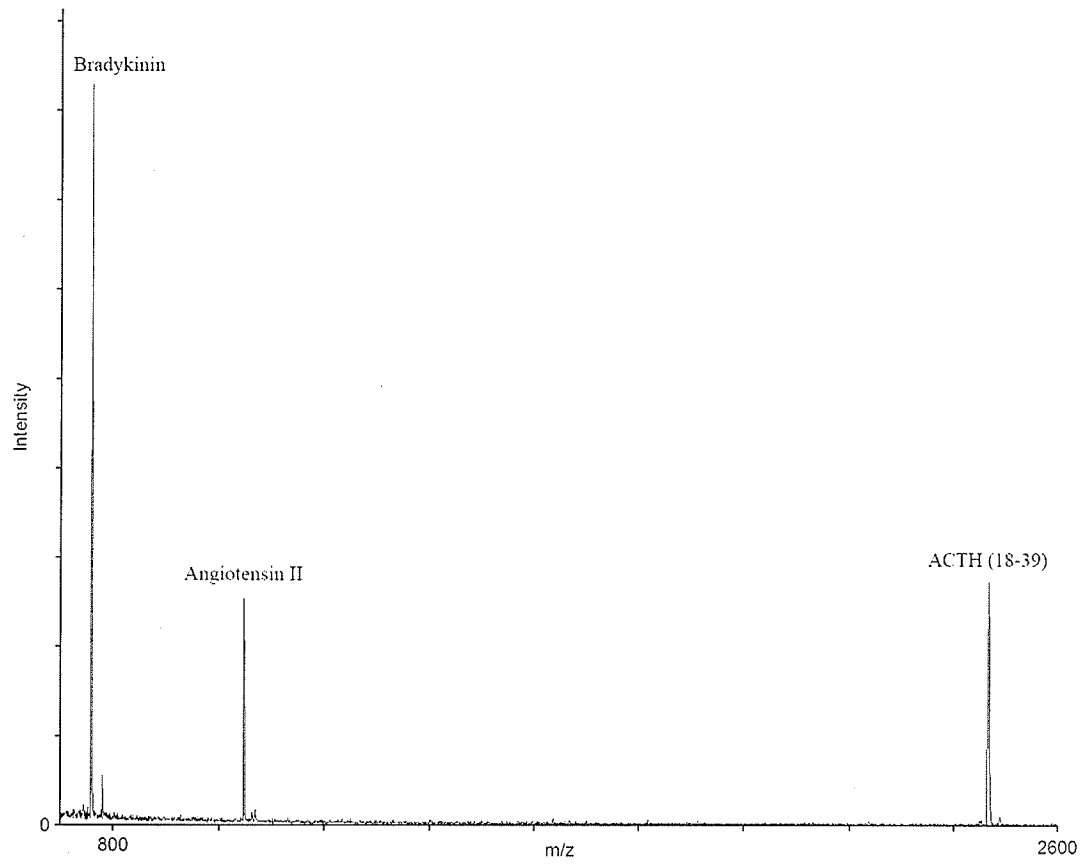


Figure 5.9: MALDI-MS of surface extract from Zone 2

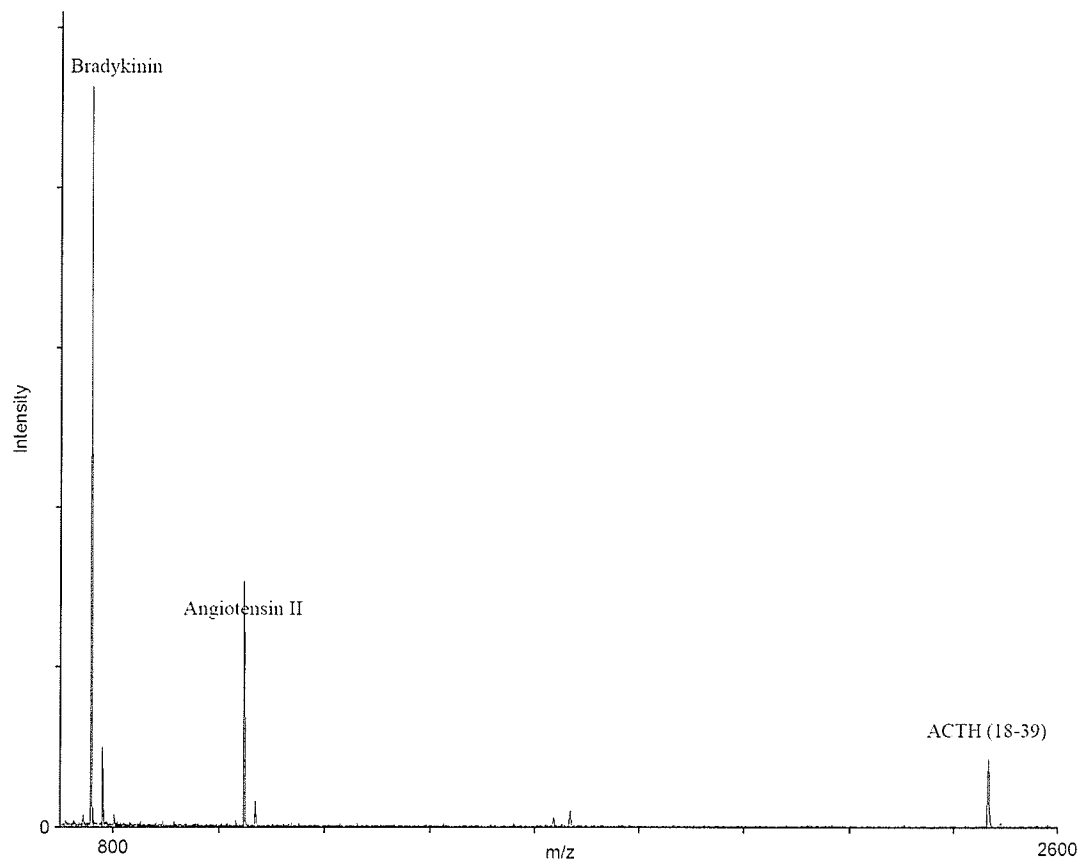


Figure 5.10: MALDI-MS of surface extract from Zone 3

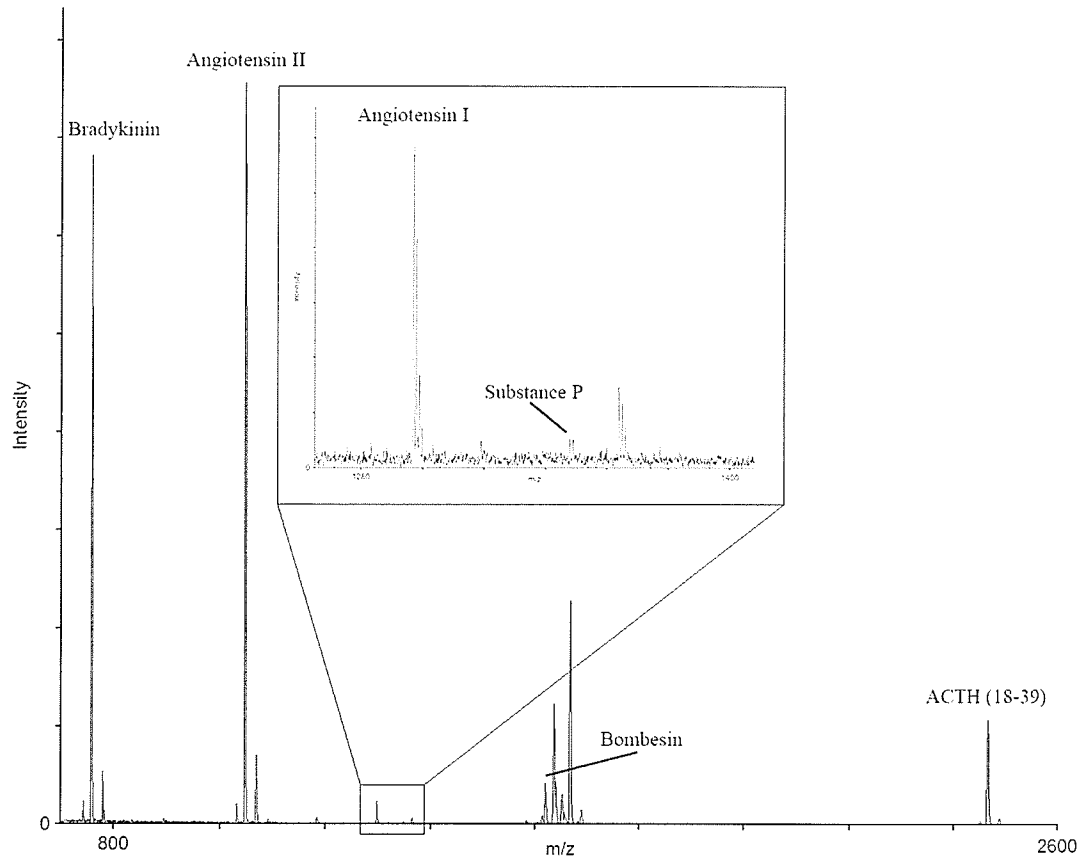


Figure 5.11: MALDI-MS of surface extract from Zone 4

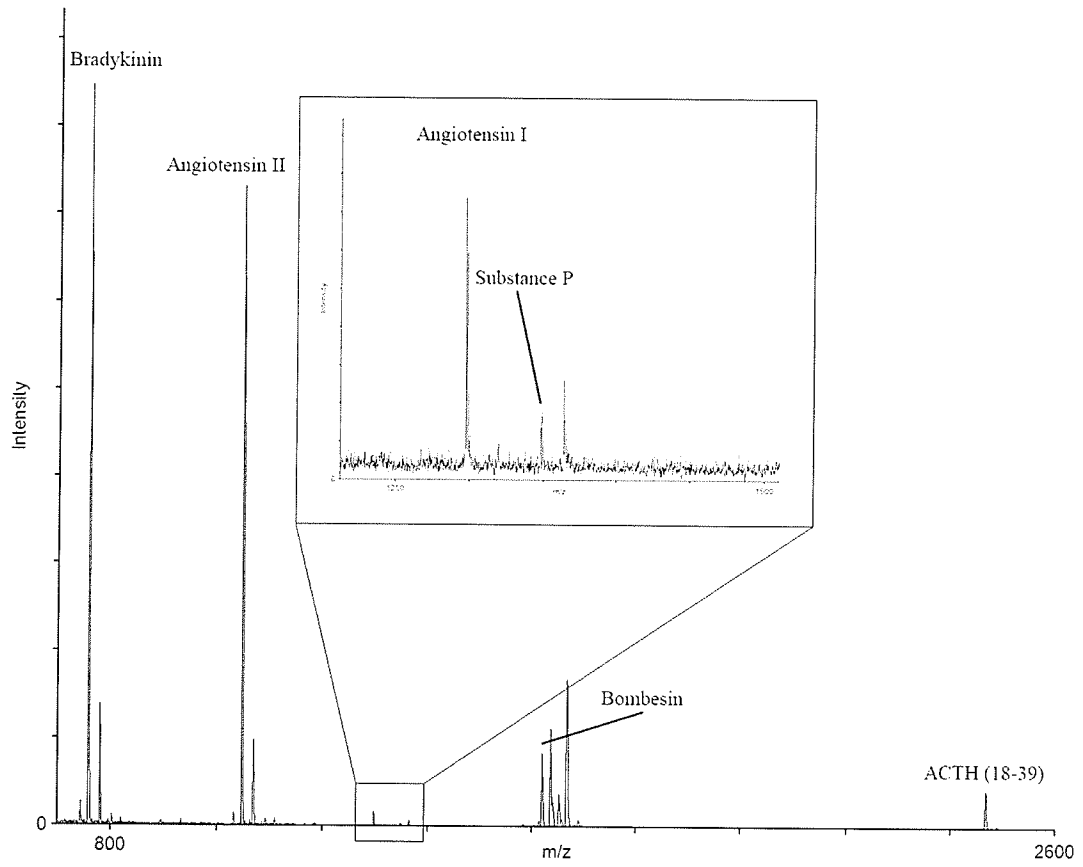


Figure 5.12: MALDI-MS of surface extract from Zone 5

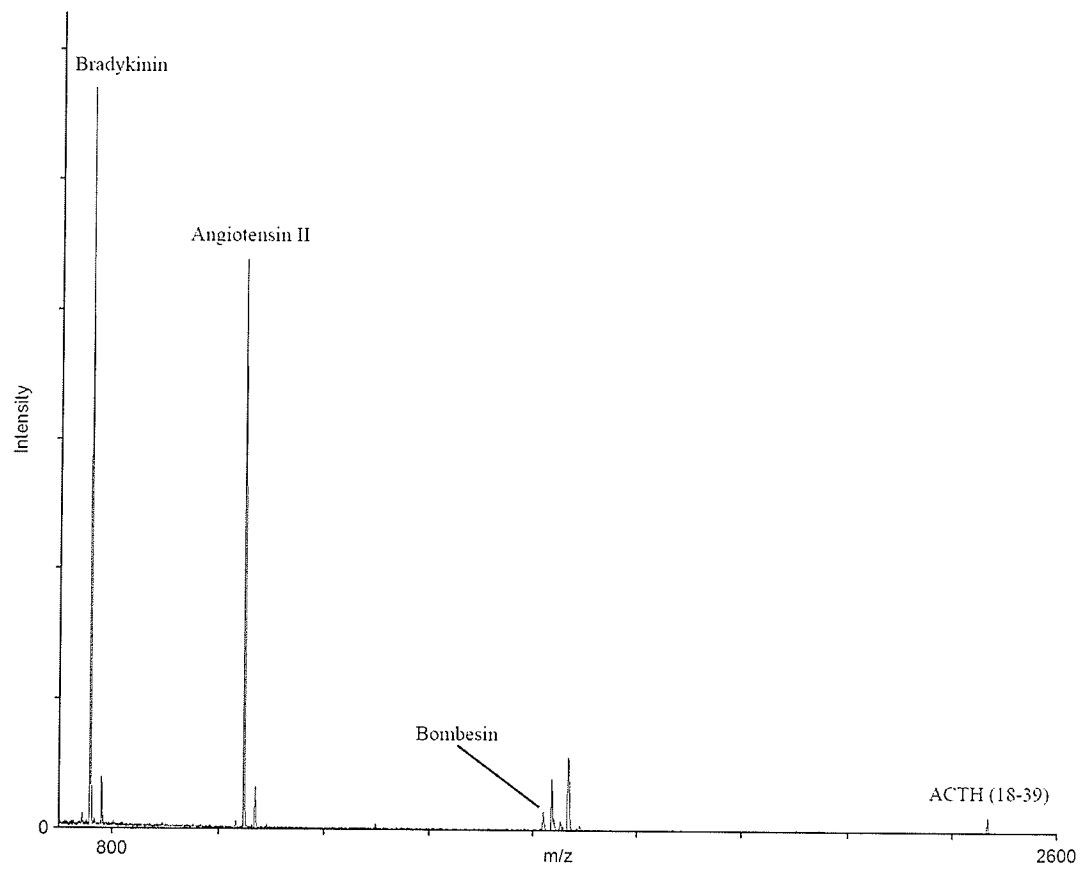


Figure 5.13: MALDI-MS of surface extract from Zone 6

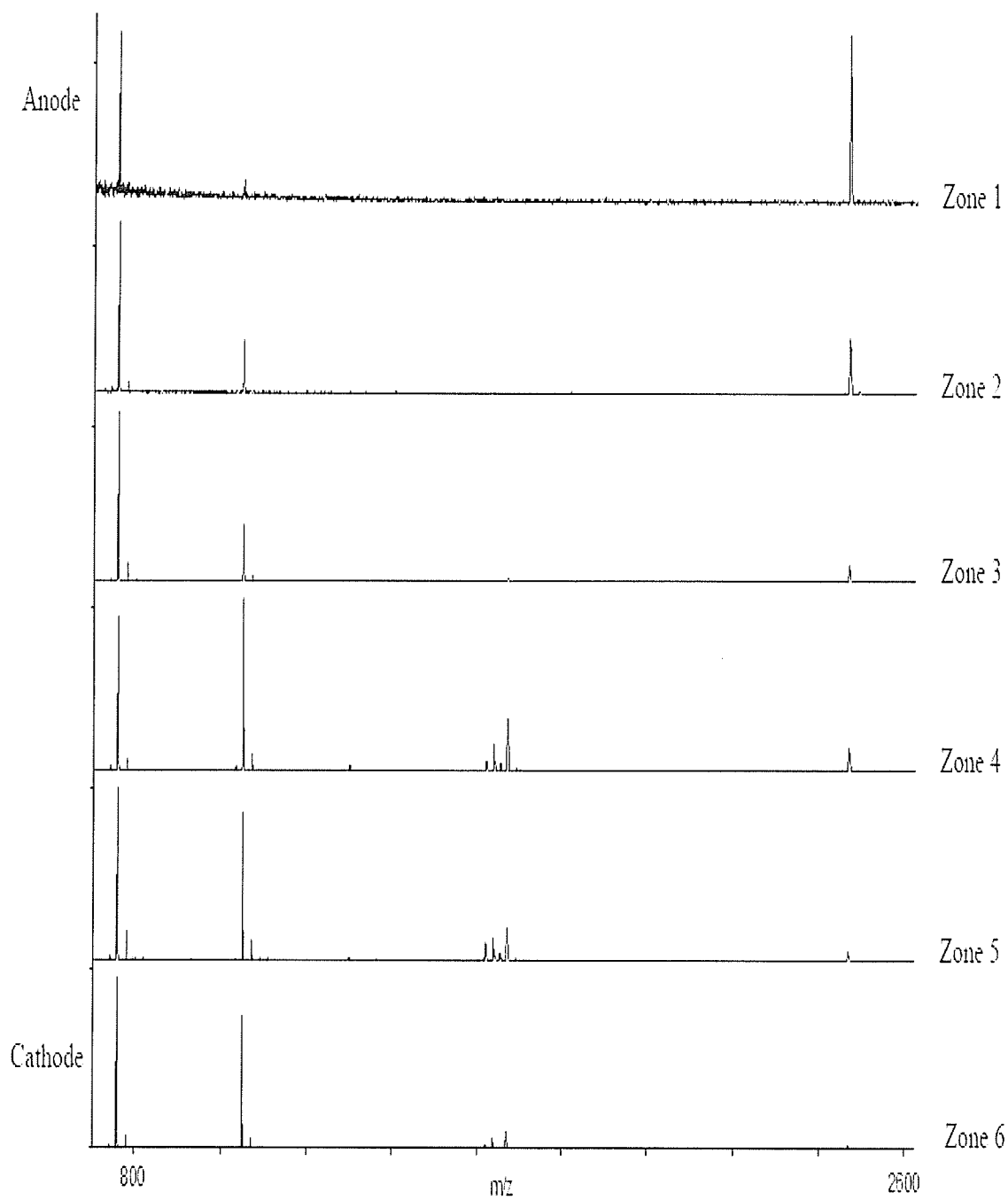


Figure 5.14: Trace spectra of MALDI-MS of zone surface extracts, showing differences between zone compositions

Analysis of the adjacent zone 2 (Figure 5.9) showed an increase in sample concentration as an equivalent number of laser shots yielded a better signal to noise ratio. Though the same components were present in this sample as in Zone 1, a reduced amount of ACTH (18-39) relative to bradykin was found. However, this zone showed an increased amount of angiotensin II relative to the previous zone, though much less than in the standard spectrum.

Zone 3 was one of the zones adjacent to the injection point, and all the peptides should be present if no separation, and only diffusion took place (Figure 5.10). The spectrum shows similarities to the spectrum of Zone 2, as the ratio of angiotensin II and bradykinin remain approximately the same. However, there is a further decrease in the ratio of ACTH (18-39) relative to bradykinin.

Also adjacent to the injection point was Zone 4. Though adjacent in the same manner as Zone 3, it was in the direction of the cathode, and the analytes detected were very different (Figure 5.11). Angiotensin II was detected in higher quantities than bradykinin which had never been observed before except in the peptide standard, while relative amounts of ACTH (18-39) remained quite low. Detected for the first time were peptides Angiotensin I, Substance P, and Bombesin which exhibited low peptide signals relative to Bradykinin.

Further towards the cathode, Zone 5 shows a similar profile. Though the amounts of Angiotensin II and ACTH (18-39) were reduced relative to zone 4, they are still easily detectable. Peaks from Angiotensin I, Substance P, and Bombesin were found again, though slightly stronger in relative intensity (Figure 5.12).

Zone 6 shows a further decrease in peak heights relative to Bradykinin. Angiotensin II, Angiotensin I, Bombesin, and ACTH (18-39) all showed decreased signals again, with Substance P not being detected (Figure 5.13).

The partial separation of the analytes shows that electrophoresis is being observed under the applied separation potential. A comparison of spectra by overlapping traces (Figure 5.14) qualitatively shows the differences, illustrating the separation of analytes over a short distance. Higher resolution of the components may be possible by decreasing the zone sizes. Extraction of the Teflon surface was performed to independently verify that sample movement had been taking place, since direct laser sampling of the Teflon surface does not give adequate resolution of the analytes to clearly show their identities. Though the electrophoretic resolution is relatively poor, the space over which the separation takes place is quite short. Considering an HPLC assay as a theoretical example for comparison, a 1 minute peak width eluting at 1 ml/min occupies nearly 20 meters of 0.010" ID HPLC tubing.

Though the trace spectra indicate some separation of the components by the relative amounts of each peptide series present, it does not fully indicate the absolute amounts of each peptide present, or the area in which it is located. An analysis of the absolute peak counts of each peptide spread across each zone of the target (Table 5.2) indicates the peak count of the peptides, and highlights the zones in which peptide were most predominantly found.

Table 5.2: Absolute peak counts of peptides from extraction zones. Numbers shown are in thousands. Highlighted boxes indicate zone of highest concentration for a particular peptide.

	Zone 1	Zone 2	Zone 3	Zone 4	Zone 5	Zone 6
Bradykinin	1200	3500	2100	3400	4200	2800
Angiotensin II	180	900	800	3800	3500	2200
Angiotensin I				120	90	25
Substance P				12	16	
Bombesin				220	450	70
ACTH (18-39)	800	700	140	380	160	35

The results indicate that the majority of peptides did not move very far in the time window during which the channel was frozen. Though injected at the midway point of the channel between Zone 3 and Zone 4, the majority of peptides did indeed move towards the cathode, showing strong peak counts mostly in Zone 4 and Zone 5. The largest concentration of ACTH (18-39) was found in Zone 1, at the anode where other peptides showed the lowest concentration.

Peptides which were distributed throughout the entire length of the channel were also found to have a second zone of high concentration, which was flanked by zones of lower concentration. Though the components are supposed to move in only one direction based upon their relative pI, the lack of a stationary phase would likely result in diffusion of the components over time, thereby giving the false impression of mobility in both directions. The presence of the majority of peptides near the injection point is likely indicative of insufficient movement of the analyte components from each other due to the short length of the separation channel. The separation of the analytes is unresolved in the time and distance available.

Though the experiment was not designed to test the sensitivity of the method, it seems to be less sensitive than results obtained from a steel target. Very low peak counts were found for most peptides. This may be due to loss of peptides during lyophilization. Results acquired directly from the surface of the Teflon insert will undoubtedly show less sensitivity than the zone extracts, given the concentration of the peptides as a result of the extraction.

Throughout the course of the analysis of the peptide extracts, some oxidation of peptides was observed. Though little Substance P was found in the target extracts, proportionately stronger peaks corresponding to oxidized Substance P were observed, with no oxidation peaks found in the peptide standard (not shown).

Bombesin is particularly susceptible to oxidation, and substantial oxidation of this peptide was seen in the standard spectrum, with up to three oxidized sites found in the peptide, along with sodium adducts (Figure 5.15). Following electrophoresis, a substantial change in the proportion of the oxidized Bombesin peaks was found. Higher proportions of multiply oxidized peaks were found. Detection of a quadruple oxidized ion was also found, which had not been observed in the concentrated standard. Absolute peak counts of the oxidized ions were also much higher than in the standard. Given that the electrophoretic separation only lasts approximately two minutes and primarily affects only bombesin, the cause of the oxidation is likely due to the long exposure of the sample to the minute amounts of atmosphere at room temperature while lyophilizing the sample. This treatment is followed by exposure to atmosphere with the sample spread over a large surface area, promoting oxidation during extraction. The increased oxidation of the sample also decreases the sensitivity

of the method for bombesin, as it is no longer the dominant peak in the spectrum (Table 5.3).

Table 5.3: Peak counts for oxidized bombesin peaks in Standard Sample and Zone 4. Numbers are in thousands.

Peak	Standard Sample Peak Counts	Zone 4 Peak Counts
1 Oxidation	100	600
2 Oxidation	25	160
3 Oxidation	70	1200
4 Oxidation	-	80

Spectra of samples directly acquired from the Teflon surface show poor sensitivity due to the insulating nature of the Teflon working against the acceleration of ions. A higher laser fluence is required to compensate for the insulating effect of the target. Laser energies used are more than twice as high as those normally used on a steel target and are approaching levels required for post-source decay, possibly decreasing sensitivity by fragmenting the analyte molecules in the source. A poor signal to noise ratio is observed for all samples, regardless of peak counts.

As a direct consequence of the high laser fluence, resolution of the peaks found is very low. Sufficient resolution is available to differentiate between sodium adducts, but isotopic resolution is not possible under these conditions.

Because the use of acetone solvent was required for preparation of the matrix, the resulting target spots formed lacked crystal formation due to the rapid evaporation of solvent. As a result, the target spots formed do not exhibit the normal tolerance that MALDI sample spots have for impurities, or normal signal intensity [35,36]. Samples are all found to exhibit high levels of sodium adduct formation, not seen in the

surface extracts of the same samples (Figure 5.16) [37]. This is likely exacerbated by the lyophilization of the water in the channel, which would concentrate any impurities such as sodium ions onto the surface of the channel. Given the volume ratio of sample to buffer is approximately 1:100, an increase in impurities present is highly likely.

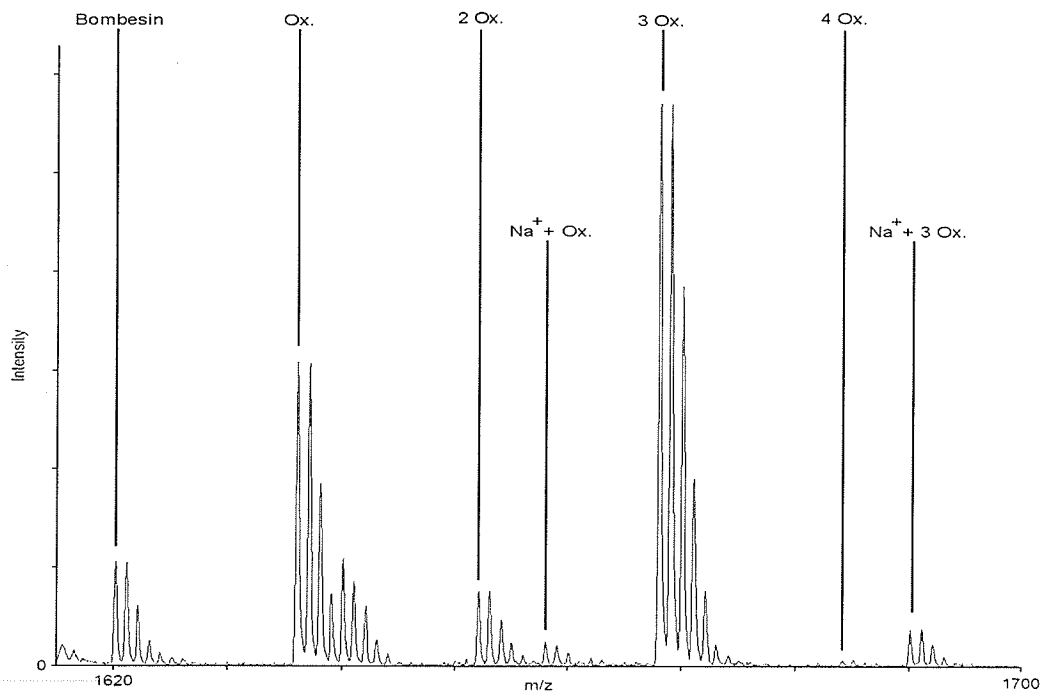
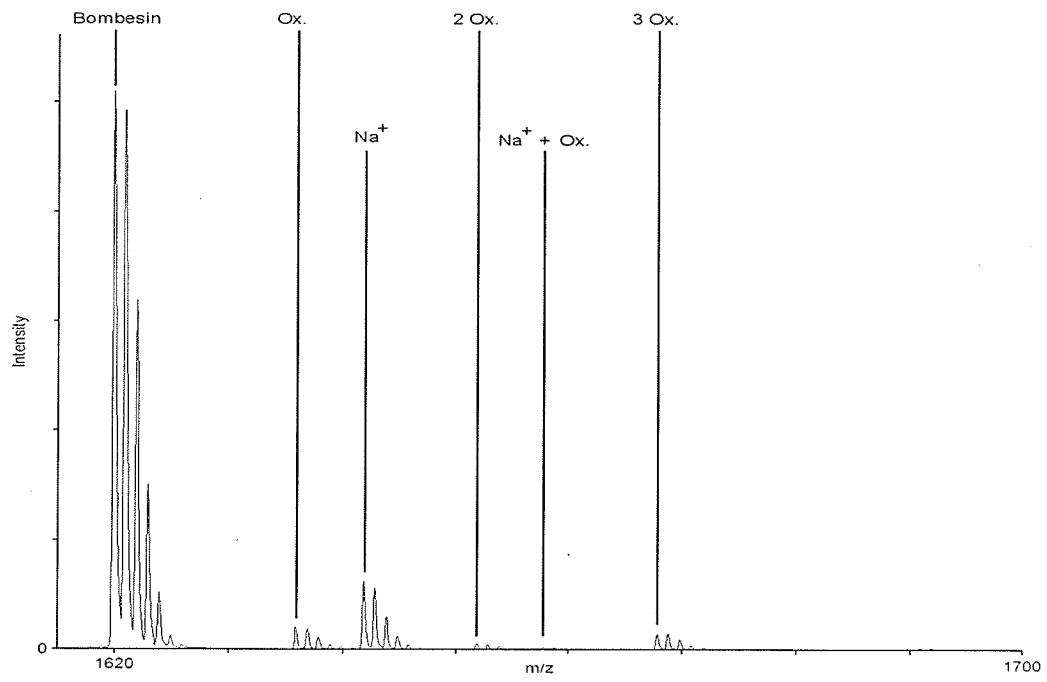


Figure 5.15: MALDI-MS showing increased oxidation of bombesin from the standard (top spectrum) to Zone 4 (bottom spectrum)

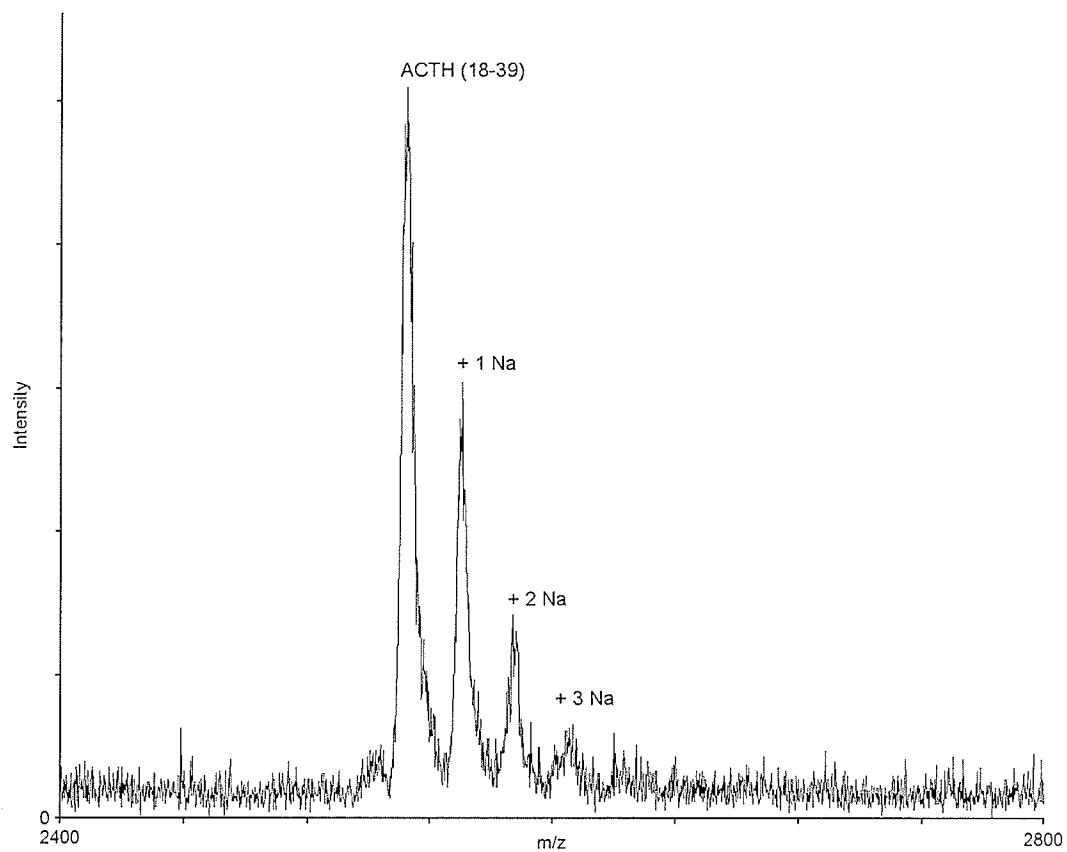


Figure 5.16: MALDI-MS spectrum directly acquired from Teflon surface showing sodium adducts of ACTH (18-39)

5.4 Conclusion

The development of on-target electrophoresis is very much at a preliminary stage. It has been shown that separation of components is possible, though diffusion of analytes is a very prominent effect. By freezing the target following electrophoresis, immobilization of the analytes can be achieved.

The use of a Teflon insert as an electrophoretic channel creates technical hurdles which have yet to be overcome. The insulating nature of Teflon also prevents ions formed during the laser shot from being accelerated from the source, reducing sensitivity. In addition, the short length of the channel which can fit into a target plate limits resolution of the system. The hydrophobic nature of Teflon also limits how much matrix can be added to the target, and reduces the tolerance of the MALDI dried drop method to impurities present. A possible solution to this problem may be found in the use of solid matrices. As fine particulates have been shown to act as matrices in ionizing samples [38-41], they could theoretically be dispersed over the surface of the sample without suffering from the hydrophobic effects of the Teflon surface. The vertical nature of the target in our instrument configuration will likely cause loss of the powdered matrices, however, requiring a different instrument to be used.

It has been shown however, that limited separation of components in a short time frame is achievable, however insensitive the current state of the method is.

Future work of this method will be focused on several key areas.

First, the limited length of the channel does not allow for adequate resolution of the components. Though a longer channel is possible, it is limited by the dimensions of the target. Because of the hydrophobic nature of the Teflon channel, it

may be possible to “bridge” two targets together to form a longer channel. By butting two targets together, the largely aqueous buffer combined with the hydrophobic nature of the Teflon surface should allow the run buffer to bridge the minute gap between the channel pieces, allowing for separation to take place. As ions move to the second channel, it should be possible to remove the second channel and replace it with a fresh channel (Figure 5.17), though movement of the channels will distort resolution somewhat. However, separation of analyte zones onto separate targets or fractions would allow for a more detailed analysis of specific components. Use of this method would require the construction of a much more sophisticated freezing apparatus, so that selective immobilization of a selected channel can be achieved.

Second, the deposition of matrix needs to be improved. Deposition of matrix by piezoelectric devices [42-44] or electrospray [45,46] would result in smaller sample spots in the channel. Resolution and characterization of peaks by our method is dependent on a combination of sample spot size, laser spot size, and the movement of the stepper motors of the mass spectrometer stage. As the deposition of matrix dissolves and mixes the components on the surface where the matrix is deposited, the matrix spot size would largely be the limiting factor, rather than the dimensions of laser spot size and stepper motor movement. Sample deposition systems have been shown to collect samples at a rate of one sample spot per 2-3 seconds of peak eluent [47] which would adequately characterize most samples.

Third, the diffusion of the components needs to be reduced to improve resolution. The addition of a monolithic packing material to the electrophoretic channel could reduce the diffusion of sample [48-52]. In this approach, the channel would resemble a

capillary electrochromatography system. It is unknown if the formation of the monolithic column would be possible inside the Teflon channel, however. Given the inert nature of Teflon, it may be impossible to bond the material to the walls, giving space for analytes to flow around the monolith.

Further analysis also needs to be performed to determine if loss of peptides during lyophilization is significant. The most direct means of determining this would be by the use of a metal-coated affinity tagged peptide as a sample, followed by ICP-MS pre-and post-lyophilization to quantitatively determine the degree of sample loss.

The lyophilization step can be circumvented, however, if the technical hurdles of IR-MALDI can be overcome [53]. The use of a buffer liquid which could also serve as a matrix in the desorption process would remove the need for a lyophilization step. Though water has been shown to be a viable matrix for IR laser desorption [54], the use of glycerol [55] as a matrix may be more useful. The higher viscosity of glycerol may reduce diffusion of components during sample injection and electrophoresis.

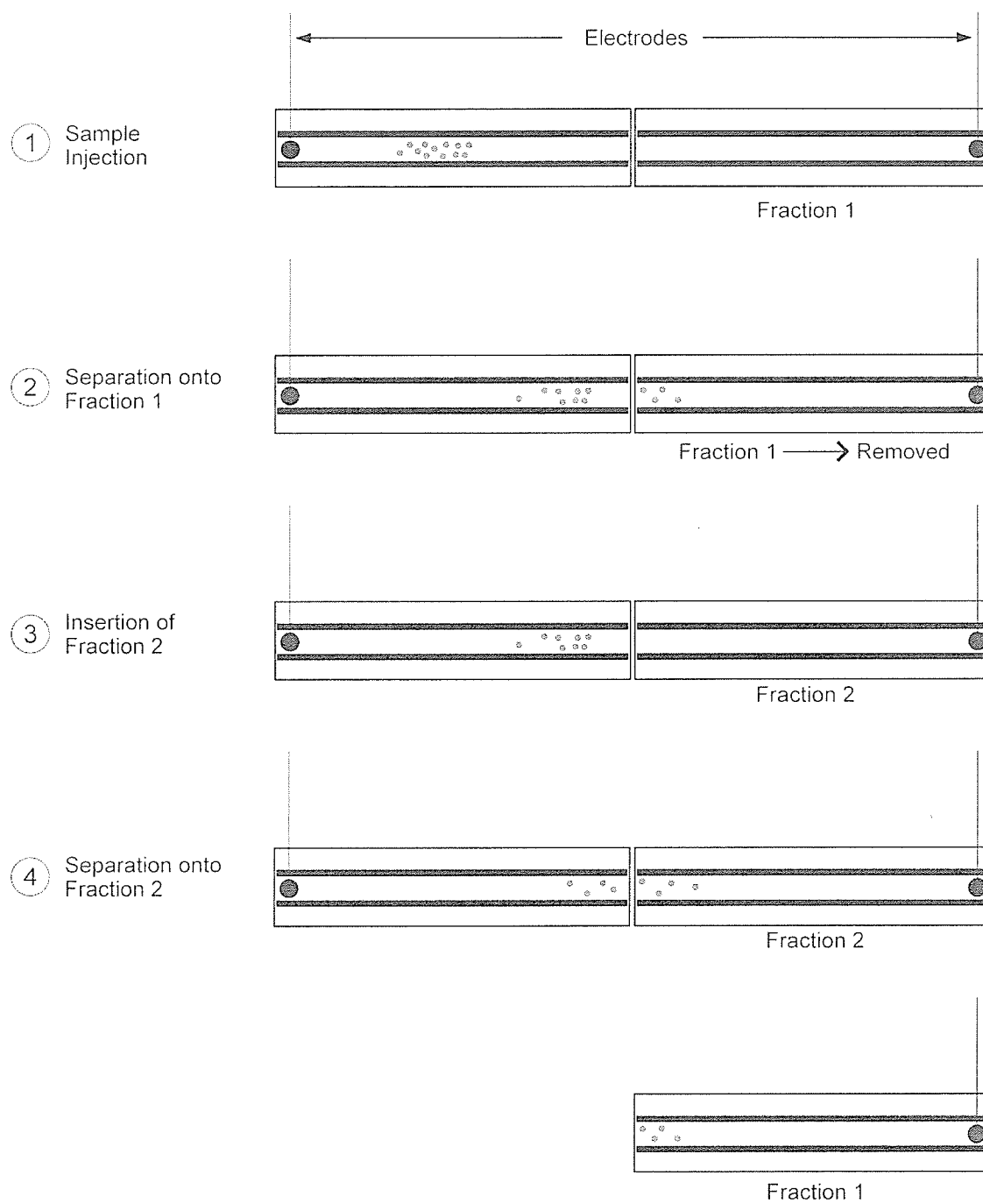


Figure 5.17: Schematic workflow of joined Teflon targets showing (1) injection of sample into the channel followed by (2) separation of the components across two targets, and (3) collection of a new fraction from the electrophoresis, and (4) further electrophoretic separation.

5.5 References

- [1] Cohen, S.L., Chait, B.T. *Anal. Chem.* **68**, 31 (1996)
- [2] Kratzer, R., Eckerskorn, C., Karas, M., Lottspeich, F. *Electrophoresis* **19**, 1910 (1998)
- [3] Amado, F.M.L., Domingues, P., Santana-Marques, M.G., Ferrer-Correia, A.J., Tomer, K.B. *Rapid Commun. Mass Spectrom.* **11**, 1347 (1997)
- [4] Zhang, H.Y., Stoeckli, M., Andren, P.E., Caprioli, R.M. *J. Mass Spectrom.* **34**, 377 (1999)
- [5] Olivares, J.A., Nguyen, N.T., Yonker, C.R., Smith, R.D., *Anal. Chem.* **59**, 1230 (1987)
- [6] Xue, Q., Foret, F., Dunayevskiy, Y.M., Zavracky, P.M., McGruer, N.E., Karger, B.L. *Anal. Chem.* **69**, 426 (1997)
- [7] Ramsey, R.S., Ramsey, J.M. *Anal. Chem.* **69**, 1174 (1997)
- [8] Figeys, D., Ning, Y., Aebersold, R., *Anal. Chem.* **69**, 3153 (1997)
- [9] Hutchens, T.W., Yip, T.T. *Rapid Commun. Mass Spectrom.* **7**, 576 (1993)
- [10] Issaq, H.J., Veenstra, T.D., Conrads, T.P., Felschow, D. *BioChem. Biophys. Res. Commun.* **292**, 587 (2002)
- [11] Walker, K.L., Chiu, R.W., Monnig, C.A., Wilkins, C.L. *Anal. Chem.* **67**, 4197 (1995)
- [12] Zhang, H.Y., Caprioli, R.M. *J. Mass Spectrom.* **31**, 1039 (1996)
- [13] Bergman, A.C., Bergman, T. *J. Protein Chem.* **16**, 421 (1997)
- [14] Preisler, J., Foret, F., Karger, B.L. *Anal. Chem.* **70**, 5278 (1998)
- [15] Rejtar, T., Hu, P., Juhasz, P., Campbell, J.M., Vestal, M.L., Preisler, J., Karger, B.L. *J. Proteome Res.* **1**, 171 (2002)
- [16] Strupat, K., Karas, M., Hillenkamp, F., Eckerskorn, C., Lottspeich, F. *Anal. Chem.* **64**, 464 (1994)
- [17] Vestling, M.M., Fenselau, C. *Anal. Chem.* **64**, 471 (1994)

- [18] Blais, J.C., Nagnan-Le-Meillour, P., Bolbach, G., Tabet, J.C. *Rapid Commun. Mass Spectrom.* **10**, 1 (1996)
- [19] Eckerskorn, C., Strupat, K., Kars, M., Hillenkamp, F. Lottspeich, F. *Electrophoresis* **13**, 664 (1992)
- [20] Eckerskorn, C., Strupat, K., Schleuder, D. Hochstrasser, D., Sanchez, J-C., Lottspeich, F., Hillenkamp, F. *Anal. Chem.* **69**, 2888 (1997)
- [21] Loo, R.R.O., Stevenson, T.I., Mitchell, C., Loo, J.A., Andrews, P.C. *Anal. Chem.* **68**, 1910 (1996)
- [22] Figeys, D., Pinto, D. *Electrophoresis* **22**, 208 (2001)
- [23] Lion, N. Rohner, T.C. Dayon, L., Arnaud, I.L., Damoc, E., Youhnovski, N., Zhi-Yong, W., Roussel, C., Josserand, J., Jensen, H., Rossier, J.S., Przybylski, M., Girault, H.H. *Electrophoresis* **24**, 3533 (2003)
- [24] DeVoe, D.L., Lee, C.S. *Electrophoresis* **27**, 3559 (2006)
- [25] Musyimi, H.K., Guy, J., Narcisse, D.A., Soper, S.A., Murray, K.K. *Electrophoresis* **26**, 4703 (2005)
- [26] Preisler, J., Foret, F., Karger, B.L. *Anal. Chem.* **70**, 5278 (1998)
- [27] Preisler, J., Hu, P.I, Rejtar, T., Moskovets, E., Karger, B.L. *Anal. Chem.* **74**, 17 (2002)
- [28] Liu, J., Tseng, K., Garcia, B., Lebrilla, C.B., Mukerjee, E., Collins, S., Smith, R. *Anal. Chem.* **73**, 2147 (2001)
- [29] Brivio, M., Fokkens, R., Verboom, W., Reinhoudt, D.N. *Anal. Chem.* **74**, 3972 (2002)
- [30] Brivio, M., Tas, N.R., Goedbloed, M.H., Gardeniers, H.J.G.E., Verboom, W., van den Berg, A., Reinhoudt, D.N. *Lab Chip* **5**, 378 (2005)
- [31] Jacksén, J., Frisk, T., Redeby, T., Parmar, V., van der Wijngaart, W., Stemme, G., Emmer, A. *Electrophoresis* **28**, 2458 (2007)
- [32] Hung, K.C., Ding, H. Guo, B. *Anal. Chem.* **71**, 518 (1999)
- [33] Yuan, X., Desiderio, D.M. *J. Mass Spectrom.* **37**, 512 (2002)
- [34] Vorm, O., Roepstorff, P., Mann, M. *Anal. Chem.* **66**, 3281 (1994)

- [35] Luxembourg, S.L., McDonnell, L.A., Duursma, M.C., Guo, X., Heeren, R.M.A. *Anal. Chem.* **75**, 2333 (2003)
- [36] Xiang, F., Beavis, R.C. *Org. Mass Spectrom.* **28**, 1424 (1993)
- [37] Cohen, S.L., Chait, B.L. *Anal. Chem.* **68**, 31 (1996)
- [38] Tanaka, K., Hiroaki, W., Ido, Y., Akita, S., Yoshida, Y., Yoshida, T. *Rapid Commun. Mass Spectrom.* **2**, 151 (1988)
- [39] Sunner, J., Dratz, E., Chen, Y.C., *Anal. Chem.* **67**, 4335 (1995)
- [40] Dale, M.J., Knochenmuss, R., Zenobi, R. *Anal. Chem.* **68**, 3321 (1996)
- [41] Schurenberg, M., Dreisewerd, K., Hillenkamp, F. *Anal. Chem.* **71**, 221 (1999)
- [42] Little, D.P., Cornish, T.J., O'Donnell, M.J., Braun, A., Cotter, R.J., Koster, H. *Anal. Chem.* **69**, 4540 (1997)
- [43] Allmaier, G. *Rapid Commun. Mass Spectrom.* **11**, 1567 (1997)
- [44] Miliotis, T., Kjellstrom, S., Nilsson, J., Laurell, T., Edholm, L.E., Marko-Varga, G. *J. Mass Spectrom.* **35**, 369 (2000)
- [45] Hensel, R.R., King, R.C., Owens, K.G. *Rapid Commun. Mass Spectrom.* **11**, 1785 (1997)
- [46] Axelsson, J., Hoberg, A-M., Waterson, C., Myatt, P., Shield, G.L., Verney, J., Haddleton, D.M., Derrick, P.J. *Rapid Commun. Mass Spectrom.* **11**, 209 (1997)
- [47] Ericson, C., Phung, Q.T., Horn, D.M., Peters, E.C., Fitchett, J.R., Ficarro, S.B., Salomon, A.R., Brill, L.M., Brock, A. *Anal. Chem.* **75**, 2309 (2003)
- [48] Hjerten, S., Liao, J.L., Zhang, R. *J. Chromatogr.* **473**, 273 (1989)
- [49] Svec, F., Frechet, J.M.J. *Anal. Chem.* **64**, 820 (1992)
- [50] Wang, Q., Svec, F., Frechet, J.M.J. *Anal. Chem.* **65**, 2243 (1993)
- [51] Svec, F., Frechet, J.M.J. *Science* **273**, 205 (1996)
- [52] Hsuan-shen, C., Rejtar, T., Andreev, V., Moskovets, E., Karger, B.L. *Anal. Chem.* **77**, 2323 (2005)

[53] Stoeckli, M., Chaurand, P., Hallahan, D.E., Caprioli, R.M. *Nat. Med.* **7**, 493 (2001)

[54] Berkenkamp, S., Karas, M., Hillenkamp, F. *Proc. Nat. Acad. Sci.* **93**, 7003 (1996)

[55] Dreiswerd, K., Berkenkamp, S., Leisner, A., Rohlfing, A., Menzel, C. *Int. J. Mass Spectrom.* **226**, 189 (2003)